ISTANBUL TECHNICAL UNIVERSITY ★ GRADUATE SCHOOL

PARTICLE-REINFORCED POLYPROPYLENE BIOCOMPOSITES BASED ON LIGNOCELLULOSIC BIOMASS FROM ORGANIC WASTES

M.Sc. THESIS

Eliz GURPINAR

Department of Chemistry

Polymer Science & Technology Programme

DECEMBER 2022

ISTANBUL TECHNICAL UNIVERSITY ★ GRADUATE SCHOOL

PARTICLE-REINFORCED POLYPROPYLENE BIOCOMPOSITES BASED ON LIGNOCELLULOSIC BIOMASS FROM ORGANIC WASTES

M.Sc. THESIS

Eliz GURPINAR
(515201021)

Department of Chemistry

Polymer Science & Technology Programme

Thesis Advisor: Assoc. Prof. Dr. Cüneyt H. ÜNLÜ

DECEMBER 2022

ISTANBUL TEKNİK ÜNİVERSİTESİ ★ LİSANSÜSTÜ EĞİTİM ENSTİTÜSÜ

ORGANİK ATIKLARDAN ELDE EDILEN LİGNOSELÜLOZİK BİYOKÜTLE ESASLI PARTİKÜL TAKVİYELİ POLİPROPİLEN BİYOKOMPOZİTLER

YÜKSEK LİSANS TEZİ

Eliz GURPINAR
(515201021)

Kimya Anabilim Dalı

Polimer Bilimi & Teknolojisi Programı

Tez Danışmanı: Doç. Dr. Cüneyt H. ÜNLÜ

ARALIK 2022

Eliz GURPINAR, a M.Sc. student of İTU Graduate School 515201021 successfully defended the thesis/dissertation entitled "PARTICLE REINFOCED POLYPROPYLENE BIOCOMPOSITES BASED ON LIGNOCELLULOSIC BIOMASS FROM ORGANIC WASTES", which she prepared after fulfilling the requirements specified in the associated legislations, before the jury whose signatures are below.

Thesis Advisor :	**Assoc. Prof. Dr. Cuneyt H. UNLU** İstanbul Technical University	.....
Jury Members :	**Assoc. Prof. Dr. Bünyamin KARAGÖZ** Istanbul Technical University	.....
	Prof. Dr. Aydan DAĞ Bezmialem Vakıf University	.....

Date of Submission : 28 December 2022
Date of Defense : 27 January 2023

To my beloved family,

FOREWORD

I would like to thank my professor, Cüneyt H. ÜNLÜ, for sharing his knowledge, experience, and guidance and for providing a friendly working environment for this dissertation. I also want to thank him for the time that he spent teaching me the parts that I had no knowledge of and for allowing me to explore the chemistry side of the project.

I would like to acknowledge Istanbul Technical University's Faculty of Science and Letters Chemistry Department and the Polymer Science and Technology family for supplying all the research facilities that are necessary for this study.

I am grateful to Ceren YARGICI KOVACI, my supervisor at Arçelik A.Ş, for her invaluable guidance and advice, as well as for assisting me in managing the workflow on this project and teaching me how to progress from a student to an engineer. I would like to thank my administrator, Dr. Gokhan SIR, for motivating, supporting, and directing me to accomplish my goals.

I would like to acknowledge Arçelik A.Ş for providing me with comprehensive lab equipment, giving me the opportunity to enhance my work, and being open to innovative solutions, re-conceptions, and different outlooks. Therefore, it was easy for me to come up with new ideas during my studies. Furthermore, I am grateful to my R&D laboratory colleagues, Metehan CIHANGIR, Sefa Yasin UZEN, Erdal PILAV, Gürkan KOCSIZ, Fatih TUTAL, and Hamit YILDIZ, for making my life easier by assisting me in completing the project work, particularly the technical portion, at a rapid pace during a heavy workload.

Finally, I want to express my gratitude to my mother for always being by my side and backing me up with everything that she has.

December 2022

Eliz GURPINAR
(Material Scientist and Nanoengineer)

TABLE OF CONTENTS

Page

ABBREVIATIONS

PP : Polypropylene

AKS : Apricot Kernel Shell

HS : Hazelnut Shell

WS : Walnut Shell

CC : Corn Cob

SA : Stearic Acid

MAPP : Maleic Anhydride Grafted Polypropylene

MFI : Melt Flow Index

TGA : Thermogravimetric Analysis

DTG : Derivative Thermogravimetry

DSC : Differential Scanning Calorimetry

ATR-FTIR : Attenuated Total Reflectance-Fourier Transform Infrared Spectroscopy

SEM : Scanning Electron Microscopy

SYMBOLS

σ_{TS}	: Tensile Strength
E	: Modulus of Elasticity
σ_{Flex}	: Flexural Strength
E_{Flex}	: Flexural Modulus
ε_f	: Elongation at Break
σ_y	: Yield Strength
ε_y	: Elongation at Yield
E_{Frac}	: Izod Impact Strength
ΔH_m	: Melting Enthalpy of the Sample
ΔH_m^o	: Melting Enthalpy of 100% Crystalline PP
ΔH_c	: Enthalpy of Crystallization
X_c	: Degree of Crystallinity
$T_{m\ onset}$	: Onset Temperature of Melting
T_m	: Melting Temperature
T_{max}	: Temperature at maximum weight loss
T_{100^oC}	: Mass loss at 100ºC
T_{200^oC}	: Mass loss at 200ºC
T_{500^oC}	: Mass loss at 500ºC
T_{950^oC}	: Mass loss at 950ºC
Mt (%)	: Moisture Content in Percentage
W_t	: Weight of the Wet Sample
W_0	: Initial Weight of the Sample

LIST OF TABLES

Page

LIST OF FIGURES

Page

PARTICLE REINFORCED POLYPROPYLENE BIOCOMPOSITES BASED ON LIGNOCELLULOSIC BIOMASS FROM ORGANIC WASTES

SUMMARY

The aim of this study was to examine the effects of lignocellulosic biomass on the properties of polypropylene (PP) biocomposites. The biomass used in this experiment was apricot kernel shell (AKS), hazelnut shell (HS), walnut shell (WS), and corn cob (CC). In the first section of the thesis, the characterization of biomasses was analyzed. For the characterization of each biomass, chemical analysis was done chemically and thermally. FTIR analysis was applied to determine the spectral analysis of biomasses. Lignin has more hydrophobic, higher available sites and more reactive groups that can bind from the surface. From the results of chemical analysis, AKS showed that it had the highest lignin content among all.

Biomass selection was critical for mass production. The biomass was selected based on its use by secondary consumers. Nut shells and corncobs could be harvested before the second consumer. In Arçelik's previous study, used coffee waste was collected after the second consumer. Coffee waste could not be cleaned or separated after collection. In some cases, undesirable substances were seen. If the unwanted external materials are not cleaned, they may damage the mold during the previous processes. AKS, HS, WS and CC wastes can be used easily in mass production.

The hydroxyl bonds of the material were determined. After titration with anhydrite and pyridine mixture, the amount of OH and the OH equation were measured. According to the results, it was seen that the OH amount was highest in WS and CC. The reason for the excess of these two is that the amount of free OH in the cellulose is high, and it is predicted that their amount is excessive. It was observed that the amount of hydroxyl bonds coming from the cellulose parts was excessive because the OH amounts in the lignin were not reached due to the structure requirement. WS and CC are more hydrophilic biomass due to their cellulose content.

When looking at the TGA analysis of biomass, the decomposition temperature of AKS and HS started later. The reason for this is that the amount of complex structured lignin is higher, and its thermal resistance is higher than other HS and CC biomass. Lignin decomposition is slower than hemicellulose and cellulose. In addition, according to the result obtained from the TGA graph, the most mass loss was seen in AKS. According to the literature research, the high amount of heavy metal in the ACS was associated with this high mass loss.

Two different PPs were used in the biocomposite process. Since the mechanical results with the two were different from each other, FTIR analysis was performed and the differences between them were examined. The isotactic ratio was determined as a result of the FTIR analysis. The ratio of isotacticity ratios to the percentage of crystallization was examined. As a result, Borealis PP was more atactic, while

Sumitomo PP was more isotactic. With the mechanical tests, the bending modulus and elastic modulus of Sumitomo PP were higher, while the impact value was lower compared to Borealis PP. The percentage of crystallization according to the difference in isotactic ratios confirmed the results. While the crystallization percentage of Sumitomo PP increased to 36%, the crystallization of Borealis PP increased to 15%. After obtaining biocomposite with AKS, isotacticity ratios were determined according to the percentage of ACS. In PP/AKS biocomposites made with Borealis, isotacticity increased as the percentage increased. The most atactic PP/10AKS was found in PP/AKS biocomposites made with Sumitomo. On the other hand, isotacticity increased with the increase of biomass ratio in biocomposites after 10%.

It was revealed that the biomass surfaces exhibit impurities and irregularities, which could degrade the biocomposite properties after compounding, because it would be harder to mechanically interlock of the biomass and PP matrix. For the removal of those impurities from the biomass surface, AKS was washed with ethanol, and it was exposed to an esterification reaction to modify its surface properties. Modification is then analyzed with FTIR spectra. The requirement for the surface modification came from the inherent hydrophilic nature of the biomass, which caused poor interfacial adhesion and incompatibility with the PP matrix. The esterification reaction reduced the hydroxyl sites of the AKS. For the modification of AKS, six different cases were experimented by changing the time, temperature, and content of the stearic acid (SA) modifier. From the characterization of modified AKS, it was revealed that just by changing the temperature from room temperature to 50 C, the modification became prominent.

The biomass was compounded with PP matrix to obtain a biocomposite form of the material. The compounding process involved melt mixing by twin screw extrusion and then injection molding. The mechanical and thermal properties of biocomposites were investigated. The effect of biomass content, type and the interfacial compatibility were examined.

For AKS, increasing biomass content resulted in agglomeration of the biomass particles according to the SEM images. This occurrence caused the matrix compatibilization to break and AKS particles detached leading to the fiber pull-out. The general trend for all type of biocomposites was an increase in proportion resulted in decreased the elongation at break and impact strength while increasing the moduli in general. TGA analysis revealed that, in the first 25% of the curve, neat PP had a higher thermal stability compared to biocomposites. Yet, in the last quartile of the graph the biocomposites had a higher decomposition temperature in comparison with the neat PP. This is an indication of in high temperature applications it would be better to use biomass-filled biocomposites. The first heating cycle of the biocomposites was studied with DSC analysis. As the biomass content increased, it was expected to have a high degree of crystallization, yet the crystallization increased up to 10% AKS biomass and then decreased afterwards. This could be attributed to the fact that at higher biomass contents, the agglomeration deteriorated the crystallization behavior.

The hydrophilic nature of biomass was inconsistent with PP matrix which could result in poor interfacial compatibility. Therefore, to improve the properties of biocomposites, maleic anhydride- grafted PP (MAPP) added as compatibilizer. The impact of MAPP on biocomposites was tested to see if the effect of the compatibilizer

enhanced the mechanical and thermal properties of the material. The improved properties of the biocomposite with the addition of 2 wt% MAPP were also confirmed with the SEM imaging, which decreased the surface roughness and provided a uniform distribution of the biomass particles inside the PP matrix.

DSC curve revealed that, the degree of crystallization was highest in the MAPP-compatible biocomposite. TGA results that the thermal stability of biocomposites were also improved with the addition of MAPP. Without compatibilizer, low molecular weight compounds were thermally decomposed earlier, and MAPP addition hold these compounds and inhibit the detachment from the PP matrix.

Finally, the rheological behavior of the biocomposites was studied with a capillary rheometer. The materials exhibited pseudoplastic fluid behavior, in which shear thinning occurs when shear rate is applied. As the biomass content increased, the power law index decreased, and the inverse proportionality of the power law index and shear thinning behavior showed that shear thinning was more distinct at high biomass contents. The viscosity of biocomposites decreased as the shear rate increased. There was no discernible difference in behavior between the viscosities of various biomass-content biocomposites.

ORGANİK ATIKLARDAN ELDE EDİLEN LİGNOSELLÜLOZİK BİYOKÜTLE ESASLI PARÇACIKLA GÜÇLENDİRİLMİŞ POLİPROPİLEN BİYOKOMPOZİTLER

ÖZET

Bu çalışmanın amacı, lignoselülozik biyokütlenin polipropilen (PP) biyokompozitlerin özellikleri üzerindeki etkilerini incelemektir. Bu deneyde kullanılan biyokütle kayısı çekirdeği kabuğu (AKS), fındık kabuğu (HS), ceviz kabuğu (WS) ve mısır koçanıydı (CC). Tezin birinci bölümünde biyokütlelerin karakterizasyonu incelenmiştir. Her bir biyokütlenin karakterizasyonu için kimyasal ve termal olarak kimyasal analizler yapılmıştır. Biyokütlelerin spektral analizini belirlemek için FTIR analizi uygulandı. Lignin, yüzeyden bağlanabilen daha hidrofobik, daha yüksek kullanılabilir bölgelere ve daha reaktif gruplara sahiptir. Kimyasal analiz sonuçlarından AKS, hepsi arasında en yüksek lignin içeriğine sahip olduğunu gösterdi. Buna zıt olarak, CC en yüksek selüloz oranına sahip biyokütle olarak sonuçlandı. Bu sebeple, en düşük mekanik ve termal değerler CC ile yapılan biyokompozitlerden bekleniyor. Bunun sebebi, CC deki selüloz miktarının yüksek olmasıyla biyokütleyi daha hidrofilik yapıda olmasını sağlar. Bu da hidrofobik yapıdaki polimer matriksiyle uyumsuzluğunu arttırır.

Biyokütle seçimi, seri üretim için kritikti. Biyokütle, ikincil tüketiciler tarafından kullanımına göre seçilmiştir. Fındık kabukları ve mısır koçanları ikinci tüketiciden önce toplanabiliyordu. Arçelik'in daha önceki çalışmasında kullanılmış kahve atıkları ikinci tüketiciden sonra toplanıyordu. Kahve atıkları toplandıktan sonra temizlenmiyor veya ayrıştırılamıyordu. Bazı durumlarda istenmeyen maddeler görüldü. İstenmeyen dış maddeler temizlenmezse daha önce gerçekleşen işlemler sırasında kalıba zarar verebilir. AKS, HS, WS ve CC atıkları seri üretimde rahatlıkla kullanılabilir.

Malzemenin hidroksil bağlarının tespiti yapıldı. Yapılan anhirit ve piridin karışımıyla titrasyon yapıldıktan sonra OH miktarı ve OH eşitliği ölçüldü. Sonuclara göre, OH miktarının en fazla çıktığı WS ve CC olarak görüldü. Bu ikisinin fazla çıkmasının sebebi ise selülozün içerisindeki serbest OH miktarlarının fazla olmasıyla miktarlarının fazla çıktığı öngörülmüştür. Ligninin içindeki OH miktarlarına yapı gerekeği ulaşılmadığından dolayı selüloz kısımlarından gelen hidroksil bağlarının miktarlarının fazla çıktığı görülmüştür. WS ve CC selüloz içeriğinden dolayı daha hidrofilik biyokütlelerdir.

Biyokütlelerin TGA analizine bakıldığı zaman, AKS ve HS nin dekompozisyon sıcaklığı daha geç başlamıştır. Bunun sebebi içerisindeki kompleks yapılı lignin miktarının fazla olmasıyla termal dayanımı diğer HS ve CC biyokütlelerine göre daha

yüksek çıkmıştır. Ligninin dekompozisyonu hemiselüloz ve selüloza göre daha yavaştır. Ayrıca, TGA grafiğinden çıkartılan sonuca göre en çok kütle kaybı AKS de görülmüştür. Literatür araştırmasına göre AKS nin içerisindeki ağır metal oranının fazla olmasıyla bu kütle kaybının yüksek olması ilişkilendirildi.

Biyokompozit prosesinde iki farklı PP kullanıldı. İkisiyle yapılan mekanik sonuçlar birbirinden farklı çıktığı için FTIR analizi yapılıp arasındaki farklar incelenmiştir. FTIR analizi sonucunda isotaktik oranı belirlenmiştir. Isotaktisite oranlarıyla kristalizasyon yüzdesinin orantısına bakılmıştır. Sonuç olarak, Borealis PP daha ataktik çıkarken, Sumitomo PP daha izotaktik çıkmıştır. Yapılan mekanik testlerle de Sumitomo PP nin eğme modulusu ve elastik modulusu daha yüksek iken darbe değeri daha düşük çıkmıştır Borealis PP ye göre. Izotaktik oranları farkına göre kristalizasyon yüzdesi sonuçları doğrulamıştır. Sumitomo PP nin kristalizasyon yüzdesi 36% çıkarken Borealis PP ni kristalizasyonu 15% çıkmıştır. AKS ile biokompozit eldesinden sonra AKS yüzdesine göre isotaktisite oranları belirlenmiştir. Borealis ile yapılan PP/AKS biokompozitlerde yüzde miktarı arttıkça izotaktisite de artmıştır. Sumitomo ile yapılan PP/AKS biokompozitlerde en ataktik PP/10AKS de çıkmıştır. Isotaktisite ise 10% dan sonraki biyokompozitlerde biyokütle oranın artmasıyla beraber artmıştır.

Biyokütle yüzeylerinin, biyokütle ve PP matrisinin mekanik olarak birbirine kenetlenmesi daha zor olacağından, bileşikleştirmeden sonra biyokompozit özelliklerini bozabilecek safsızlıklar ve düzensizlikler sergilediği ortaya çıktı. Bu safsızlıkların biyokütle yüzeyinden uzaklaştırılması için AKS, etanol ile yıkandı ve yüzey özelliklerini değiştirmek için bir esterleşme reaksiyonuna maruz bırakıldı. Modifikasyon daha sonra FTIR spektrumları ile analiz edilir. Yüzey modifikasyonu gereksinimi, zayıf ara yüzey yapışmasına ve PP matrisi ile uyumsuzluğa neden olan biyokütlenin doğal hidrofilik doğasından geliyordu. Esterleştirme reaksiyonu, AKS'nin hidroksil bölgelerini azalttı. AKS'nin modifikasyonu için, stearik asit (SA) değiştiricinin süresi, sıcaklığı ve içeriği değiştirilerek altı farklı durum denendi. Modifiye edilmiş AKS'nin karakterizasyonundan, sıcaklığın oda sıcaklığından 50 C'ye değiştirilmesiyle modifikasyonun öne çıktığı ortaya çıktı.

Biyokütle, malzemenin biyokompozit formunu elde etmek için PP matrisi ile birleştirildi. Birleştirme işlemi, çift vidalı ekstrüzyon ve ardından enjeksiyon kalıplama ile eriyik karıştırmayı içeriyordu. Biyokompozitlerin mekanik ve termal özellikleri incelenmiştir. Biyokütle içeriğinin, tipinin ve arayüz uyumluluğunun etkisi incelenmiştir.

AKS için, artan biyokütle içeriği, SEM görüntülerine göre biyokütle parçacıklarının topaklaşmasına neden oldu. Bu olay, matris uyumlaştırmasının kırılmasına ve AKS parçacıklarının ayrılmasına yol açarak fiberin çekilmesine neden oldu. Tüm biyokompozit tipleri için genel eğilim, genel olarak modülleri arttırırken, kırılmada uzamayı ve darbe dayanımını azaltan orantısal bir artış olmuştur. TGA analizi, eğrinin

ilk %25'inde saf PP'nin biyokompozitlere kıyasla daha yüksek termal stabiliteye sahip olduğunu ortaya çıkardı. Yine de, grafiğin son çeyreğinde biyokompozitler saf PP'ye kıyasla daha yüksek ayrışma sıcaklığına sahipti. Bu, yüksek sıcaklık uygulamalarında biyokütle dolgulu biyokompozitlerin kullanılmasının daha iyi olacağının bir göstergesidir. Biyokompozitlerin ilk ısıtma çevrimi DSC analizi ile incelenmiştir. Biyokütle içeriği arttıkça, yüksek derecede kristalleşme olması beklenirken, kristalleşme %10 AKS biyokütlesine kadar artmış ve daha sonra azalmıştır. Bu, daha yüksek biyokütle içeriklerinde, aglomerasyonun kristalleşme davranışını bozduğu gerçeğine atfedilebilir.

Biyokütlenin hidrofilik doğası, zayıf arayüz uyumluluğuna neden olabilecek PP matrisi ile tutarsızdı. Bu nedenle biyokompozitlerin özelliklerini iyileştirmek için uyumlaştırıcı olarak maleik anhidrit aşılı PP (MAPP) eklenmiştir. MAPP'nin biyokompozitler üzerindeki etkisi, bağdaştırıcının etkisinin malzemenin mekanik ve termal özelliklerini geliştirip geliştirmediğini görmek için test edildi. Biyokompozitin ağırlıkça %2 MAPP ilavesiyle iyileşen özellikleri, yüzey pürüzlülüğünü azaltan ve biyokütle partiküllerinin PP matrisi içinde üniform bir dağılımını sağlayan SEM görüntüleme ile de doğrulandı.

DSC eğrisi, MAPP uyumlu biyokompozitte kristalleşme derecesinin en yüksek olduğunu ortaya koydu. TGA sonuçları, biyokompozitlerin termal kararlılığının da MAPP ilavesiyle iyileştirildiğini göstermektedir. Bağdaştırıcı olmadan, düşük moleküler ağırlıklı bileşikler daha önce termal olarak ayrışmıştır ve MAPP ilavesi bu bileşikleri tutar ve PP matrisinden ayrılmayı engeller.

Son olarak, biyokompozitlerin reolojik davranışı bir kılcal reometre ile incelenmiştir. Malzemeler, kesme hızı uygulandığında kayma incelmesinin meydana geldiği psödoplastik sıvı davranışı sergilemiştir. Biyokütle içeriği arttıkça, güç kanunu indeksi azaldı ve güç kanunu indeksi ile kayma incelmesi davranışının ters orantılılığı, yüksek biyokütle içeriklerinde kayma incelmesinin daha belirgin olduğunu gösterdi. Biyokompozitlerin viskozitesi, kesme hızı arttıkça azalmıştır. Çeşitli biyokütle içerikli biyokompozitlerin viskoziteleri arasında davranışta gözle görülür bir fark yoktu.

1. INTRODUCTION AND AIM

Globally, 1,3 billion tons of organic food waste are discarded each year. Most wastage occurs in the production of fruits and vegetables. Food waste, which is produced in significant amounts as a byproduct of food processing in food manufacturers, is one of the main sources of organic waste. Because some of this organic waste cannot be composted, thus corporations must spend resources and energy to get rid of it, which harms the environment. For the sake of preserving human health, environment, and economy, upcycling the waste to turn it into a useful product has become essential.

Finding novel materials with high economic and ecological value is one of science's top priorities. In this direction, waste recovery turns into a lucrative resource. Due to their unique characteristics, such as low density, high strength, and non-abrasiveness during processing, organic wastes are fascinating reinforcement materials for composite production. Moreover, they are inexpensive, abundant, renewable, and biodegradable. In this regard, the use of waste as a biomass in composites assists the emergence of biocomposites, which give rise to an economic and environmental viewpoint and exemplify sustainable, circular, and environmentally friendly reinforcements.

The first chapter of the thesis revealed the differences between biomasses. Due to the structural differences such as chemical composition including cellulose, lignin and hemicellulose content and hydroxyl content create different properties. Therefore, the characterization of biomass will be done by FTIR, TGA and DSC analysis. In the second chapter biomass will be compounded with polypropylene matrix and results are expected to be different due to the structural variations of molecule itself.

To leave a clean and healthy environment for future generations, there is continuous development in our products that incorporate biomasses. To do this, we ensure energy gain through resource efficiency by reducing environmental impacts across the entire production process. In Arçelik A.Ş, we evaluated the coffee waste products produced by espresso machines and discovered that they have no economic value in our coffee

machines. We used tea fiber as an industrial waste product that is produced during the processing of tea leaves, in our tea machines. As a result, we shorten the plastic end time by using the waste of plastics, which is the most critical problem in the environment of the future. In addition, we add value to the waste material and increase the quality of the waste. Therefore, trying different kinds of organic waste to produce ground-breaking materials has become the goal of this project.

In the current study, it is envisioned that polypropylene is as polymeric matrix and the recovered organic wastes are combined as biomasses to create biocomposite materials. Due to the imcompatible characteristics of the biomass and the matrix, the characterization of the biomasses and compounded materials will be done by mechanical, thermal, morphological, and rheological analysis. As a result, by creating biocomposite compound formulations for Arçelik products, it will aid in generating sustainable materials that will reduce carbon emissions. The intended formulations are based on particle-reinforced biocomposites from polypropylene with different kinds of biomasses, conducted by literature research which will be evaluated regarding their mechanical and thermal properties.

2. TEORETICAL SECTION AND LITERATURE REVIEW

2.1 Polymeric Materials

Polymeric materials have a crucial role in everyday life. They are extremely useful and are utilized in all facets of society. The lightweight, adjustable mechanical and thermal properties, ease of workability and processability of these materials have superior benefits over other materials. Due to their characteristic features, the use of polymeric materials is very common throughout the world. Today, global plastic production is approximately 350 million tonnes and 99% of plastics are based on fossil fuels which means they are made from oil or natural gas. The main issue with these materials is the risk of exhaustion of fossil fuels being non-renewable resources. A small part of this plastic has been recycled (9%), some has been burned (12%), and the remaining part (79%) has ended up in landfills or the environment. Plastic items can take up to 1,000 years to decompose in landfills. This causes air and water pollution; rise in mercury emissions; acid rain; climate change; and so many other environmental and health problems for the environment and human health.

Any group of natural or synthetic compounds known as polymers is made up of macromolecules, which are just multiples of simpler chemical building blocks known as monomers. They are composed primarily of carbon and hydrogen hydrocarbons. They are relatively greater molecular mass compounds, and these properties produce unique physical properties such as hardness, high elasticity, viscoelasticity, and a tendency to form amorphous and semi-crystalline structures rather than crystalline ones. They have relatively low melting temperatures compared to metals. The utilization of these types of materials is very abundant due to being lightweight, and inexpensive to make, most are very resistant to the environment, have poor conducting capabilities of heat and electricity, are easy to bend, easy to process either in molds, as sheets, or as coatings. Many of them have high plasticity, and a few have good elasticity. Some are transparent while some are opaque. Some of the polymer applications are adhesives, containers, moldable products, clothing, coatings such as

paint and varnish, biodegradable products, biomaterials, low friction materials such as Teflon, synthetic oils and greases, gaskets, soap, and surfactants. Depending on how they are used, polymers are categorized into three classes: commodity, engineering, and high-performance polymers. Commodity polymers, which include polyethylene, polypropylene, polystyrene, and polyvinyl chloride, make up 70% of all plastics used in large quantities due to their lightweight, affordability, and formability [1, 2]. These materials are used in construction, packaging, insulation, and cushioning because of their low strength and stiffness.

Engineering polymers are the 25% of plastics used in automotive and electronics that use polyamide, polyester, ABS, polyurethane, epoxy, and polycarbonate to improve strength and high-temperature performance. Finally, high-performance high-performance polymers contain 5% with significantly increased stiffness, higher temperature properties, and chemical resistance. Examples include PEEK's high-temperature resistance; aramid's high strength and stiffness, aromatic polyester's high strength and stiffness; fluoro/silicone polymers' high chemical resistance; and polyacetylene's conductivity.

The three main types of polymers are thermoset, thermoplastic, and elastomers. If we classify polymers based on their properties from a scientific point of view, thermoplastics are mostly solid, like physically entangled amorphous and semi-crystalline structures. Thermosets, on the other hand, are mostly liquid-like, crosslinked structures and it is required to have another component to be formed and reacted, namely a curing agent or crosslinking agent. Elastomers have very large elastic deformations, and they could be thermoplastic or vulcanized to be thermoset. Thermosetting polymers cannot turn back to their original form once cured, which gives them durable and heat-resistant characteristics. The resin can be epoxy, phenolics, polyester, and so on. In other respects, thermoplastics can be reheated and molded again by Van Der Waals and hydrogen bonding weak intermolecular forces, which are better in terms of toughness and recyclability. For instance, epoxy resin and polyester resin are used for casting, encapsulation, and adhesives, while melamine formaldehyde is used for laminating work surfaces, electrical insulation, and tableware. Finally, viscoelastic amorphous structured elastomers have weak intermolecular forces that allow the material to gain elastomeric properties with a high elastic deformation region. High strain values in elastomers decrease the modulus of

elasticity. With a high elastic deformation region, the material can recover from stretching and return to its original shape. Elastomers can be flexible even at low temperatures, and examples include polyurethane to be used as clothing for lycra, silicone for prostheses and for lubricants, and natural rubber for automotive applications.

All polymers have a structure when they are in their solid form. When polymers turn from melt to solid, the polymer chain becomes aligned, and that is when the crystallization happens with the creation of lamellae. The features of plastics are considerably impacted by their degree of crystallization. The parts that remain uncrystallized are called amorphous regions, which may be due to the restricted time during processing, as chains cannot find time to align. The degree of crystallinity in semi-crystalline polymers designates stiffness, toughness, and solvent resistance [3]. The amorphous polymers include polystyrene, polycarbonate, acrylonitrile-butadiene-styrene, and polyvinyl chloride. Polyethylene, polypropylene, and nylon are semi-crystalline polymers. Crystalline structures are like glasses in that they cannot distribute energy when struck. So, the hit point absorbs all the energy and breaks from that point, whereas in amorphous polymers there are gaps in between the molecular chains due to the branching structure that could distribute energy and the material is not breakable but rather flexible. Crystallization can be disrupted by the asymmetry introduced by the R-side group. The three stereoregularity configurations of the chains are isotactic, in which crystals always form; syndiotactic, in which crystals occasionally form; and atactic, in which crystals never form. In other words, the material becomes semi-crystalline when all the R groups are on the same side of the chain, whereas an amorphous polymer results from all the R groups being randomly oriented.

2.1.1 Polypropylene

Polypropylene is a thermoplastic polymer produced by the addition polymerization reaction of its monomer propylene. The polymerization of polypropylene was exemplified in 1951 for the first time by Phillips Petroleum, J. Paul Hogan, and Robert Banks [4]. It is a partially crystalline and nonpolar polyolefin. It is the most widely used commodity plastic after polyethylene, with a 5.8% enlargement up to 2021. The low-density feature assists in the production of moldings with lighter parts and more

pieces per mass of plastic. In the production of plastics, biomasses are being incorporated as resins for many reasons. They are used to minimize the cost, to process it better, to control the density and to manipulate the optical, magnetic, thermal, flame retardancy and mechanical characteristics of a material [5]. However, the biomass addition could substantially change its density. It shows low impact strength, particularly the melt flow index, which is relatively low. Yet, its working temperatures and tensile strength are better than the most widely used commodity plastic, polyethylene. It has high toughness and heat resistance. It ensures good resistance to organic solvents, degreasing agents, electrolytic attack, acids, and alkalis, but it is not resistant to aromatic, aliphatic, and chlorinated solvents. The non-polar molecular structure provides low moisture absorption. Due to these features, it is commonly used in packaging, labeling, textiles, laboratory equipment, automotive, and so on.

2.2 Overview of Composite Materials

The composites could be structured to compose stronger, lighter, and cheaper materials [6]. The term "composite" originates from the matrix and the filler including two or more different constituents inside. The matrix is assigned to save the filler against environmental degradation and mechanical deterioration. The filler, on the other hand, is a reinforcement phase embedded in the continuous matrix phase. Typical reinforcements are talc, glass fiber, silica, mica, graphite, and calcium carbonate, whereas natural and renewable sources are being used as fillers in biocomposites.

Preliminary composites were made of bamboo, tendon, silk, horn, and pine resin to be used as weapons [7]. Later, it continued with the polymerization of synthetic resins. Polymers were designed to reinforce to ensure rigidity and strength. The synthesis of bakelite has led to the formation of new products such as electrical insulators, toys, radios, kitchenware, etcetera. They started to use composites in automotive manufacturing by compression molding, sheet molding, and bulk molding. Then production novelty endured with pultrusion, filament winding, and vacuum bag molding. By the time of progress, composites had started to be used in aerospace, consumer goods, home appliances, insulators, infrastructure, and so on. The future trend is to look for eco-friendly composites that can be recycled and bio-based, which will satisfy the need for stronger, lighter materials to be used in more applications.

Composite materials are composed of two or more different materials combined to meet the requirements of the desired implementation by providing multifunctional properties to the material. The composition can include nano, micro, or macro components that are not soluble in each other. A composite material is made of two basic parts: a matrix and reinforcement. The reinforcement generally has much higher mechanical properties and serves as the principal load-bearing member. The role of the matrix phase is to transfer the load between the fibers, carry them under stress, protect the reinforcement from chemical and humid environments, and improve the matrix properties by providing high mechanical strength. The reinforcement and matrix material can be organic or inorganic. There are different types of composites, including particle-reinforced (large particle or dispersion strengthened), fiber-reinforced (continuous or discontinuous), and structurally reinforced (laminates and sandwich panels).

Composite performance depends on the materials of which the constituents are composed, the form and structural arrangement of the constituents, particularly size, shape, diameter/length, orientation, and the interaction between the constituents.

The fiber-matrix interface is a crucial parameter to consider since the matrix acts as a stress carrier and transfers the stress to the fiber with the help of the fiber-matrix interface. The interface can be created by mechanical, chemical, or reaction bonding where there can be more than one bond at the same time. Mechanical bonding is created by the surface roughness of the material, which leads to a mechanical interlocking between the fiber and the matrix. The chemical bonding is formed at the surface of the fiber and the matrix, which can be spontaneous or non-spontaneous depending on the fiber itself. If it is nonspontaneous, the surface of the fiber can be compounded with some coupling agents to form chemical bonding. Reaction bonding occurs when the matrix and the fiber disperse and penetrate the interface and form a distinctive interfacial layer. The interfacial layer assists in generating a reaction bonding along with the fiber microcracks, which could lower the strength. Factors that affect the mechanical properties of the composites are as follows: reinforcement aspect ratio, fiber/matrix interface, resin/fiber ratio, types of resin and fiber, fiber orientation, resin-fiber interface interaction, and method of processing.

Certain chemicals are used in composite materials for different purposes, such as fillers, additives, and pigments. Fillers are commonly used to reduce weight and cost

by using less polymer in the composition, and they can also improve material properties. Organic waste was used as a filler in this study to reduce costs and plastic usage while also lowering the carbon footprint. Generally, fillers improve the modulus but impair the strength of a material; thereby, the filler content should be optimized. The most widely used fillers are calcium carbonate, talc, silica, and so on. On the other hand, additives are commonly used for better processing, extending the lifetime as well as achieving the intended chemical properties. Even though it is used in small amounts (5%), it can considerably impact the performance of the material with enough alterations. Some additives include UV stabilizers, viscosity stabilizers, flame retardants, suppressants, conductors, release agents, colorants, and so on. The classification of composite materials depends on the sort of material used for the matrix. It involves metal matrix composites, ceramic matrix composites, carbon matrix composites, and polymer matrix composites (PMC). This research is focusing on thermoplastic polymer matrix type matrix-type composites.

2.2.1 Polymer matrix composites

Most polymers' properties are inadequate for many structural purposes, as their strength and stiffness are quite much lower than those of fibers. So, they need to be improved by reinforcing them with fibers. In polymer matrix composites (PMC), the continuous phase is made up of various organic polymer types, and the dispersed phase is made up of reinforced fibers. To effectively transfer load between the fibers, the continuous phase acts as a matrix to hold the fibers together. The matrix acts as a crucial foundation for evenly distributing the fibers throughout the structure. The resin matrix must have the physical properties necessary to improve the performance of fibers and be able to wet and penetrate the bundles of fibers that serve as the reinforcement, replacing any impurities that are coming from air spaces internally. Therefore, the matrix, reinforcing fibers, and interphase contents of PMC affect its mechanical and physicochemical properties. The PMC's fracture toughness, tensile strength, and stiffness are modified by the reinforcing fibers. Normally, the matrix completely encases the reinforcement, and it is the matrix that should be able to endure the aggressive environmental conditions when the composite is subjected to higher temperatures. The overall composite strength also deteriorates because of temperature on the interfacial area. Therefore, the qualities of composites that make them resistant to high temperatures are more closely tied to the matrix than to the reinforcement. This

implies that polymer matrix composites could only withstand service temperatures of around 300-350 °C. Moreover, polymer matrix composites frequently have higher specific strength and modulus than metal and ceramic matrix composites. The processing of polymer matrix composites is much easier and cheaper compared to that of metal and ceramic matrix composites. Moreover, they have low densities, good corrosion resistance, low thermal and electrical conductivities, translucence, and aesthetic color effects. However, the limitations of such polymer matrix composites are low service temperature, high thermal expansion coefficient, low fire performance, sensitivity to radiation and moisture, and material cost, which incorporates the total cost of each material inside the composite. Furthermore, polymer matrices are viscoelastic materials that are usually lacking in force and stiffness, and the reinforcement fiber ensures the strength of these types of composites [8].

Having said that, even though these types of renewable materials are promising for the environment, they are facing some challenging features. They may undergo, mechanical deterioration, thermal degradation, fungal decay, etc., which could be related to the unpredictable properties, moisture susceptibility, poor dimensional stability, low processing temperature, flammability, incompatibility of those polar natural fillers and nonpolar polymer matrices, and so on. The incompatibility between biomass and polymer matrix is the major drawback of these types of materials. The focus of my project is to find solutions to these kinds of problems. The compatibility of the filler and the matrix will improve the properties of the biocomposite material with the aid of various additives.

2.3 Lignocellulosic Biomass

Particulate biomasses are widely used in composite production for the modification of material properties. For an environmentally friendly approach, instead of using generalized particulate biomass, lignocellulosic biomas could be used, and organic wastes are one of the options for the use of biomass. Organic waste is considered biodegradable and could be obtained from either a plant or an animal. They have high levels of moisture content, around 80%. The biodegradability of these types of waste comes from breaking down into methane, carbon dioxide, and plain organic molecules. Food waste in landfills also contributes to nitrogen pollution, which results in dead zones and algae blooms. There is a wide variety of green waste involving food waste,

food-soiled paper, wood waste, pruning waste, and so forth. They could come as industrial, household as well as agricultural waste. As reported by the food and agriculture organization of the United States, one-third of all food produced worldwide is wasted [9].

There are different types of waste disposal methods, including landfill, recycling, composting, and incineration. Almost 70% of the waste is going to landfills, whereas only about 19% is recycled [9]. Throwing wastes into landfills and incinerating them are the most common methods for disposal due to low-cost alternatives in which the material will decompose anaerobically because of the absence of oxygen and induce biogas such as methane, carbon dioxide, and very small amounts of hydrogen and hydrogen sulfide. As a result of this methane formation, atmospheric concentrations of greenhouse gas emissions will increase and become more hazardous for the environment. If this condition continues, the amount of waste is expected to grow exponentially to 5.6 billion in 2050 [9]. Figure 2.1a depicts global waste consumption in percentage terms. Figure 2.1b depicts the total municipal solid waste material that is landfilled in 2018 as 146.1 million tons. As can be seen from the chart, food and plastics contain large amounts of waste than other materials.

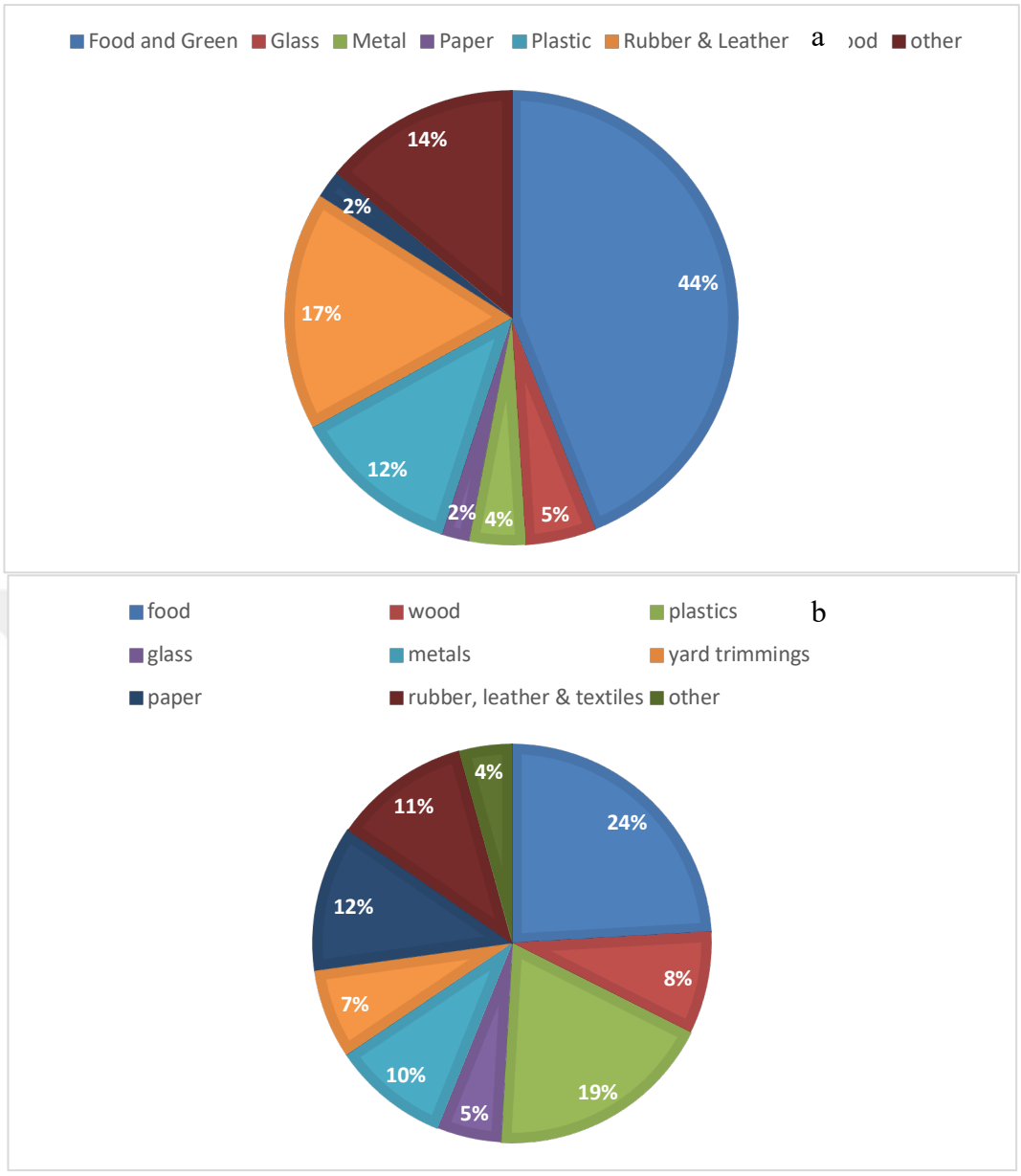

Figure 2.1 : a) Waste consumption b) Solid waste [9].

Food waste is a material that has been wasted after being consumed by people and is then discharged, evanished, degraded, or polluted. These types of waste represent 30% of the overall organic waste. The classification of food waste is divided as follows: food loss depicts food processing that causes loss in goods; unpreventable food losses occur while consuming it, such as fruit peel, core, leaves, and outer skin; and preventable wastes, which include edible foods yet loss happens during consumption [10]. There is no long-term solution for utilizing food waste. Nearly 50% of emissions come from food waste. The problem has many facets and a complex foundation. In USA, households account for most of the food waste. This is followed by occupations like restaurants, grocery stores, food services, and so on. If no changes are made in the

sector, solid waste-related emissions are predicted to rise to 2.8 billion tonnes of CO_2-equivalent per year by 2050 [9]. For this reason, the improvement of bio-composites from food waste could be the solution to sustainable food waste administration.

2.3.1 Chemical composition of lignocellulosic biomass

The chemical composition of organic wastes is already being used in the composite industry due to the commonly used wood plastic composites, which are similar in respect to the chemical structure of organic wastes. Wood itself is a composite material made of cellulose fibers and lignin. The lignin matrix links the fibers and provides the stiffness, whereas the cellulose fibers are relatively flexible but have higher tensile strength. It is thought that the hemicellulose included in natural fibers acts as a compatibilizer between cellulose and lignin.

The main constituents of biomass are cellulose (α-cellulose), hemicellulose, lignin, pectins and waxes. Their content varies with the use of diversified bimass. Cellulose is a linear chained organic polysaccharide formed from D-glucose monomer and it is the principal component that builds up the cell walls of natural products, whereas lignin is an organic binder for cellulose that puts stiffness, strength, and rigidity to the cell walls. The polymer structure of lignin is inordinate. In the structure of cellulose, hydroxyl groups link the linear chains to one another, which in turn holds the chains together. The hydroxyl groups make the cellulose structure hydrophilic by forming intramolecular hydrogen bonds inside the macromolecule, intramolecular hydrogen bonds with the other cellulose molecules and hydroxyl groups from the air as shown in figure 2.2. Therefore, biomass turn out to be naturally hydrophilic [11].

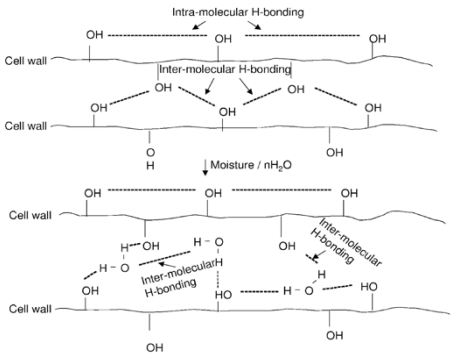

Figure 2.2 : Hydrogen bonding variations of lignocellulosic biomass [11].

When fibers are relatively longer, the number of celluloses increases much more with the increase in cellulose crystallinity and in the presence of hydroxyl groups, which

makes water an attractive material, which could cause swelling. The swelling due to the water absorption ends up with the voids in the interface of the composite material and lowers the mechanical strength.

2.3.2 Effect of particle size

The particle size of fillers has a huge impact on the final composite properties, particularly strength, since the incorporation of filler directly affects the stiffness of a material. It is usually known as "when the size of the particles decreases, strength increases [12]." This might be because finer particles are more likely to aggregate into larger particles at higher surface energy since they have a higher surface-to-volume ratio. Even though the finer particles tend to form agglomerates, the larger contact area in touch with the polymer matrix could increase the mechanical properties of the material. The factors that influence particulate filled composites are as follows; particle size, size distribution, aspect ratio, attrition during processing, fiber-matrix adhesion, stress transfer at the interface and mixing temperatures.

The physical and mechanical properties of composites are affected by the aspect ratio, length, and diameter of the fiber. Smaller particle size fillers are typically expected to have higher mechanical properties than larger ones. However, in some cases, bigger particle sizes could give higher mechanical properties only if they have a higher aspect ratio than the smaller ones, since a higher aspect ratio will result in better mechanical properties. On the other hand, a higher aspect ratio also increases the water absorption, melting viscosity and speeds up the biodegradation [13].

2.4 Organic Waste Reinforced Thermoplastic Biocomposites

One of the most urgent concerns facing humanity today is recovery from waste resources and non-renewable plastic consumption. This is a result of depleting resources and environmental problems [14]. Finding workable ways for producing novel materials with excellent performance, functional, and aesthetic attributes that may be employed in a variety of industries is the solution for not only manufacturing original materials but also contributing to a circular economy with an ethical point of view.

From the point of life cycle analysis, carbon footprint reduction would be positively affected if byproducts or wastes could be used as the matrix and the reinforcement.

There are a wide variety of bio fillers composed of agricultural wastes and natural fibers, including wheat straw, hemp, flax, coconut, sugarcane, banana, eggshell, hazelnut shell, and so on. The cost of food waste disposal and potential pollutant emissions are avoided by upcycling of food waste to make new biocomposites with novel physical and chemical properties. Food waste lowers the cost of biobased composites, provides for the new material's biodegradability and CO2 neutrality, and produces a biobased product that is distinct from the norm, such as biofuels or bioenergy [6]. Organic waste composites are becoming more popular in this sector due to factors including their widespread availability, renewable nature, biodegradability, affordability, low density, non-abrasive, strong and reduced risk of skin and respiratory irritation. Moreover, they are corrosion free, insect or rot resistant, paintable, and give a wood look without splinters. When compared to pristine plastic it gives high strength and stiffness, and high creep resistance, and it can be used in the same way as wood (cut, glued, and secured with the same screws, nails, or staples).

Even though these items are highly noticeable when they are first introduced to the market, not every customer segment may find them appealing. Customers who are more concerned about the environment would be of interest. Furthermore, such biomaterials are still facing some challenges. Biocomposite applications that proceed during the manufacturing process are slow in comparison with conventional composites due to the innate features of their subcomponents that make them unique. Furthermore, those distinct characteristics change as plants, climate, and seasons change [36]. The alteration of those conditions leads to an instability in the mechanical properties of the intended material. Therefore, there is no certain and valid data to be sure if the desired properties of those materials are obtained or not. To ensure consistency in bio products, companies should work with gatherers that provide almost the same harvested raw material that they gave as before.

Additionally, biomass such as agricultural wastes and natural fibers are incompatible with the polymer matrix due to the polar nature of biomass and the predominantly nonpolar structure of polymer matrices, eventuating weak interfacial adhesion between the filler and the matrix. The poor adhesion at the interface could deteriorate the material and hence result in poor mechanical properties. Therefore, to improve the compatibility of the filler and the matrix coupling agents and surface

modifications would be noteworthy. In addition, the polarity of those biomass leads to a hydrophilicity that makes them highly susceptible to moisture. Moisture absorption could arouse a failure by weakening the interfacial adhesion, alteration in dimensions, fungal or microbial decay, as well as hydrolytic cleavage by the addition of water molecules and hence depolymerization. As a result, their long-term implementations should be carefully monitored [15]. The amount of humidity in biomass is generally around 6-12 wt% and to be applicable for composites, it is required to lower them down to less than 3 wt% [36].

Apart from that, those natural materials are thermally unstable, which could result in a restricted processing temperature range. They generally cannot withstand temperatures above 220 C because their degradation temperature is between 150 and 220 C. The degradation and shrinkage of those biofillers chemically and physically deteriorate them, which could undermine the color change, recrystallization, hydrolysis, oxidation, depolymerization, and so on [36].

The literature has been reviewed for biomass filled polymer matrix composites [15-19]. In one article, Coffee grounds were pulverized to ensure uniform particle size distribution [16]. The mixing ratios of 10, 20, and 30% of coffee grounds were prepared with Homo-PP and Block-PP. Due to the existence of only propylene in Homo-PP, it gives a high degree of regularity and crystallinity whereas Block-PP exhibits a relatively lower crystalline polymer due to the additional ethylene polymerization into the propylene. Spent coffee grounds met the criteria of a handy composite with up to 30 wt% filler contents. In general, higher amounts of filler results in lower mechanical properties, however, the impact strength and young's modulus increased with the addition of higher amounts of spent coffee grounds in the Homo-PP. In another work, apricot kernel shells (AKS), hazelnut shells (HS), and pistachio shells (PS) were all ground into fine powder particles with dimensions of 300–425 mm and added from 0 wt% to 15 wt% to the polyester matrix to form a composite material. [17] Chemical analyses were used to evaluate the concentrations of cellulose, ash, humidity, and metal in these particles. The moisture content has changed with the changing ratio of cellulose, lignin, and hemicellulose. Overall, the compression strength, hardness, specific weight, and heat conductivity of the polyester were improved with the addition of reinforcement. A different article examined how alkaline treatment affected the thermal and mechanical characteristics of 5-30% macadamia nutshell-filled polypropylene composites [18]. The fibers were subjected

to an alkaline treatment and a compatibilizing agent (MAPP) was utilized to enhance the contact between the fiber and matrix. The findings suggested that bio-filled composites had a higher thermal resilience at higher temperatures illustrated by the deterioration peak. In comparison with the neat PP, the addition of raw and processed macadamia fibers increased the composites' stiffness together with the addition of a coupling agent. The results show that the more the filler the filler added to the matrix, the greater the stiffness and lower the impact strength will be. In a review of biocomposites, ground sunflower husk was added to polymer composites based on isotactic polypropylene in amounts of 10 and 20 wt% [19]. It has been demonstrated that the larger particle size of the filler being employed directly affects the rise in the composite stiffness at high temperatures. In the case of composites with larger filler content, a correlation between the filler's size and the degradation of tensile strength was shown. The morphological changes were assessed using SEM, the composites were analyzed for mechanical properties, thermomechanical properties, Vicat softening point VST, and heat deflection temperature HDT. Based on an examination of the surface topology of the injected composites, the resulting composites' quality was determined. A further study investigated waste polypropylene and sisal fiber were combined with 5%, 10%, 15%, and 20% fiber loading to create the biocomposite [20]. Based on the results of the characterization, the composite with a fiber content of 15% is thought to be the ideal ratio. By etching the surface of the composite with chromic acid and then treating it with stearic acid, the surface made the material hydrophobic. The FTIR and SEM images of the composites' unmodified and modified (superhydrophobic) surfaces, in both, make obvious the considerable differences in their distinct chemical compositions and surface structures. The self-cleaning and low wettability characteristics of the surface-modified biocomposite were used to determine its superhydrophobicity.

2.4.1 Processing

Technologies used in polymer processing involve chemical reactions, molding, compounding, and other procedures to transform monomers such as bio-based raw materials into finished goods. So, the processing occurs through heating/melting and shaping.

When manufacturing polymers, several additives and fillers may be added to enhance the desired material’s qualities [21]. While biopolymers have a lot of

promise and many benefits, they also have certain fewer desirable qualities or downsides as compared to traditional petroleum-based polymers. These can be overcome by improving the quality in accordance with the needs of certain applications. One way is blending, which greatly enhances the properties of biopolymers and is a reasonably quick, practical, compatible, and inexpensive process. If physical blending is involved, then basic compounding of polymeric components is done without any chemical reaction. Blending can be done with basic conventional equipment. In many instances, it has been found that polymers containing biomaterial blend interactions are insufficient. Co-polymerization, reactive modification, stepwise polymerization, grafting, and trans-esterification are further methods of processing to enhance the characteristics of biopolymers [22]. For compounding and mixing, the following polymer processing implementation could be done by, blenders, extruders, pulverizers, mills, and mixers. There are three different ways of shaping: melting, which can be used for injection molding, compression molding, melt spinning, blow molding, calendaring, or extrusion depending on the task at hand. Secondly, it can be shaped in a rubbery state by thermoforming and calendaring. Finally, it could also be shaped in a wet state where wet spinning, fiber spinning, spreading, and dipping could be applied with the aid of polymer solution. The mentioned polymer processing techniques are not always practical for large-scale production.

2.4.1.1 Extrusion processing

With the aid of pressure, extrusion is a continuous process where the polymer is forced to move inside the barrel and then through a shaped die. The pressure is generated from the action of screw rotation. The basic functions of an extruder are as follows: to transport polymer from hopper to die; to melt the polymer; to carry out mixing; and to generate homogeneous polymers. The machine is divided into three parts: the solid conveying zone (compaction, feed); the transition zone (melting); and the metering zone (melt pumping), as shown in figure 2.3. At the compaction zone, there is no melting; instead, it is used to get the polymer forward and push it inside into the barrel. The transition zone is where the polymer begins to melt, and the pumping zone is the final section of the machine where the polymer is transferred to the outside via pumping. As the screw rotates, it pushes the polymer through the barrel. From the beginning till the end, the diameter of the screw is increasing, thereby the channel

depth is decreasing, and pressure builds up, which induces the polymer to be pushed out of the die section. Table 2.1 depicts the temperatures of PP at different zones in the extruder.

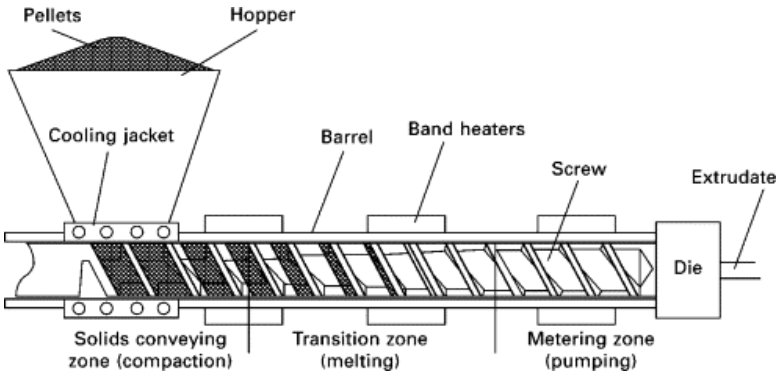

Figure 2.3 : Single-screw extruder [23].

Table 2.1 : Heating strategy of different zones in the extruder for PP.

Feed Zone (˚C)	Transition Zone (˚C)	Metering Zone (˚C)	Die Zone (˚C)
190	210	221	221

In biocomposite manufacturing, selecting the correct feeder for a specific material is crucial. Hence, ingredient properties such as flowability become an important factor for the success of the feeder in the extrusion process. For instance, pellets have good flowability, whereas powders have poor flowability characteristics. The poor flowable ones also have flooding features in which air is trapped in the powder particles and thereby the powder acts as a liquid [22]. Particles can be in the form of beads, pellets, chunks, crumbs, dust, flake, fiber, irregular shape, or granule crystalline. Particle size is also considerable from various viewpoints. As such, fine powders determine the flow and flood characteristics of the material. Fiber flowability changes with particle size, whereas pellets, granules, and irregulars are to determine the physical feeding features like clearance between tube and screw when choosing feeder size. Furthermore, ingredient properties such as bulk density, compressibility, angle of response, angle of slide, packing and compaction, and moisture content also affect the feed rates of the extrusion process.

Cellulosic material, which is a component of organic waste composites, contains water and produces water vapor bubbles. At the surface, bubbles could deteriorate the shape, which is not acceptable for a decorative site. If there are cavities in the massive part of the product, that would decrease its mechanical strength. Before

the extrusion process, the bio fillers needed to be dried to remove moisture from inside. The moisture content is preferred to be under 0.3%. If we are not considering decorative or mechanical problems, then we do not have to spend time preheating. Instead, degassing units could be used. Otherwise, if we feed a moist material directly, when the extrusion temperatures rise to 200 C, the vapor depolymerization might occur. Furthermore, the processing temperature should not exceed 200 C since bio fillers are thermally stable up to 200 C.

In this project, a lab-scale twin screw extruder has been used to process the desired materials. Twin screw extruders have better mixing characteristics, which gives the ability to compound additives. It has good feeding that can handle pellets, powder, and liquid forms of materials. The melting area is shorter in twin screw extruders; 14 is enough for melting, which indicates that it has more place to mix. Furthermore, it has good dispersion and distributive mixing.

2.4.1.2 Injection molding

In thermoplastic processing, injection molding is the most important technique for forming a material. Step by step, plastic granuels are melted, mixed and injected into molds. Depending on the shape of the item, different kinds of mold can be used. After feeding the polymer through a hopper and sending it to the barrel, the pressure of the barrel must be sufficient for a specific cavity pressure to meet pressure flow limits coming from the plasticator into the mold cavity. The materials are propelled toward the nozzle by a plunger inside the plasticator barrel, and while they do so, they melt due to a heating system around the barrel. The polymer is inserted between the surface of the barrel and the torpedo. Polymer is forced between and forms a film-like layer in the torpedo's midsection. At the end of the machinery, there is a nozzle tip through which the material readily comes out. In this capillary passage, homogeneous melting takes place. This kind of machinery has no function like mixing. The injection molding machinery is illustrated in figure 2.4.

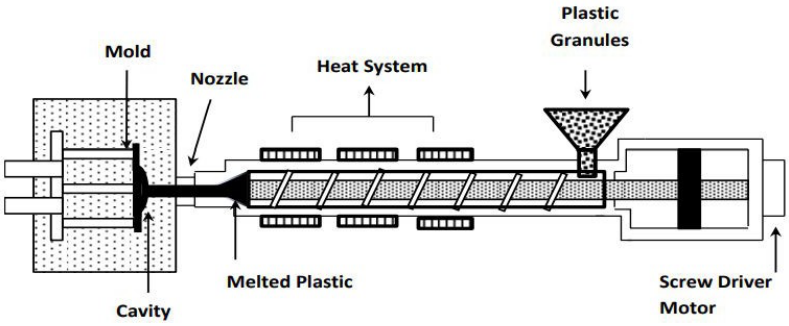

Figure 2.4 : Injection molding machinery [24].

There are numerous operational temperature and pressure configurations, each with a range of lower and upper bounds. improper temperature and pressure. Lower production quality results from improper pressures and temperatures. To illustrate, a melt temperature that is too low can leave a void that is not filled, also called a "short shot," whereas a melt temperature that is too high causes the material to degrade thermally. Low holding pressure can result in immoderate shrinkage, while high holding pressure can result in the flash phenomenon, which happens when pressure exceeds the clamping force of the machine and the melt flies across the mold separating lines. Figure 2.5 represents these complications by means of a pressure versus temperature diagram. Sink marks are a result of cooling-related material shrinkage. Process variables that generate non-symmetric stress concentrations throughout the part thickness are what cause deformations. Rapid cooling is primarily to blame for remaining tensions [25]. For large volumes of products, higher pressures are required to meet the needs of the material. 13 of the injection molding cycle belongs to the holding pressure (melt pressure) stage, which is crucial to preventing shrinkage problems.

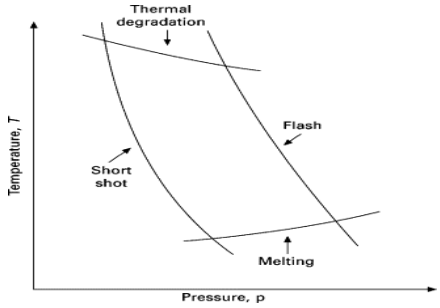

Figure 2.5 : The molding diagram [23].

Moreover, melt flow rate index (MFI) is also critical, which affects the cooling time and plasticizing (recovery). The simplicity of molding and high output rates is caused by high MFI. The cylinder temperature will be lower, and the surface finish will be adequate as the MFI increases, which will increase the production rate.

The benefits of this technique are as follows: good surface finishes, highly automated, high-quality parts at high rates, relatively low labor costs, and intricate shapes are possible. However, the machine and molds are very expensive because they require a lot of pieces to make the purchase worthwhile. Moreover, close monitoring of process parameters is required for high throughput and product quality.

2.4.2 Improving the properties of organic waste biocomposites

Natural filled polymer composites are economically preferred materials with a slight footprint on the environment and mechanical properties that are acquired if there is strong adhesion at the interface of the polymer matrix, which is related to wettability and the fillers, with proper dispersion of the filler into the matrix [26]. The efficacy of composite materials mainly depends on their capability to transfer stress from the polymer matrix towards the fillers. Due to the hydrophilic properties of natural fillers, it is a common problem that they face incompatible bonding with the polymer matrix, forming an inhomogeneous dispersion. Lack of stress transfer from the polymer matrix to the load-bearing natural fillers causes poor composite strength.

To enhance the adhesion at the interface of composites, various approaches can be applied. The various routes are as follows: adjustment of surface free energy, functionalization, roughness, as well as dispersion. Adjustment of the surface free energy of the filler could have an impact on the wetting capability and thus improve the adhesion to the polymer matrix [27]. Functionalization of the fillers increases the reactivity through the matrix and advances chemical coupling. For further reaction, involving coupling agents additionally inside the matrix could also be done. Mechanical interlocking can be obtained by monitoring the surface roughness. Finally, the dispersion of those fillers should be controlled to improve the specific surface area of the fillers.

In the case of functionalization, before the use of additives that contain grafting groups or different kinds of coupling agents, surface cleaning of the filler provides better access to the desired functional group [28]. The presence of these additives

is expected to considerably enhance the interfacial adhesion, providing a strong interfacial layer that changes the local stress distribution and thus contributes to the deformation and fracture mechanisms. The existence of impurities in the chemical structure of natural fillers, namely hemicellulose, lignin, oil, wax, and dust, reduces the accessibility of hydroxyl groups. Surface modification could improve surface wettability, water resistance, and allow accessible hydroxyl groups to create adhesion between the filler and the matrix. Surface modification techniques are divided into two categories: physical and chemical treatments. Physical treatments involve plasma treatment, corona treatment, ultrasound treatment, and ultraviolet treatment. Chemical treatments cover alkali, silane, acetylation, benzoylation, permanganate, peroxide, isocyanate treatments, acrylonitrile grafting, maleated coupling agents and so on. Coupling agents are compounds with dual purposes. The first one is aimed at reacting with the hydroxyl groups of natural fillers, whilst the latter is meant to react with the functional groups of the matrix, establishing a link of chemical linkages between the fiber and the matrix [29]. More than 40 coupling agents have been tried out and applied in research and manufacturing thus far [46]. These substances are divided into three groups: organic, inorganic, and organic-inorganic substances, with organic substances being superior to inorganic substances due to higher interfacial adhesion. Typically, anhydrides, fatty acids, isocyanates, organosilanes, and various short-chain compounds are the most frequently utilized coupling agents.

Compatibilizers: Compatibilizers are macromolecules used to ensure compatibility in the boundary layers between the filler and the polymer matrix. The most common compatibilizers are block and graft copolymers, which are considered physical compatibilizers, whereas the chemical compatibilizers are the ones that are in situ reactive. In reactive compatibilizers, generally one phase is modified with the placement of a chemical group along the backbone of the polymer chain. The newly introduced chemical group reacts across the interface with a chemical group in other phases and creates an anchor. In physical compatibility, on one hand, the molecule has more affinity for the polymer matrix, and on the other hand, it has more affinity for the filler. It needs to be migrated at the interface and create entanglement for interfacial adhesion. When choosing a compatibilizer, it needs to be fit into the anchoring criteria, which is the depth of penetration that the

compatibilizer achieves in each phase. Therefore, the compatibilizer's chemical and molecular structure, which refers to the placement of segments along the chain and molecular weight of each segment are the ones to be considered.

In high molecular weight compatibilizers, it could have better entanglement and anchoring with molecules on two sides. Hence, it could be more advantageous to use them, but it would be harder to get them to the interface because of the mobility of such long and high molecular weight molecules. Its mobility to move to that interface would be more difficult. Shorter or low molecular weight molecules have better molecular mobility to pass through and having that interface is much easier. If processing time is not that long, with the addition of a long compatibilizer, it won't take any time to get entangled due to the low molecular mobility. As a result, shorter molecules are more efficient due to the faster kinetics and could have better efficiency, although the entanglement of the longer one is more efficient. Yet, for proper anchoring, there needs to be an optimum length with respect to processing time. All these occur through increasing interfacial adhesion and interfacial interaction by reducing the interfacial tension between the filler and the continuous phase.

3. EXPERIMENTAL WORK

3.1 Materials Used

Polypropylene homopolymer was supplied from Borealis with a grade of HE125MO and had been with the features of good flowability and high stiffness of 1,550 MPa. The data sheet of this type of grade states that it had a density of 908 kg/m^3, a melt flow index at 230°C under 2,16 kg was 12 g/10 min, a melting temperature of 220-260°C, holding pressure of 200-500 bar and mold temperature 20-40°C with a high injection speed according to ISO 1873-2.

Compatibilizer was maleic anhydride-modified polypropylene (MAPP) polymers. Two compatibilizers were used in the study. One of them was Polybond 3200 brand, it had high a maleic anhydride content in a range of 0,8 to 1,2% and a melting point of 157°C. The other compatibilizer was Scona TPPP 8112 FA type BYK brand. The technical data sheet describes its properties as follows; the melt flow index at 190°C under 2,16 kg was higher than 80 g/10 min, and maleic anhydride content was 1.4% with a drying loss for 3 hours at 110°C was lower than 0.5%.

As reinforcements, 4 types of lignocellulosic biomass were used to investigate the properties of bio-composites. Apricot kernel shell (AKS), walnut shell (WS), hazelnut shell (HS), and corn cob (CC) supplied from Yelisan in the form of powder and the particle size of those powders are in the range of 0-255 μm.

3.2 Characterization of Biomass

3.2.1 Determination of hydroxyl content of lignocellulosic biomass

Determination was carried out according to ASTM D4274-21 and E222-17 standards. First acetic anhydride was distilled to obtain its purest form, then a 12,7% (v/v) solution in pyridine was prepared. Lignocellulosic biomass weighed 0,1 g and was acetylated with 31,75 ml of the solution determined by Büyükdere et al. [30]. The reaction was carried out at 98 °C for 2 hours. To terminate excess anhydride 30 ml distilled water was added to the reaction mixture. Once the reaction mixture cooled to room temperature it was titrated against 0,5 aqueous NaOH solution. For the titration, 0,1 ml phenolphthalein was added into the solution as an indicator. The spent amount of NaOH was reported, V_1. To obtain the blank NaOH amount, V_0, the method was

applied without using the biomass sample. Hydroxyl number and OH equivalent was determined using equations (2.1) and (2.2) [30].

$$OH\ Number = \frac{v_0 - v_1}{0{,}1\ g\ biomass} \times\ 0{,}5\ M\ NaOH\ \times\ 56{,}1\ g\ KOH \qquad [30] \quad (2.1)$$

$$OH\ equivalent\ (g\ equivalent^{-1}) = \frac{56\,000\ mg\ KOH}{OH\ number} \qquad [30] \quad (2.2)$$

3.2.2 Determination of chemical composition of lignocellulosic biomass

The chemical composition of lignocellulosic biomasses were determined by the method offered by Abebayehu et al. [20].

3.2.2.1 Estimation of the extractive content

The extractive volume in biomass solvent extraction was designated by mixing 300 ml of acetone with 5 g of biomass (A). The mixture was placed into a water bath to maintain a 90 °C temperature for 2 hours and vacuum filtration was applied. [20]. Thereafter, the sample was dried for 2 hours at 105–110°C in an oven to achieve a constant weight (B). The equation (2.3) identifies the extractive volume:

$$\text{Amount of extractive (g)} = A - B \qquad [20] \quad (2.3)$$

3.2.2.2 Estimation of the hemicellulose content

1 g of B was added to 150 ml of 0.5M NaOH solution and vacuum filtration was performed for 3,5 hours in an 80 °C water bath. For the removal of Na+, the sample was cleaned with deionized water and dried in an oven at 105–110 °C. The hemicellulose volume can be calculated by the equation (2.4):

$$\text{Amount of extractive (g)} = B - C \qquad [20] \quad (2.4)$$

3.2.2.3 Estimation of the lignin content

For 24 hours, 1 g of B was mixed with 30 ml of 98% H_2SO_4 and placed in the heating mantle. Then, the sample was heated to boiling for one hour on a heating mantle at a regulated temperature of 100 °C after being left at room temperature for 24 hours. The mixture was vacuum filtered, and the sediment part was thoroughly washed with distilled water until no sulfate ions were observed checking with aqueous 10% $BaCl_2$. The presence of sulfate ions can be understood from the precipitation of barium sulfate

as a white substance. The sample was then dried in an oven at 105°C and the amount of lignin was calculated as the total weight of the remnant shown by the equation (2.5):

$$\text{The amount of lignin (g)} = D \quad [20] \tag{2.5}$$

3.2.2.4 Estimation of the cellulose content

The amount of cellulose (E) in the sample can be determined by calculating the difference between the starting weight of the sample and the weights of the other three components calculated during the experiment and shown by the equation (2.6):

$$(A - B) + (B - C) + D + E = 1 \text{ g} \tag{2.6}$$

3.2.3 Surface modification of the biomass with esterification

Stearic acid (SA) was being used to modify the surface of the AKS powder. The modification method was appointed by Chun et al. [31] The ratio of AKS to SA was optimized by giving them different amounts. To find the most effective method, time, temperature, and ratios of AKS:SA was altered. First, 3 g of SA was dissolved in 10 ml of ethanol at 75°C, followed by the addition of AKS powder. The mixture was blended with a mechanical stirrer for 1 hour and immersed in it throughout the night or two nights in the water bath for an esterification reaction.

3.3 Compounding Process

To create polymer material with organic waste fillers, the fillers are first dried in the oven for 4 hours at 80°C and then pre-mixed manually with the polymer. After pre-drying the bio fillers, moisture content was analyzed at 100°C for 10 minutes with a moisture analyzer, Mettler Toledo Hg63 Halogen. A laboratory-size twin screw extruder prism 24l/D was used for the melt compounding. The gravimetric feeders that would be used in this procedure were first calibrated. Based on a review of the literature. the barrel temperature parameters that were suitable for the polymerization process were chosen [32]. Tables 3.1 display the barrel temperatures that were employed during the testing based on the various types of polymers. The screw speed used during the compounding stage was 16 rpm, and the continuous strands were then chopped into 2-3 mm pellets using a four-blade saw.

Table 3.1 : Barrel temperatures of PP for extrusion compounding.

Temperatures (˚C)	Feeder 1	2	3	Sections 4	5	6	7	Die
Set	70	175	180	185	190	190	185	180
Melt						204		

Following that, the plastic components that had been compounded in the extruder and then they were injected molded to create the test samples. After extrusion, biocomposites were chopped to small chips with an average diameter of 2 mm and the length of 2 to 3 mm. Then the granules were oven dried for 4-hour at 80 °C.

The Arburg Allrounder 320˚C injection machine was used to perform the injection process. For the injection processing the pressure of injection for biocomposite were set at and 800 bar initially. There are 3 steps of injection pressure, the pressure is continuously increasing by starting at 22 ccm meaning until 22 ccm the injection speed stays at 800 bar. Then from 22 ccm to 12 ccm the injection speed increased to 810 bars. In the third step, when injection lowers from 12 ccm to 6 ccm the injection speed increased to 820 bars. Then the material goes into holding part of the machinery. Since the holding pressure should be higher than injection pressure it was set to 850 bar for 4 seconds. The barrel temperatures were between 180 and 190 °C. The mold temperature was 40 °C with an injection speed of 85 ccm (cm^3/s).

The formulations were prepared for lignocellulosic biomass-filled polypropylene biocomposites. The biocomposites were prepared using mass proportions of 5, 10, 15 and 20%. Also, another biocomposite was prepared using 20% biomass and 2% MAPP with Borealis PP. The study continued with Sumitomo PP and the formulations was repeated with uncompatibilized biocomposites and 5%, 10% and 20% biomass filled 2% MAPP compatibilized biocomposites were added. The percentages of the biomass and the use of compatibilizer were arranged to observe the change in mechanical and thermal properties in polypropylene-based biocomposites.

3.4 Physical Tests

3.4.1 Density Measurement

The density of the samples was measured by Archimed's principle: a body submerged in liquid would appear to lose weight in proportion to the weight of the liquid it displaces. This straightforward idea allows for the straightforward gravimetric measurement of density using a laboratory balance. The weigh of the sample scaled in

the air first, then the sample was put into alcohol and weighed. The difference between the weights were taken as a result.

3.4.2 Melt flow index

The Zwick 4106 tester was used to determine the material flowability. Tests are conducted at predefined weights and temperatures. The standard for this test was ISO 1183. With the aid of the pusher, the polymer that had melted in the chamber pours out of the mold. The device creates samples by cutting the flowing polymer at times determined by the operator. The weights of these samples are quantified. The amount of material flowing in 10 minutes was measured by the melt flow index, which was computed as in (2.7) where W was average sample weight (g), and t was cutting time (s).

$$Melt\ Flow\ Index\ (MFI) = \frac{W \times 600\ s}{t} \tag{2.7}$$

3.4.3 Ash content

The identification of mechanical properties of a material was influenced by the presence of inorganics. The ash test was used to establish the inorganic content of plastic materials. A microwave ash oven was used to burn the material at temperatures between 600 °C and 900 °C to determine the ratio of additives in the material for 1 hour with ISO 3451/1 method. The sample weights are measured both before and after heating, and the additive content was determined.

3.5 Mechanical Tests

3.5.1 Tensile strength

A tensile test was a mechanical test in which the specimens are exposed to a controlled tensile load until failure. The samples are stored at 23 °C for 48 hours after the injection procedure in preparation for the tensile test. The Zwick Z020 tester was used to draw tensile samples at a rate of 5 mm/min at 23 °C with a standard ISO 527 standard. The thickness of dog bone shaped samples were measured 4 mm ± 0,2 mm while the gage width were measured 12,5 mm ± 0,25 mm [33]. Figure 3.1 illustrates the dog bone shaped test specimen for tensile test.

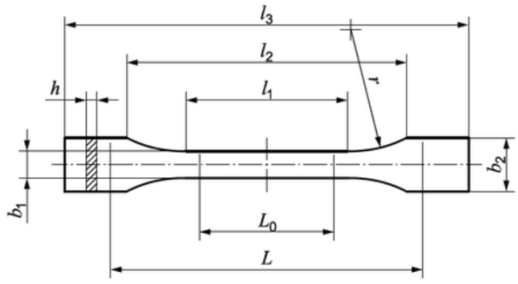

Figure 3.1 : Test specimen for tensile test mm [33].

3.5.2 Flexural strength

The bending strengths of the materials are determined by a 3-point bending test using the Instron 4505 tester. The specimens, whose force (F) and length of the carrying span (L) were divided into two with the materials' width (w) and thickness (h), were measured in each formula below in equation (2.8). According to the ISO 178 standard, the flexural modulus (E_{flex}) depicted by the equation (2.9) was the ratio of stress to strain during flexural deformation, where d represents the deflection beam in equation 2.9. It was subjected to a 3-point bending test at 23°C, under a 5 kN load, at a speed of 1 mm/min.

$$\sigma_{bend} = \frac{3\,F\,L}{2\,w\,h^2} \qquad \text{[33]. (2.8)}$$

$$E_{flex} = \frac{L^3 F}{4wh^3 d} \qquad \text{[33]. (2.9)}$$

3.5.3 Notched Izod Impact Strength

Injection-made impact samples that are 4 mm x 10 mm x 80 mm are also stored at 23 °C for 48 hours, and the width and thickness of these samples are measured to determine the cross-sectional area. The notching tool was then used to open the 2 mm notches. The samples are shattered when they are inserted into the impact test equipment with the notched surface facing the weight.

3.6 Thermal Tests

3.6.1 Thermogravimetric analysis (TGA)

Thermal analysis was conducted by TGA using a TA Instrument Q550 analyzer to determine the characteristic degradation temperatures and mass losses at temperatures of biomass and biocomposite samples.10 mg samples were taken and heated from room temperature to 950 °C at a rate of 10 °C/min in a nitrogen atmosphere.

3.6.2 Differential Scanning Calorimetry (DSC)

Differential scanning calorimetry analysis was another thermal analysis to establish the transition temperatures and enthalpies of each material. The ramp (heating rate) of the materials was from 20°C to 300°C at a rate of 10 °C/min using the TA DSC250 Discovery. The sequence of the heating program are as follows: isothermal 2min, ramp 10°C/min to 300°C, isothermal 2 min, ramp 10°C/min to 20°C, isothermal 2 min, ramp 10°C/min to 300°C, isothermal 2 min, ramp 10°C/min to 20°C and isothermal 1 min. Melting temperature, T_m, heat of fusion, ΔH_m, and degree of crystallinity, X_c, were calculated using the first heating cycle. The degree of crystallinity could be evaluated from the formula depicted as (2.10):

$$X_c = \frac{\Delta H_f}{\Delta H_f^0} \times 100 \qquad \text{[34] (2.10)}$$

The heat of fusion, ΔH_f, was obtained by integration of the melting signal of the first heating run of biocomposites, while ΔH_f^0=207 J/g was heat of fusion belonging to 100% crystalline PP which was obtained from the literature [34].

3.7 FTIR-ATR Spectroscopy

Fourier transform infrared (FTIR) analysis was performed with Bruker Tensor 27 along with platinum high refractive index attenuated total reflectance (ATR) apparatus. FTIR was used to identify the different chemical bonds between the unmodified and modified AKS. The specimens were captured using 16 scans with a resolution of 4 cm^{-1} and wavelengths between 4000-500 cm-1.

3.8 Rheology

The melt rheology of the materials was tested by using a Göttfert Werkstoff-Prüfmaschinen capillary rheometer model RG25 at constant piston speed ranging from 0.0036 to 0.9 mm/s. The entrance angle of the material was 90°. After a 30-minute

residence period, the material was inserted into the extrusion chamber's barrel and pushed down through the capillary with a piston. The temperature was set to 200°C. The power law equation was commonly used to determine the viscous flow behavior of non-newtonian fluids as depicted in the equation (2.11) below.

$$\tau(\gamma) = A \cdot \dot{\gamma}^{n} \qquad [81]\ (2.11)$$

Where τ = shear stress, $\dot{\gamma}$ = shear rate, A = consistency factor, and n = flow index. When n < 1, it was called pseudoplastic fluid (shear thinning); when n > 1 it was called dilatant fluid (shear thickening), and when n=1 it was called Newtonian fluid. Flow index was determined by regression analysis of shear rate-shear stress data.

4. RESULT AND DISCUSSION

4.1 Characterization of Biomass

This chapter focused on the differences among different kinds of biomass (namely AKS, HS, WS, and CC) using spectral (FTIR) and thermal methods (TGA and DSC).

The physical appearance of the biowastes (Figure 4.1) was different according to the source. However, they were all fine powders with a particle size of 0-200 µm. Prior to compounding, the moisture content of biomass should be lower than 3% for the process, therefore, it was ensured that all biomasses had lower than 2,5% moisture content. To characterize the lignocellulosic biomass, chemical and elemental analyses were previously performed.

(a) (b) (c) (d)

Figure 4.1 : Waste biomass sources a) AKS b) HS c) WS d) CC [42].

The major constituents of this biomass, which are cellulose, hemicellulose, lignin, and waxes, may be subdivided into two parts: cellulosic and non-cellulosic constituents. The cellulosic part is the hydrophilic section and holds the whole structure together by forming intra- and intermolecular hydrogen bonds through hydroxyl groups themselves and other cellulose chains, respectively. The existing hydroxyl groups in the macromolecule could also form bonds with the hydroxyl groups of air, which could be irrelevant during the reaction. Hence, they are also called reactive hydroxyl groups. Non-cellulosic parts of the structure have poor binding ability, meaning they could be effortlessly removed from the polymer structure by chemical or mechanical treatments. They are also called impurities because they create irregularities at the surface of the biomass that reduce the accessibility of hydroxyl groups. Some of the impurities are hemicellulose, oil, wax, and dust. In our case, oil, wax, and dust become impurities.

The characterization of biomass and its chemical composition were important factors. All the mentioned components of the biomass contain hydroxyl groups as active sites in their chemical structures. However, the behavior characteristics of those hydroxyl groups are slightly different from one another. Lignin was a stiff material due to its highly branched, resin-like structure via linkages of aliphatic and aromatic OHs and double bonds, leading to forceful intra- and intermolecular bonding. Cellulose also had naturally formed intra- and intermolecular H-bonding among hydroxyl groups. This bonding ability could create agglomeration among biomass particles during biocomposite manufacturing. Lignin had both polar and non-polar groups inside its structure, whereas cellulose had the most hydrophilic content inside. Therefore, the highly hydrophilic structure of cellulose would create a greater problem by forming an agglomerated appearance inside the polymer matrix. These differences would change the mechanical and thermal properties of the biocomposites. Therefore, the chemical composition of biomasses was determined by the following method: Since the binding site of the biomass will be hydroxyl groups, the amount was also calculated. The differences will affect the interfacial compatibility between the biomass and polymer matrix. It is expected to have better mechanical and thermal properties in high-lignin biomasses.

4.1.1 Determination of chemical composition of lignocellulosic biomass

The main difference among different parts of a plant is mainly regarding the proportion of the components, i.e., the stem of the plant contains a higher amount of cellulose compared to the leaves (higher lignin) or the fruit (higher pectic polysaccharides). Thus, the main constituent may differ in terms of the proportion among similar parts of different materials. The chemical composition of lignocellulosic biomass was also affected by growing region, climate, health status, and type of the source. Therefore, the biomass content, including cellulose, hemicellulose and lignin may vary as a natural source [20].

The differences might lead to different responses during and after production of biocomposite. To find the chemical structure and percent mass of the extractives, lignin, hemicellulose and cellulose inside the biomass, several experiments done. Due to the percent differences in chemical composition changes the compatibility between the biomass and PP matrix. Lignin is inherently hydrophobic whereas cellulose more

dominant with its hydrophilicity. Results were given in Table 4.1. As seen from the table, the major component was lignin for the shells and cellulose for CC. The results were consistent with the literature which used the same materials; however, small deviations were acceptable due to sources [14, 35–37]. Nut shell including fruit stones generally have higher lignin content when compared to biomasses like CC [37]. However, among all the highest lignin content was belong to AKS which was also true for Çelik et al. [38].

Table 4.1 : Chemical composition of lignocellulosic biomass in percent.

Samples	Extractives (%)	Lignin (%)	Hemicellulose (%)	Cellulose (%)
AKS	11	48	17	24
HS	18	40	14	28
WS	11	35	24	30
CC	15	15	30	40

4.1.2 Determination of hydroxyl content of lignocellulosic biomass

The number of available hydroxyl groups in biomass may vary. The portions of cellulose, hemicellulose, and lignin are different from each other, which will affect the binding sites of the reinforcement. Here, the number of available binding sites for each biomass was investigated. Thereafter, chemical analysis was done to determine the number of extractives, hemicellulose, lignin, and cellulose compositions. The amount of KOH needed to neutralize the acetic acid that had been absorbed after acetylating 1 gram of a chemical compound that contains free hydroxyl groups was known as the "hydroxyl value" in analytical chemistry. The typical analytical procedure for calculating hydroxyl value entails acetylating the material's free and accessible hydroxyl groups using acetic anhydride in pyridine solution. The residual unreacted acetic anhydride was terminated by adding water and converting to acetic acid when the reaction was complete, and the amount is then determined by back titration using an adjusted NaOH solution.

The OH content of the biomass will determine the compatibility of the biomass and the polymer matrix. The hydroxyl number defines the available binding sites in the biomass. If biomass is not compatible with the polymer matrix, those hydroxyl groups could be manipulated by different methods, such as surface modification. Therefore, it is important to know the hydroxyl number of the biomass. When comparing the

results, WS had the highest OH number, followed by CC, HS, and AKS. The large number of sites will get sanitized with the aid of SA.

The results of the hydroxyl contents of the biomasses are listed in Table 4.2. As indicated in the table, the highest OH number belonged to WS, followed by CC. WS had both higher in cellulose, hemicellulose and lignin. The high percentage of these substances could result in high OH content. The occurrence in CC could be related to its high cellulose and hemicellulose content. As cellulose was more hydrophilic compared to lignin, which was higher in proportion for AKS, HS, and WS, CC would have a higher level of accessible, free, and reactive OH groups. This result was also supported by the high OH number of WS, which had the highest cellulose content among other biomass samples.

Table 4.2 : Hydroxyl contents of lignocellulosic biomass.

Samples	OH Number	OH equivalent
AKS	280	200
HS	841	66
WS	2889	19
CC	1318	42

4.1.3 Characterization of lignocellulosic biomass (FTIR-TGA-DSC)

After determining the chemical composition of lignocellulosic biomass, the resultant samples were confirmed by FTIR spectra in AKS. Figure 4.1 shows the samples that formed after the determination of chemical composition, in which B stands for acetone-treated AKS, C stands for hemicellulose, and D is the lignin part inside the AKS.

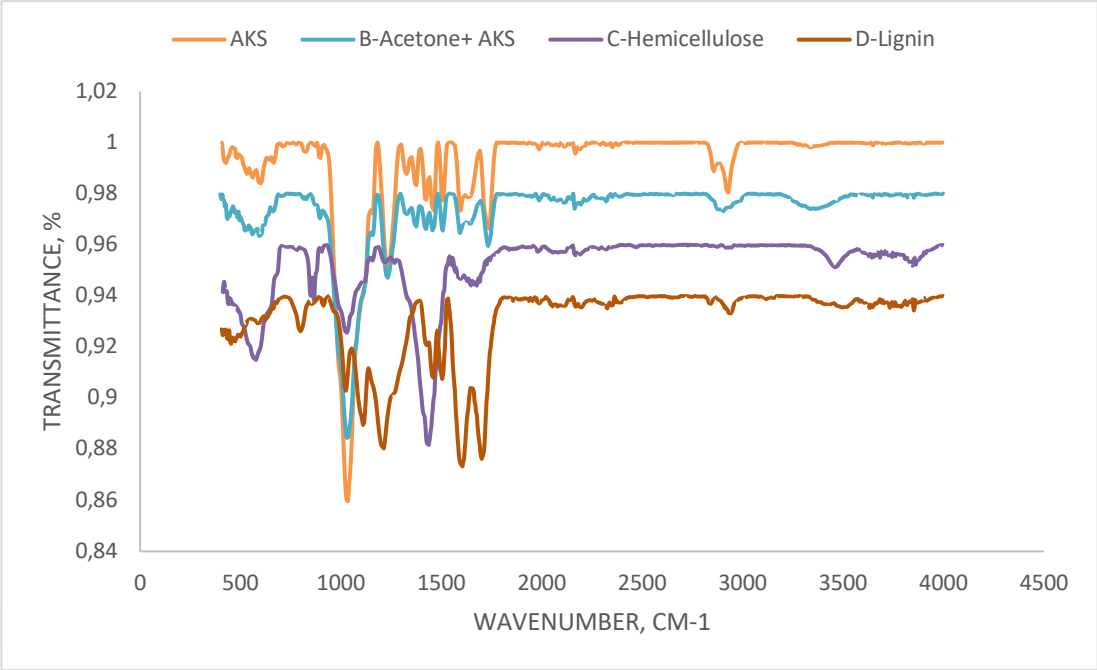

Figure 4.2 : Determination of chemical composition of AKS illustrated by FTIR spectra.

For the determination of chemical composition, one of the biomasses was chosen to investigate its FTIR spectrum. AKS was examined because later, surface modification will be applied to this biomass. The constituents of this biomass, including acetone and AKS, hemicellulose, and lignin, contain esters at 1750–1735 cm^{-1} as C=O carbonyl stretching, alkene at 1680–1640 cm^{-1} as C=C, ketone at 1715 cm^{-1} as C=O carbonyl stretching, alcohol, and oxygen-bonded groups in the spectra illustrated with OH at 3400–3200 cm^{-1}, C=O stretching at 1765–1715 cm^{-1} of hemicellulose from ketone, aliphatic groups, and carbonyl groups. The C=O stretching peak could also come from ester carbonyl stretching of extractives for the acetone AKS spectrum. C-O-C asymmetric stretching of cellulose at 1270 cm^{-1} and C-O-H at 1050 cm^{-1}. C-O-C also exists in lignin as an ether bond. There were also distinctive peaks to illustrate the differences among them. For instance, cellulose had the largest peaks of OH and C-O whereas hemicellulose had a larger C=O peak. The complex structure of lignin was expected to have methoxyl-O-CH3, stretching of C-O-C and aromatic C=C groups in it [39]. The characteristic peak of lignin is at 1510 cm^{-1} which designates aromatic skeletal vibrations, and aromatic ring vibrations are at 1590 cm^{-1} [40]. C-O stretching of lignin is at 1245 cm^{-1} [41].

The variant peak numbers were at 2924 cm^{-1}, which was less sharp in the case of CC which was indicating methyl and methylene groups [30].

Under the signals of 1800 cm^{-1} the bending vibrations of the biomasses are defined, and those vibrations come from adjacent neighboring groups of the molecular structure. Moreover, due to the structural differences of biomass the peak at 1732 cm^{-1} occurred in a different shape. The peak was coming from C=O stretching vibration of hemicellulose. At 1643 cm1, the water content inside the biomass may have created the differences among them. There was also a different view at the 1145 cm^{-1} peak, which was attributed to 4-O-methylglukuronoksilane [42].

Finally, the distinctive difference occurred at 1037 cm^{-1} which was due to the stretching of the C-OH molecule that was coming from cellulose and hemicellulose. At this peak, CC has high hemicellulose and cellulose content, and the peak appears as the strongest one among all

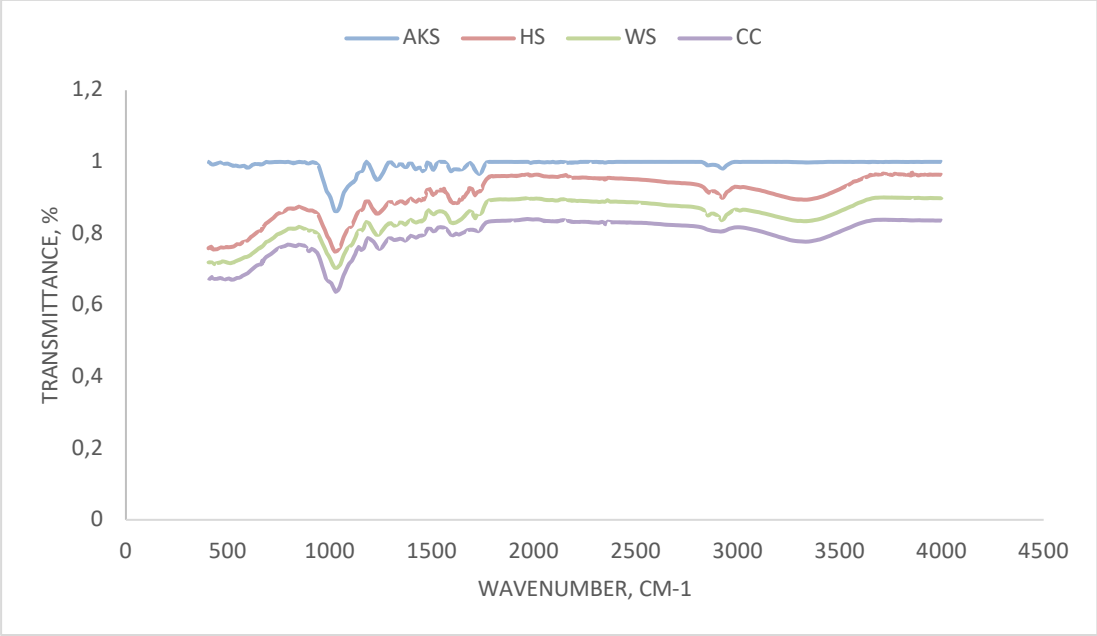

Figure 4.3 : FTIR spectra of AKS, HS, WS and CC.

Table 4.3 illustrates the characteristic FTIR spectrum peaks of AKS powder. The FTIR spectrum of AKS was particularly investigated. The following explains the surface modification of AKS: The hydroxyl groups (-OH) of AKS were referred to as the broad peak at 3344 cm^{-1} for cellulose, hemicellulose, and lignin. The C-H stretches belong to the 2924 $cm^{-1}$and 2864 cm^{-1} peaks. The wavelength number of C=O stretching

occurred at an intensity of 1732 cm^{-1}. The absorption peak of the carboxyl group (C=O) indicates the stretching of the ester bond or acetyl group that exists in hemicellulose [31]. This peak is also related to aldehydic groups that exist in the structure of lignin [15]. The peak intensity of CC at 1732 cm^{-1} is smaller than that of other biomasses, which is due to the lower amount of lignin. The peak at 1631 cm^{-1}could be related to the H_2O bending [17]. The peak intensity at this wavelength is higher than that of other biomasses, which is due to the high lignin content of AKS. At 1594 cm^{-1} the aromatic ring of lignin made C=C stretching possible. From 1422 cm^{-1} to 500 cm^{-1} C-C-H, C-O-C, C-C-O bending and C-C, C-O stretching vibrations were observed [43].

Table 4.3 : Characteristic FTIR spectrum peaks of AKS.

Wavelength (cm^{-1})	Chemical Bond
3344	-OH
2924-2864	C-H stretching
1732	C=O stretching
1594	C=C stretching from lignin
1615-1631	H2O molecules
1422-500	C-C-H, C-O-C, C-C-O bending, C-O stretching

Figure 4.3 compares the FTIR data of several biomass resources. The study of the biomass resources found that they all had similar peaks with slightly different intensities. The following is a summary of the major peaks seen in the chemical composition of the biomass. The broad peak seen around 3300 cm^{-1} belongs to the stretching of -OH in the molecules of lignin and cellulose. At 2924 cm^{-1} and 2854 cm^{-1} was the asymmetric stretching of C-H bonds began. However, in the structure of lignin, these two peaks belong to aromatic methoxyl groups and the side chain's methyl and methylene groups [44]. The peak intensity of these two peaks was higher in AKS, HS, and WS due to the existence of a large amount of lignin inside the molecular structure. The lignin inside the CC is much lower than that in the other biomasses, and hence these two peaks appear less distinct. The peak at 1732 cm^{-1} defines the C=O stretching, and the peak at 1600 cm^{-1} shows the C=C stretching of lignin [44]. The peaks at 1600 cm^{-1} 1515 cm^{-1} and 1426 cm^{-1} depicts the aromatic skeleton vibrations, and 1462 cm^{-1} showed the aromatic ring vibration of lignin [44]. The peak intensities varied at that wavelength: AKS was at 1594 cm^{-1}, HS occurred at

1612 cm^{-1}, WS was at 1608 cm^{-1}, CC was at 1632 cm^{-1} and 1601 cm^{-1}. At 1370–1375 cm^{-1} phenolic hydroxyl and aliphatic C–H methyl groups appeared, which also came from the structure of lignin itself. The existence of aromatic groups in the structure of lignin made these peaks distinguishable. From 1422 cm^{-1} to 500 cm^{-1}, C-C-H, C-O-C, and C-C-O bending and C-C, C-O stretching vibrations were observed [42]. The location of the 1267 cm^{-1} peak is also changing with the biomass type. This peak defines the C-OH in a plane and when there is a change in crystal structure of cellulose, or the crystal structure is different from one another the location of the peak changes [15]. The peak appeared in AKS at 1232 cm^{-1}, HS at 1231 cm^{-1}, WS at 1233 cm^{-1} and CC at 1240 cm^{-1}. These peaks could be attributed to the crystal structure of cellulose 1. However, there was one additional peak in CC, which was at 1159 cm^{-1} , this may have come from another cellulosic structure called cellulose 2 [45]. The largest peak occurred at 1031 cm^{-1} in CC. This is due to the lower lignin content inside the molecular structure of CC. This peak defines the stretching of hemicellulose and cellulose functional groups [15]. Overall, the structure of lignin differentiated itself by phenolic, aliphatic Oh, meO, double bond and aliphatic bonds.

The chemical composition of hemicellulose was extremely connected to the kind of biomass that is comprised of a sugar part, which comes from β-(1◊4) which the linearpart,t and several kinds of branched ones connected in various routes to the linear chain [46]. At 1512 cm^{-1} the peak intensity of CC is lower than other ones, whereas the signal at 1050 cm^{-1} is more intense [30]. This is because, as depicted in the content analysis above, the amount of lignin was lower than other ones, while the amount of cellulose was higher for CC.

As a result of the spectroscopic FTIR data, signals were seen that came from the structure of lignin and cellulose. The molecular structures of cellulose and hemicellulose are similar. However, the aromatic ring of phenyl units in the structure of lignin changes the characteristic peaks. Some of the peaks were more distinct. Therefore, it was determined that the difference between the spectra was mainly due to the ratios of lignin and cellulose inside the biomass.

The following part investigates the thermal behavior of biomasses by TGA and DSC analysis. Thermogravimetric analysis, also called thermal gravimetry, is the subtype

of thermal analysis that determines the physical and chemical properties of materials during heating and cooling. Thermal energy transfers into a material sample.

The keystone of TGA is that the sample is heated and mass change occurs. This mass change could be beneficial for examining the composition or thermal stability of the material up to 1000 °C. Typically, a sample loses weight when heated due to reduction, evaporation, or decomposition. Likewise, it could gain weight due to oxidation or absorption. Temperatures can be monitored with a thermocouple. To form an equilibrium phase, changes in internal energy due to chemical reactions or phase transformations could be examined. There was a dynamic process in time and temperature, thereby making it kinetically related. It determines synthesis, temperature, and duration during mass change. In short, TGA measures mass change as a function of temperature or time. Thermal decomposition with the formation of gaseous reaction products, corrosion, metal oxidation (formation of non-volatile oxides), combustion of carbon black on gas switching, multi-step decomposition, and explosive decomposition with recoil effect are examples of TGA chemical reactions. Many gravimetric effects are not related to chemical reactions or melting. For instance, dehydration, desorption of other substances (solvent residues or monomers), sublimation of lower molecular weight organic compounds, evaporation, oxidation, reduction, vaporization, and absorption The TG curve could alter with changes in sample mass, volume, shape, sample holder, atmosphere pressure, and scanning rate. The vertical axis represents percent mass change, whereas the horizontal axis depicts temperature or time. From the graph, TGA gives a continuous weighing of the sample in a controlled atmosphere.

Polymer degradation could be seen in three different ways: random scission, systematic chain scission, or the junction of two. Random fusion could happen with the radicals or reactive products, and they could become volatile by breaking into small pieces, or they could attack other chains, which could result in cross-linking. They had less capability to degrade, which could induce high-temperature residue. TGA gives information about the loss of volatile parts of polymers caused by decomposition. However, it cannot analyze the chemical changes and degradation properties given by cross-linking. TGA could support the polymers through the determination of their thermal stability, compositional analysis, and identification of their unique decomposition patterns. Moreover, the representation of TGA could be used to

designate the kinetics of the thermal decomposition of polymers and curing processes such as condensation polymerization.

Materials for TGA analysis are as follows: thermogravimetric analyzer, pure and dry nitrogen gas with low pressure, cooling spare for below room temperature searches, 0.0001 gram balance measurement. The specimens should not contain any impurities such as monomers, water, or solvents.

Firstly, the temperature and heat calibration samples should be loaded into the sample holder. Afterward, the temperature range should be set and the temperature controller should be operated. Later, a data acquisition system should be set up, and, with the help of a data analysis system, a graph can be interpreted.

Thermogravimetric analyses were also performed on biomass samples to investigate thermal behavior. TGA is a method based on the measurement of mass loss with heat. The pyrolysis of ingredients including cellulose, hemicellulose, and lignin is expected to be predicted from the TGA curve since all biomass contains those constituents.

In the literature review, the pyrolysis characteristics by TG/DTG analysis divide the curve into three parts: mass loss of water (25–250 °C), rapid pyrolysis (250–410 °C), and slow decomposition, also called carbonization (410–900 °C) [38,47,48].

The water loss peak appears at T 100 °C, and the loss may both come from the physical and chemical adsorption of water molecules. Concurrently, the chemically unstable structure of hemicellulose starts to decompose. The mass loss at this temperature range is usually between 2% and 10%. Rapid pyrolysis shows itself as the most distinctive mass loss at 300–350 °C in the curve. In this part of decomposition, hemicellulose completely detaches from cellulose at 300 °C, and cellulose starts to lose mass at 350 °C. Up until this part, 80% of the biomass thermally decomposes. At slow decomposition step 5% of the biomass decomposes with residue. Table 4.4 showed the mass loss steps of four types of lignocellulosic biomass, which were obtained from the TGA curve.

Table 4.4 : Mass loss steps of biomass waste derived from TGA curve.

Sample	T100 (˚C)	T200 (˚C)	Tmax (˚C)	T950 (˚C)	Total mass loss
AKS	5,3	7,3	72,29	4,5	89,39
HS	3,6	5,1	66,49	5,9	81,12
WS	2	3,2	71,91	4,9	82,01
CC	3,2	4,8	73,71	3,5	85,21

It is known that hemicellulose easily and quickly decomposes at around 180–325 °C due to the existence of short side chains and its branching and amorphous structure [49]. The TG/DTG curve shows that the decomposition started at around 180˚C. The hemicellulosic parts decompose earlier in AKS, HS, and WS the peak became larger and distinct at 190˚C whereas CC had a later decomposition at 220˚C and the ongoing decomposition peak for hemicellulose was larger than the other biomasses which also confirmed by the 30% hemicellulose content of CC. The second largest peak between in the range of hemicellulose decomposition was belong to AKS. However, the hemicellulose content appeared to be lowest among the biomasses by 17% which was not coherent with the TG/DTG curve.

The secondary ingredient to decompose was cellulose, which is around 300–400 °C. Since cellulose had a longer linear chain and a higher molecular weight than hemicelluloses, it had higher thermal stability [50]. A portion of cellulose also possessed a crystalline structure composed of organized microfibrils [49]. At the decomposition temperature of cellulose, the largest decomposition occurred at CC, which was also predicted from the chemical composition in which the cellulose content was highest of all. Therefore, the chemical composition of CC confirmed this result.

Finally, the decomposition of lignin continues throughout the entire temperature range from the beginning (280 ˚C) until 950 °C because the complex molecular structure and aromatic rings with branches make decomposition more difficult [50,51]. The highest rate of decomposition in lignin occurs at 350˚C and 450˚C. The amorphous structure of lignin is analysed by FTIR spectra. The complex structure of lignin gradually decomposes over a large temperature range and is primarily responsible for the synthesis of biochar. This was because lignin contains benzene rings, which indicate the portion of the polymer with higher carbon levels, as also confirmed by FTIR spectra [49]. Cellulose, hemicellulose, and lignin were each distinguished by diverse chemical structures and bond couplings that affected their thermal stabilities. Therefore, the structural differences among them caused these kinds of behaviors. The

phenolic part of the lignin decomposes over the non-phenolic units. Therefore, lignin decomposes in a wide temperature range. In the temperature range of 350˚C and 500˚C, greatest mass loss expected to occur in highest lignin content biomass. This range is also called the ‘’second combustion step’’, which comes after the first combustion step (250˚C and 350˚C) which is usually correlated with the amount of lignin [52].

The mass loss at this second combustion range was highest in AKS, the results of HS and WS were similar to each other and came in the latter; and CC was the lowest, which was also correlated with the amount of lignin inside the biomasses. Therefore, the chemical composition confirmed this result. The Tmax in the DTG curve occurred between 350˚C and 450˚C for AKS, HS, and WS. However, the Tmax value for CC was earlier than 350˚C. Since the largest decomposition of lignin occurs between 350˚C and 450˚C, the existence of a higher content of lignin in AKS, HS, and WS describes this behavior. The faster decomposition of CC than other biomass could be attributed to its higher cellulose content. The results of this kind of behavior are confirmed by the chemical composition of biomasses.

The TGA curve showed there were decomposition peaks coming from hemicellulose, cellulose, and lignin. All the organic waste variations, including AKS, HS, WS and CC, experience non-isothermal degradation in the ambient air through three consecutive phases followed by mass losses, as depicted in figure 5.7. It began with a small loss step of below 5.3% until 100 °C, a temperature at which water loss occurs which was 5,3% for AKS, 3,6% for HS, 2% for HS and 3,2 for CC. In the literature, it was expected that the thermal stability of organic waste would be up to 200 °C. In all four cases, the thermal instability started at different temperatures. The onset temperatures of thermal decompositions are as follows: the onset of AKS is 250 °C, the onset of HS is 250 °C, the onset of WS°C is 244 °C, and the onset of CC is 233 °C. The high lignin content inside the AKS and HS may have delayed the onset temperature of the biomass and as a result it both started to decompose slightly later than other biomasses. Moreover, high hemicellulose content inside the WS and CC may have initiated the decomposition temperature slight earlier than other ones due to the poor thermal stability of the structure than lignin. The temperatures at which maximum weight loss occurs are shown by the derivative curve; Tmax of AKS is 350 °C, Tmax of HS is 375 °C, Tmax of WS is 360 °C, and Tmax of CC is 346 °C. The

percentage of residue at 950 °C indicates the output of biochar that was produced after pyrolysis [49]. The percentage residue is related to nonvolatile metals that exsit in biomass. The heavy metal content of AKS is higher than that of other biomasses. Therefore, it is expected that the ash content of AKS would be higher than that of other biomasses [49]. In addition, elements such as carbon, nitrogen, oxygen, and hydrogen could also affect this ash ratio. Generally, carbon and oxygen content are higher in these kinds of biomasses. The change in carbon and oxygen content could cause these variations in residues. The residue of AKS is 19,48% at 600 °C and 17,11% at 950 °C; the residue of HS is 26,35% at 600 °C and 23,37% at 950 °C; and the residue of WS is 23,58% at 600 °C and 21,18% at 950 °C. Finally, the residue for CC is 21,13% at 600 °C and 19,53% at 950 °C. From the elemental analysis, it was revealed that the highest heavy metal content was belonged to AKS which was also confirmed by Çetin et al. [43], yet the ash content of AKS was minimum among all. This may be due to the different ratios of carbon, oxygen, and nitrogen. HS had the highest residue content which may be due to the amount of carbon and oxygen.

The greatest mass loss occurs from 200 °C to 500 °C, which is also called the "active pyrolytic zone," in which the material loses a significant amount of mass [49]. So, the mass loss of AKS, HS, WS, and CC at the active pyrolytic zones is 72,29%, 66,49%, 71,91%, and 73,71%, respectively. In this zone, two peaks appear at the DTG curve. Two DTG peaks represent the pyrolysis of hemicellulose and cellulose, respectively [49] .The size of the DTG peaks at that zone is different from one another. The first small peak was discernible at both AKS and CC, and mass loss was greater in CC. The overall size of the peak was smallest in HS, and the largest size belonged to CC. The larger peaks may correspond to the amount of cellulose and lignin inside the molecular structure of AKS and CC. AKS had the highest lignin content among all, whereas CC had the highest cellulose content. The high amount of cellulose inside the CC and lignin inside the AKS could increase the mass loss in the TGA curve. The total mass loss of AKS was the greatest, which could be attributed to the lignin content within the AKS due to its high molecular weight structure. The difficulty in the decomposition of lignin creates lower mass loss rate and makes the decomposition in a broad temperature range [53,54].

In my opinion, instant decomposition of the molecule would be harder than the decomposition of cellulose and hemicellulose. The DTG peak of CC was sharper than the rest of the biomass, meaning the polymer molecules decomposed more quickly. The other biomasses had a broader and less sharp decomposition. This is due to the low content of lignin inside the CC. The second sharp peak has belonged to AKS, the highest content of lignin in AKS may have cause this appearance. Tonset of HS started later than other biomasses which was also the same case in TGA curve. The results of Tmax revealed that AKS and HS had a later decomposition. Thereby, it could be said that the thermal stability of those two biomasses was higher than that of WS and CC. The Tmax values was also higher in TGA curve.

The DSC curve of biomasses had no melting peak. The moisture inside the biomass decomposes at 100˚C. In TGA curve, the mass loss at this temperature coincides with this loss at DSC curve. Low molecular weight components might decompose at this temperature. The highest water loss occurred at AKS, and DSC data confirmed this result. Table 4.5 display the DSC results of biomasses.

Differential Scanning Calorimetry (DSC) measures heat flow in and out of a sample and reference material as a function of temperature as the sample was heated, cooled, or held isothermally (at constant temperature). The measurement signal shows the energy absorbed by or released by the signal, and it detects endothermic and exothermic effects. Exothermic heat flows out of the sample and endothermic heat flows into the sample. It determines peak areas in transition and reaction enthalpies. It additionally allows for the determination of caloric values such as heat of fusion, and heat of crystallization by measuring heat flux and change in temperature converted to heat flux difference by an appropriate calibration. Table 4.5 depicts the Tonset and Tmax values of biomasses.

Table 4.5 : DSC results of biomasses.

Sample	Tonset (˚C)	Tmax (˚C)
AKS	172	218
HS	176	218
WS	168	215
CC	160	203

It specifies temperatures that characterize a peak or other effects and measures specific heat capacity. The usual measurement mode of DSC includes low heating rates (0.5 to

5 K/min) with good temperature resolution and detects small effects, whereas high heating rates (> 20 K/min) with poor temperature resolution, large effects, and medium rates of 5 to 20 K/min. It can ensure qualitative and quantitative information regarding physical and chemical alterations that cover endothermic or exothermic processes or changes in heat capacity. [55]. The reference could be an inert material (alumina) or an empty aluminum pan. The temperature of both the sample and the reference was increasing at a constant rate. It regulates itself at constant pressure, and heat flow was equal to enthalpy changes. The equation represents the heat capacity where the enthalpy change occurs.

In endothermic processes, the heat flow of the sample was higher due to the absorbed heat in comparison with the reference (i.e., phase transitions, decomposition, reduction, dehydration), thereby dH/dt was positive, whereas in exothermic processes, dH/dt was negative (i.e., crystallization, crosslinking, oxidation) peaks [56]. The current was for two heaters to increase the temperature and the power difference between the two holders was required to resume the holders at the same time. Temperature was used to calculate enthalpy change as a function of time. There was also nitrogen gas, which gives a repeatable and dry atmosphere while excluding the sample oxidation of air at high temperatures. The sample needs to be sealed into a tiny aluminum pan (which could carry from 1 to 10 mg at most), while the reference stays empty. Crystallization was an exothermic process, and melting was an endothermic process. Enthalpy change can be calculated in the area under the peaks. Materials for DSC analysis are as follows; pure and dry nitrogen gas with low pressure; DSC equipment with data collector system and its cell; cooling apparatus for below room temperature searches; pointed tip forceps; balance capable of measuring to at least 0.0001 g; DSC aluminum sample pan and lids; crimper.

The specimens were taken as samples without any impurities in them. Temperature and heat calibration should be done first. Crimping the sample pan and then loading it with samples was necessary. Finally, temperature operation with the controller and adjustment of the temperature ranges are done. A sample should be prepared according to the rules of the device. Using forceps to manage the sample pan and lid and then procurement of the tare weight of the pan and the lid. Both masses should be recorded. Around 1–10 mg of polymer should be weighed (the powder version increases the thermal contact). With the help of forceps, the polymer sample pan and lid should be

removed, and it should be protected from external factors that could influence the mass. Samples should be crimped, and the lid should be closed on top of the sample pan. Also, another empty sample pan and lid should be crimped as a reference pan.

As a result, to compare the characteristics of each biomass, FTIR, TGA, and DSC analyses were conducted. When looking at the FTIR spectrum, CC mainly contains cellulose and hemicellulose while the others contain mainly lignin, but different results have been given due to the differences in lignin structure. These differences have a significant effect on the thermal and mechanical properties of the organic waste-filled polypropylene composite.

4.2 Modification of Biomass

The hydrophilic structure of these biomasses and the hydrophobic feature of polypropylene make them incompatible in compounding process. Therefore, if we could apply structural changes to the biomass and make it more hydrophobic than itself, it is expected to become compatible with the polymer matrix. Surface modification of biocomposites was dependent on the hydroxyl content in the structure. To improve the interfacial compatibility, biomass needs to be modified first. Because the modification prior to compounding processing occurs with the reactive OH groups of the molecule, biomasses with a higher OH number are expected to modify more than others. The esterification of biomass with SA was thougt as a method to increase hydrophobic character of the biomass. It was expected that the more the hydroxyl content inside the biomass, the higher the modification will be because carboxylic acid group will have access to hydroxyl group to form an esterified material. Therefore, it was important to note that the number of hydroxyl groups inside the biomass. Moreover, it is expected to form ester bond from the hydroxyl groups of lignin. The hydroxyl groups of lignin are more reactive than the hydroxyl groups of cellulose which facilitates the binding ability of the modifier. In addition to that, the availability of those hydroxyl groups in lignin is much higher than hydroxyl groups of cellulose. The lignin content was highest in AKS, thereby, the modification is expected to become successful in this biomass and hence the surface modification applied to AKS. The determination of chemical composition of lignocellulosic biomass is also crucial for the prediction of modified parts of the material. To observe any changes in the surface structure of a biomass, modification was first introduced to the AKS. To obtain

the better results of the experiment the conditions of temperature, time and amount were altered. For this, 6 different types of reaction conditions were introduced. Then esterified AKS powder was filtered before being dried in an oven for 24 hours at 80°C. The ratio, temperature, and time were changed to 10:1 50C 24h, 10:2 RT 24h, 10:2 RT 48h, 10:2 50 ˚C 24h, 10:2 50 ˚C 48h, and 10:1 50 ˚C 48h respectively. A summary of the esterification reaction conditions of AKS with SA could be seen in Table 4.6.

First, AKS needed to be washed with ethanol. Because there were parts that dissolved in ethanol. To remove the ethanol-soluble parts, AKS were first washed with ethanol (AKS-etOH), then it was modified. To make sure of this, AKS poured in ethanol and mixed for a few hours, mixed and dried to get FTIR spectra.

Table 4.6 : Reaction conditions for surface modification of AKS with SA.

Experiment no	T(˚C)	t (h)	AKS (g)	SA (g)	AKS:SA(g:g)	Obtained polymer (g)	Yield (%)
AKSSA1	50	24	1	0,1	10	0,93	84
AKSSA2	25	24	1	0,2	5	0,92	76
AKSSA3	25	48	1	0,2	5	0,82	68
AKSSA4	50	24	1	0,2	5	0,84	70
AKSSA5	50	48	1	0,2	5	0,87	72
AKSSA6	50	48	1	0,1	10	0,86	78

After washing with ethanol, the signals at 2924 cm $^{-1}$ and 2864 cm $^{-1}$ were gone. This indicated that by washing the AKS with ethanol oil and wax type hydrocarbons were removed from the chemical composition of AKS. These hydrocarbons were already soluble in terms of its structure. These types of hydrocarbons prohibit to reach the reactive functional groups of the biomass and behave like a barrier within the interface of the biomass and the matrix. In other words, it deforms the interlocking of the biomass and the matrix and create poor interfacial adhesion by acting as an irregularity and inequailities of biomass surface. After removing these impurities from the surface, the yield of the surface modification could be improved. So, the modification was done with the washed one so that they do not affect the result. The FTIR spectra of AKS and AKS that were washed with ethanol (AKS-etOH) were compared in the figure 4.4.

c

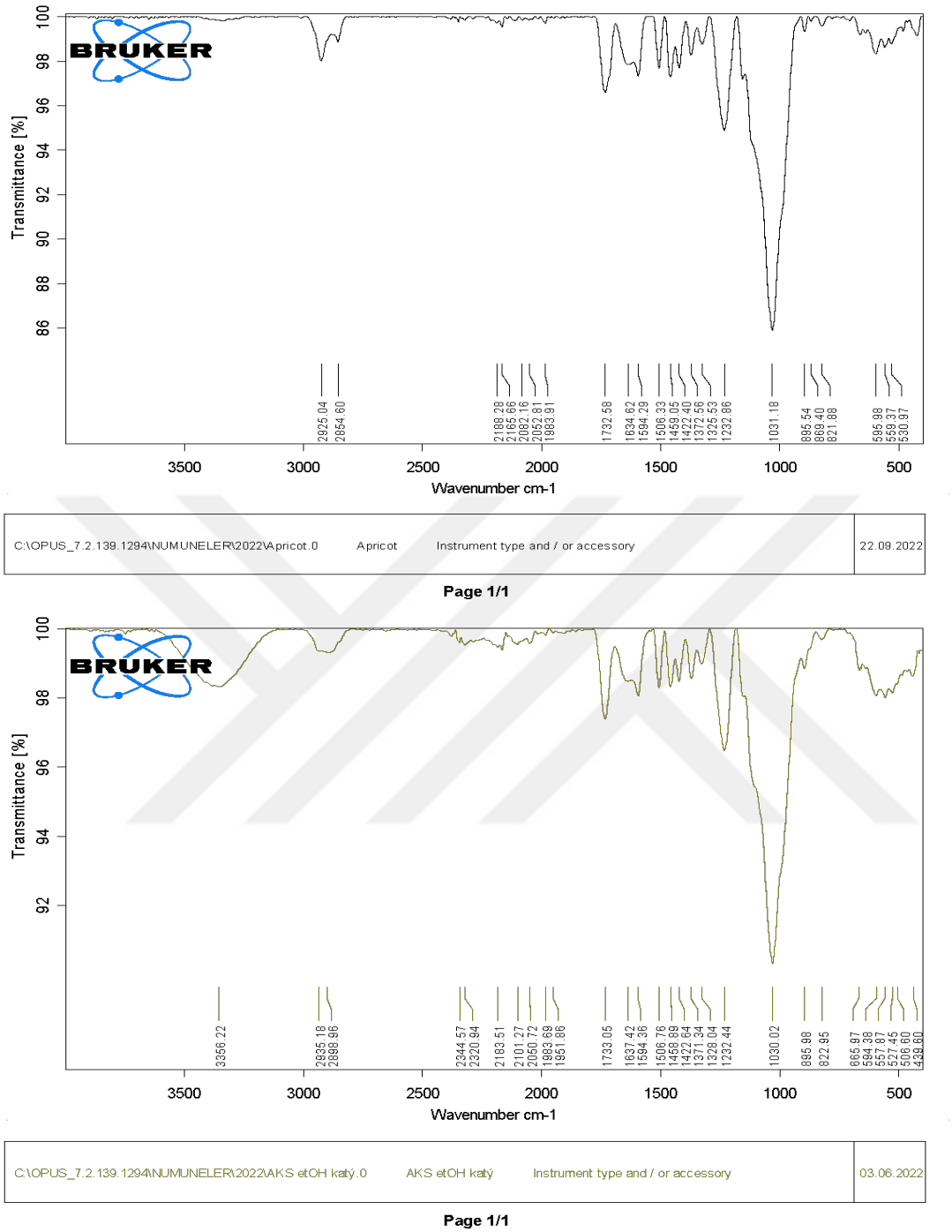

Figure 4.4 : FTIR spectra unmodified AKS and AKSetOH.

In the FTIR spectra of SA and AKSSA which was shown by figure 4.4, 2955 cm^{-1} indicates the stretching vibrations of -CH_2-. The high intensity peaks at 2914 cm^{-1} and 2847 cm^{-1} showing the asymmetric and symmetric stretching of -CH_2- respectively. The absorbed peak at 1698 cm^{-1} was coming from -COOH vibrations of SA [57]. The characteristic peaks of AKSSA shown in the table 4.7.

Table 4.7 : The main characteristic FTIR spectra of AKSSA.

Wavelength (cm^{-1})	Chemical Bond
3328	-OH bonding
2920	C-H stretching
2850	C=O stretching
1724	C-O ester bonding

In all cases the OH bonding of modified AKS was decreased in intensity at 3328 cm^{-1} while C-H stretching at 2920 cm^{-1}, C=O stretching at 2850 cm^{-1} and C-O cm^{-1} ester bonding at 1724 cm^{-1} were increased. The peak at 1724 cm^{-1} explained that the biomass powder was successfully modified with SA by forming an ester bond which was also supported by Chun et al. [31]. Figure 4.5 depicts the differences between the 6 type experiment conditions in IR spectra. It could be said that, when temperature of the reaction increased from room temperature to 50˚C the peak after the modification becomes larger. However, there were no difference when the time had changed. Among all, the best modification occurred at experiment 5. As a result, the increase in SA content did not change the modification yield, yet the only difference occurred with the temperature increase.

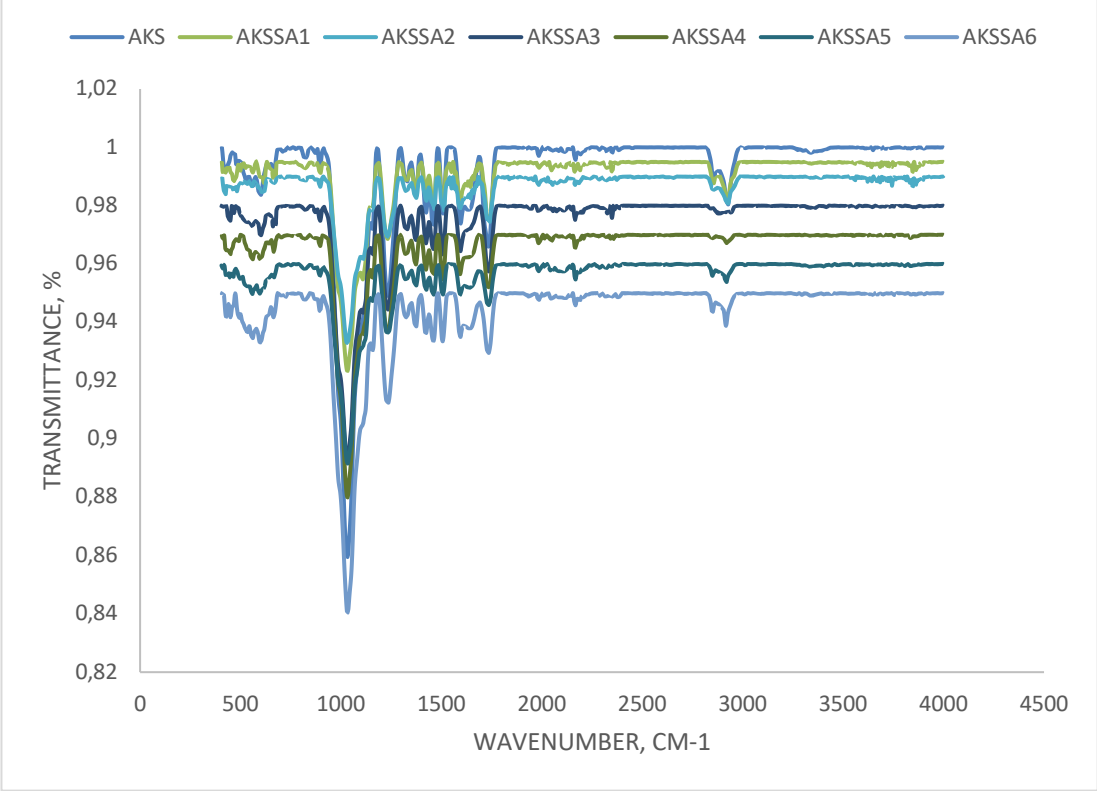

Figure 4.5 : FTIR spectra of time, temperature and amount dependent modified AKS.

For further investigation and confirmation TGA data were also performed. Figure 4.6 depicts the TGA curve of modified (AKSSA) and unmodified AKS. The AKSSA was investigated in two different terms which was by changing only the temperature of the reaction. When looking at TGA analysis of AKS, SA and AKSSA, it was revealed that just by changing the temperature from room temperature to 50˚C and keeping the time and amount of SA constant, the thermal stability of AKS biomass was improved considerably.

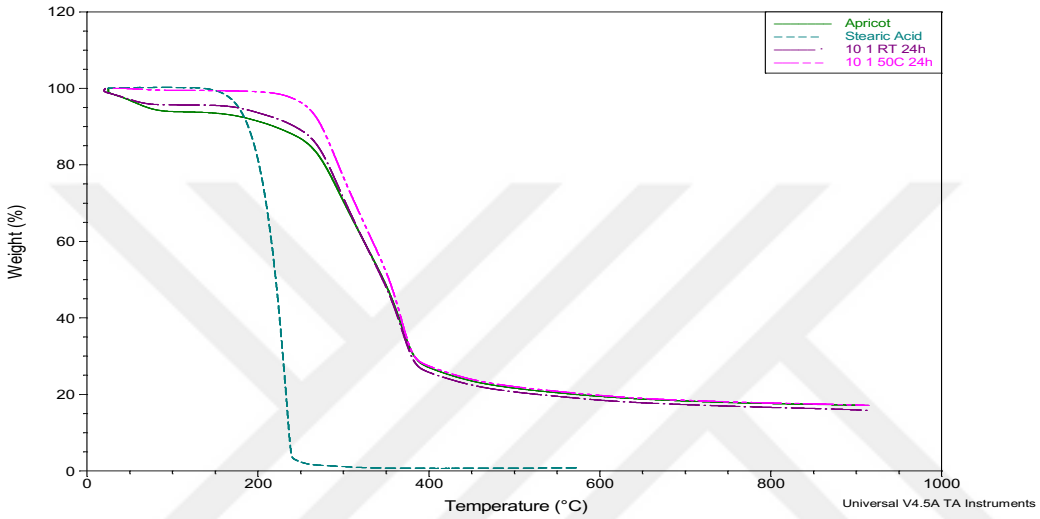

Figure 4.6 : TGA curve of temperature dependent modified AKS.

4.3 Biocomposite Production

This chapter was focused on the mechanical and thermal behavior of the biocomposites after the compounding process of polypropylene with different kinds of lignocellulosic biomass and compatibilizer. The use of a compatibilizer is essential to meet the specifications of the desired material. The compatibilizer worked by attaching to the reactive hydroxyl groups of the biomass. For this reason, the more the biomass gets cleaned up from the impurities, the higher the hydroxyl groups will be able to bind with the compatibilizer. The interconnection between the anhydrite groups of maleated coupling agents and the hydroxyl groups of those biomass results in an ester bond with the polymer matrix.

The biomass content in the compound had a significant effect on the overall properties of the composites; therefore, the effect of biomass content was investigated as well. When the biomass added into the polymer matrix, the most common property change

occurs in the stiffness of the material. Therefore, it was expected to increase in Moduli with the addition of biomass.

4.3.1 The effect of biomass and biomass content on biocomposites

To see the appearance and the color effect of biomass, color plates were injection molded. The color plates that had no compatibilizer inside came out dark brown, indicating that the material was burned during processing. It was expected that, as the amount of biomass increases, the darker color we obtain, yet the color of a 5% filled biocomposite comes out much darker than the one with a 20% filled and compatibilized biocomposite. This shows the material was burned without the addition of the Scona modifier which was shown in figure 4.7 below.

Figure 4.7 : a) Color plates of AKS-filled PP biocomposite b) Color differences between PP/20AKS (dark brown) and PP/20AKS/MAPP (light brown).

As PP was combined with WS, WS and CC during compound, the resulting composite materials were compared regarding the appearances of the altered filler contents. Each composite had an organic waste content of 10%, 15% and 20%. The color density of organic waste-filled composites increased with increasing biomass content. While the relatively low content-filled composites depicted a lighter color, the high content-filled composites appeared darker. It was easier to see the dotted pattern that was coming from the biomass itself in the lighter colored composites as seen in figure 4.8.

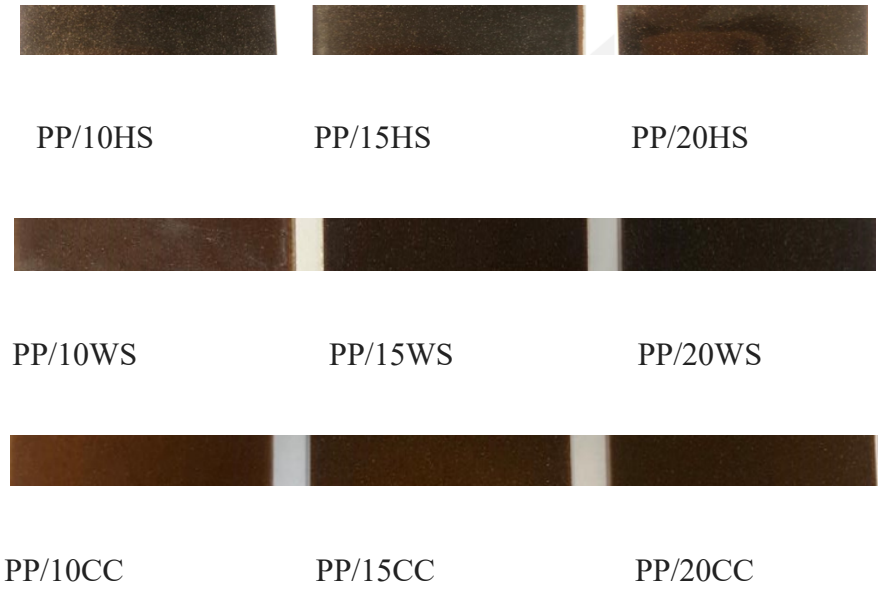

Figure 4.8 : Color plates of HS, WS and CC filled PP biocomposites

To enhance biocompatibility of PP some biowaste materials were compounded with Borealis HE125MO PP first. For further investigations, the compounding process continued with Sumitomo PP because we got Sumitomo PP and continued with it. Afterwards, waste biomass sources were investigated in the biocomposite form. The spectroscopic analysis and mechanical properties of the biocomposites were investigated first and thermal properties comes in the latter. Finally, the rheological behavior of those compounded biocomposites were studied.

4.3.1.1 Spectroscopic Analysis

Initially, IR spectroscopy was practiced to identify any variations inside the molecular structure of the biomass parts and analyse the probability of bond formation between the biomass and the polymer matrix [58]. Figure 4.9 depicts the FTIR spectrum of neat PP.

PP could have different kinds of tacticity. Isotacticity is directly correlated with the crystallinity of the composites, and isotacticity may alter with different grades of raw polymer. The isotacticity and crystallinity of the materials could be detected from FTIR spectra [59-61]. The signals of the FTIR peak are altered by the number of repeating units [59,62].The signals at 1220 (C-H wagging), 1167 (C-C stretching), 998 (CH3 rocking), 900 (CH3 twisting), 841 (C-C stretching, and CH2, CH3 rocking), and 808 cm-1 (C-H out-of-plane bending) were closely related to the number of repeating units in helical form [63]. If the number of repeating units in the polymer chain is

lower than 10, the signal appears at 998 cm $^{-1}$, if it is higher than 13, the peak occurs at 841 cm $^{-1}$. The rest of the signals needed a higher number than 15 to be observed [64] . All signal intensities were relative to the signal intensity at 1460 cm-1 (asymmetric CH3 deformation); because it was an asymmetric C-H deformation of the methyl group and was used as an internal standard. Approximate values for pure isotactic PP were presented as A998/A1460 = 0.265 and A841/A1460 = 0.255 by Kissin et al. [61]

Changes in isotacticity form various conformational orders. This study investigates the impact of the conformational order of the biocomposites on their crystallization and thermal bearing. The peak below 1400 cm $^{-1}$ shows the isotacticity of PP. The most visible isotactic PP peaks are 1170 cm1, 998 cm $^{-1}$, and 841 cm $^{-1}$. If there is syndiotactic conformation in the polymer chain, the peaks appear at 1005, 997 and 867 cm $^{-1}$[64].Lanyi et al. discovered that the degree of crystallinity can be calculated by dividing the height of the peak at 998 cm-1 by 974 cm-^{1}[60].

On the other hand, Luongo et al. state that, the peaks 974 cm $^{-1}$ and 995 cm $^{-1}$ define the isotacticity of the polymer, in which if the peak intensities of those two appear in the same size, it becomes 100% isotactic, whereas if only 974 cm $^{-1}$ appears as a distinctive signal, then the polymer becomes 100% atactic [65]. The ratio of isotactic to isotactic could be found by comparing these two peaks. When the size of the peaks is the same, the ratio is equivalent to 1, indicating 100% isotactic polymer. As the size of 995 cm $^{-1}$ decreases, the ratio increases. The smaller the size of 995 cm $^{-1}$ signal, the higher the ratio, indicating greater atacticity.

In our case, the signals occurred at 972 cm $^{-1}$ and 995 cm $^{-1}$. The sizes of the two peaks were different from one another, and the 972 cm $^{-1}$ signal was much more distinctive than the 995 cm $^{-1}$ peak. Therefore, it could be said that atactic conformation is higher in comparison with isotactic polymer chains. The size of the Borealis PP peak at those signals was larger than Sumitomo PP. The data in the below illustration displays the isotactic/atactic ratio of the neat PPs and biocomposites. The ratio of Sumitomo PP was 1,35, whereas Borealis PP was 1,37. Because 1.35 is closer to 1, the percent isotacticity is slightly higher in Sumitomo PP than in Borealis PP, making the polymer more atactic. More isotactic polymer is expected to have higher crystallinity, and higher crystallinity would result in low impact toughness, high elastic modulus, and high flexural modulus due to the increased stiffness of the aligned and oriented chains.

When some of the additives were added, the isotactic ratio decreased to 20% and some increased. In this section it will be discussed whether they are directly proportional to their degree of crystallinity. Overall, the highest atactic material was PP/10WS by 2. The rest of the materials were lower than 1,6. In Sumitomo PP/AKS biocomposites, the highest atacticity occurred at PP/10AKS followed by PP/5AKS, whereas highest isotactic material was PP/20AKS followed by PP/15AKS. In Borealis PP/AKS biocomposites, as the filler content increased isotacticity also increased, accordingly.

In Sumitomo PP/CC biocomposites, there were no relevant relationship between the isotacticity of the materials and filler content, yet the highest isotactic value was belonged to PP/10CC. In Sumitomo PP/HS biocomposites, the percent atactic value increased with increasing biomass content after PP/10HS, and PP/10HS had the highest isotactic value. Figure 4.9 depicts the isotactic ratio of neat PPs and biocomposites and FTIR spectra of Borealis PP and Sumitomo PP.

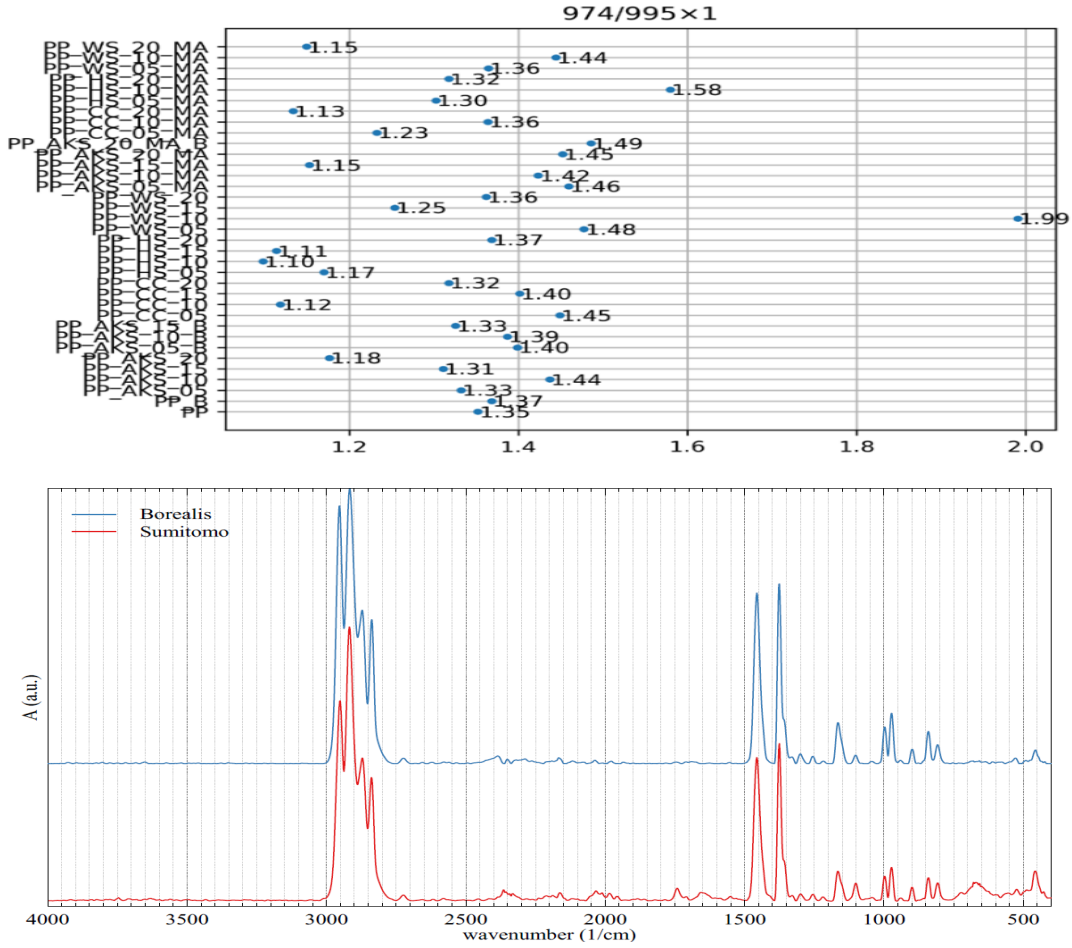

Figure 4.9 : A) Isotactic/atactic ratio of PP and its biocomposites. B) FTIR spectra of neat PPs.

4.3.1.2 Thermal Analysis

Secondly, thermal tests were performed to observe the behavior of the biocomposite when it exposed to high temperatures. Ther analyses were carried out with thermogravimetric analysis and differential scanning calorimetry. TGA showed the percent mass loss according to the increasing temperature profile. The mass losses depict the thermal stability of the material and TGA curve illustrates the starting and ending point of thermal decomposition of the material. In addition to this, DSC analyzed the crystallization behavior of the biomass and biocomposites. To compare the produced materials, neat PP (Borealis and Sumitomo) were analysed initially. The reference was taken as neat PP as shown in figure 4.10.

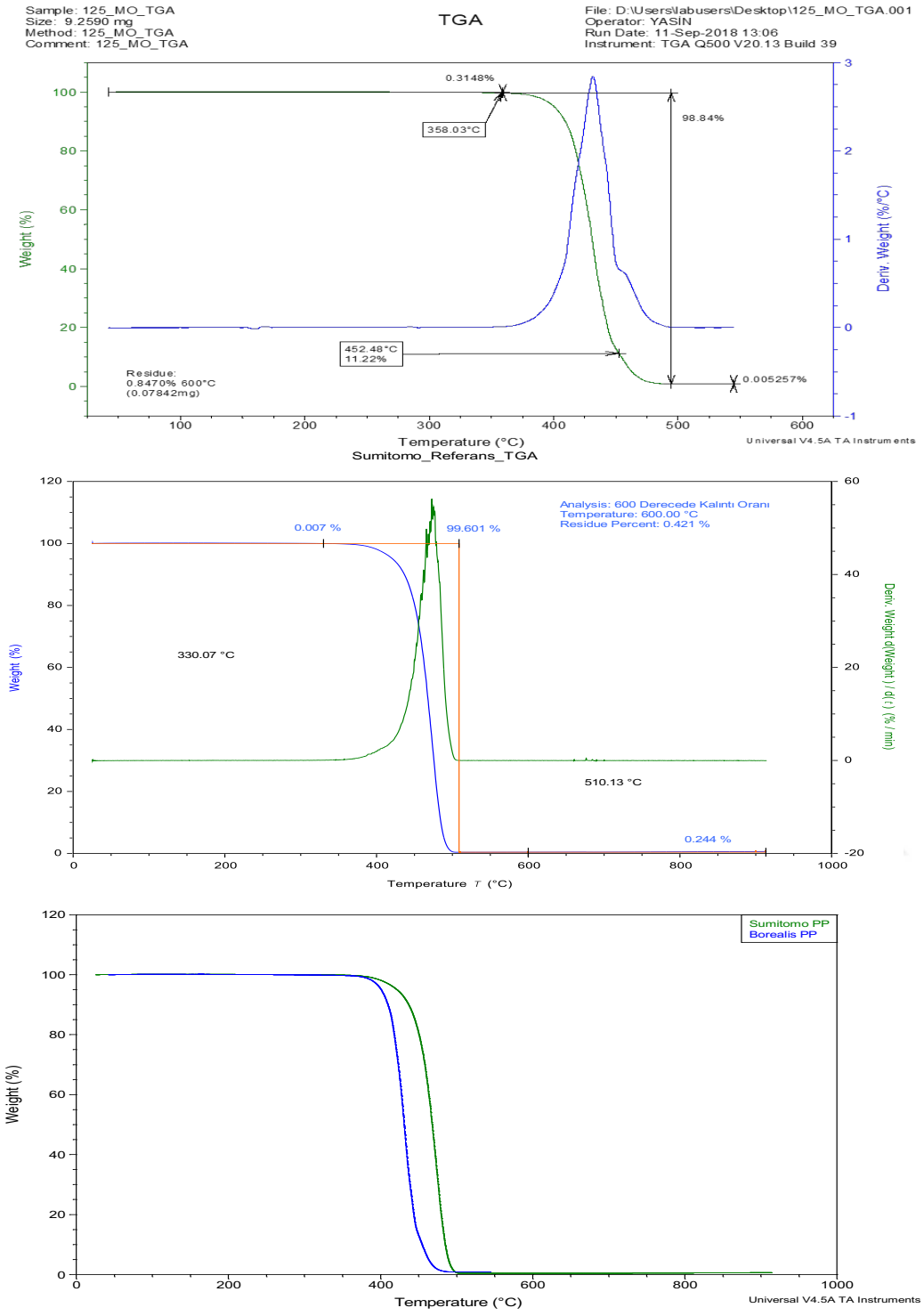

Figure 4.10 : TGA curve of a) Borealis PP b) Sumitomo PP.

The temperature at which the sample begins degradation was the onset temperature, which was 358 °C in the case of Borealis PP and 330 °C for Sumitomo PP. It was also called Ti (initial temperature). 425°C was he temperature at which half of the sample degrades (At 50%). Even though the Tonset is higher in Borealis PP, thermal stability

of Sumitomo was slightly higher than Borealis PP which could be seen from the Tmax values. Tmax of Sumitomo PP (474 °C) was higher than Borealis PP (431°C) .

To compare the behavior of those two different PPs, the thermal characteristics of biocomposites were investigated. The addition of biomass to the PP matrix changed the thermal behavior of the material. Even though the same amount of biomass was put into the polymer matrix, the thermal characteristics changed with the PP grade. PPS/5AKS performed better than PPB/5AKS prior to 450 °C. However, at high temperatures, PPS/5AKS became more thermally stable. At Tonset, there was a greater mass loss at PPB/5AKS, which was coming from poor interfacial compatibility of biomass and Borealis PP. The thermal decomposition graph of PPB/10AKS was very good in terms of stability and endurance to high temperature applications at 10% biomass loadings, whereas the decomposition of PPS/10AKS began much earlier than that of PPB/10AKS. This situation was also the same at 15% and 20% biomass loadings.

When comparing compatibilized biocomposites with Sumitomo PP and Borealis PP, PPB/20AKS/MAPP and PPS/20AKS/MAPP were also different from one another. In my opinion, PPS/20AKS/MAPP was less compatible than PPB/20AKS/MAPP because, at Tonset, the decomposition of the biocomposite was not going straight and there were 2 additional derivative peaks in that curve. This showed that the biomass inside the PP matrix detached and decomposed earlier than the biocomposite itself. The low-molecular-weight compounds inside the biomass also detached and burned earlier since they were not bound to the PP matrix. On the other hand, in PPB/20AKS/MAPP, the TGA curve was more straightforward, and there were no additional peaks that designated a proper binding of biomass with the PP matrix, but it resulted in poor thermal stability at high temperatures. Figure 4.11 illustrates the DSC curve of neat PP.

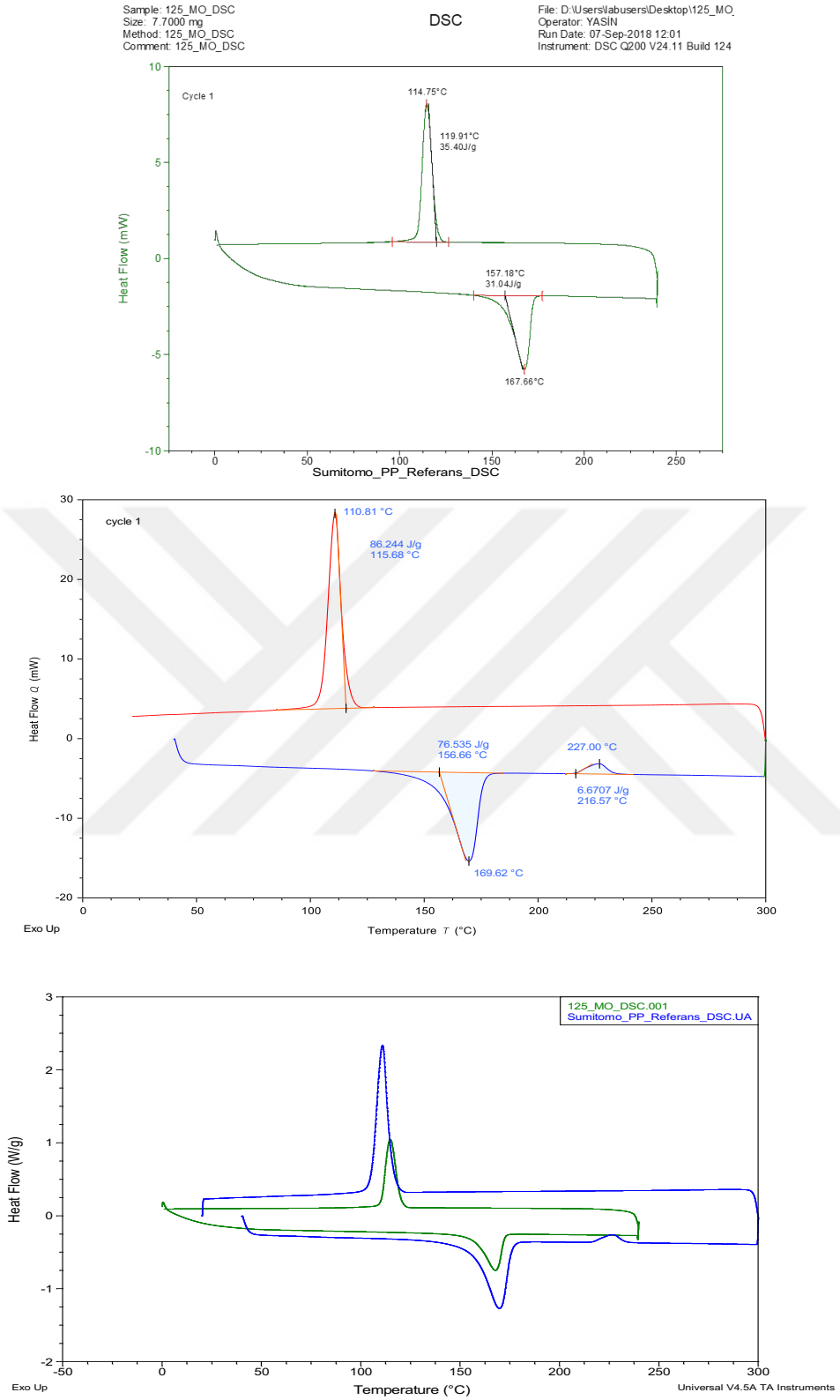

Figure 4.11 : DSC curve of PP.

The thermal behavior of PP/AKS biocomposites was investigated with TGA and DSC analysis. Figure 4.12 depicts the decomposition behavior of PP/AKS biocomposites.

Initially, there was a small amount of moisture loss up to 200 °C due to the amount of biomass used being small. The degradation of uncompatibilized biocomposites showed three-step decomposition at 290 °C, 375 °C, and 465 °C. The first two steps of degradation are seen at the derivative curve with slight and smooth peaks, which indicated that without compatibilization of biocomposites, some molecules started to degrade and depolymerized before the main decomposition temperature at which the maximum mass loss occurs. The second step of degradation was where the maximum mass loss occurs during decomposition. This can also be seen from the DTG curve. With the addition of biomass into the polymer matrix, the decomposition started earlier than the neat PP. The reason for this behavior was that there was an incompatibility between the biomass and the polymer matrix. When the biomass and the polymer matrix are compounded, the molecules that exist in the biomass cannot be coupled with the polymer matrix. The second reason was that the biomass itself begins to decompose initially. This also explained the first two-step decomposition of uncompatibilized biocomposites. Nonetheless, even though the thermal decomposition of PP/AKS composites started earlier than that of neat PP, a more thermally stable material had been obtained with the addition of biomass. The AKS started decomposing at more elevated temperatures due to the thermal preservation provided by the more thermally robust PP that enclosed the biomass. The influence of the bimass may had impaired the free radicals developed during the beginning of the decomposition of the polymer bond and hindered the dispersion of volatile byproducts through the interconnection with the biomass, which was likely the reason for the greater stability of the PP biocomposite [66]. In the first 25% of the TGA graph, neat PP seems to be advantageous on its own, but 75% of it degrades later than neat PP. It might be said that, if higher temperatures are needed for the application, the AKS-filled PP biocomposites are more advantageous since the portion of 75% was more thermally stable than the neat PP. As a result, the incorporation of biowaste increased the thermal stability of the composite, which was one of the expected goals for this research.

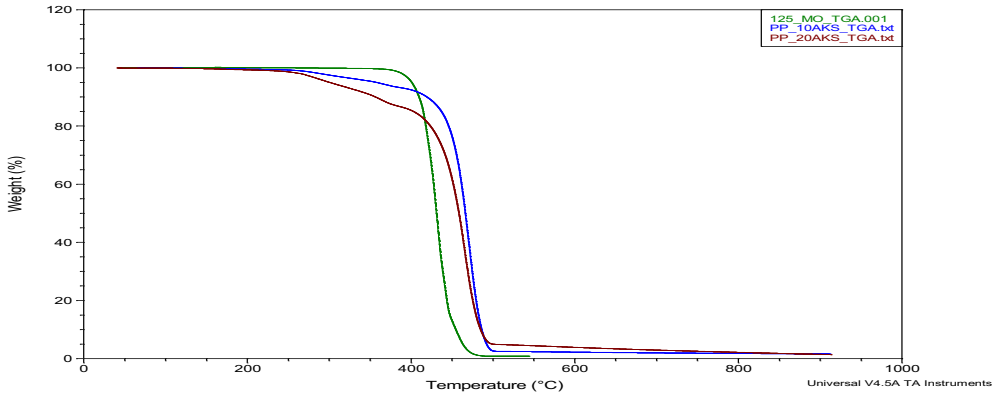

Figure 4.12 : a) TGA curve of PP/AKS biocomposites.

It was normal to expect higher mass loss with increasing biomass content until 100°C because the water content was expected to be higher in the higher weight filled weight-filled content due to the hydrophilic feature of AKS. PP/10AKS loosed a higher percentage of moisture than PP/5AKS. However, PP/15AKS loosed less moisture than PP/5AKS and PP/10AKS until 100°C. This could be explained by the fact that as the biomass content increases, agglomeration also increases, and the agglomerated part could remove the water that was in touch with the surface. The surface side of the PP/15AKS could had been decreased due to the aggregation that was formed by the biomasses themselves. The water attached to the surface may be removed by the formation of agglomeration. It could also happen during processing since the material was exposed to heat, and by heating, the water content may had gone away more clearly. Table 4.8 shows the mass loss steps of PP and PP/AKS biocomposites. The numbers were derived from the TG-DTG curve and shown by table 5.8.

Table 4.8 : Mass loss steps of PP and PP/AKS biocomposites.

Sample	T100 (˚C)	T200 (˚C)	Tmax (˚C)	(%) Residue at 600˚C	(%) Residue at 900 ˚C
PP	0,1162	0,0836	429	0,08	-
PP/5AKS	0,0584	0,5921	472	4,33	2,73
PP/10AKS	0,0872	0,4061	469	2,26	1,63
PP/15AKS	0,0399	0,4175	467	3,58	2,30
PP/20AKS	0,0856	0,6524	465	3,90	1,44

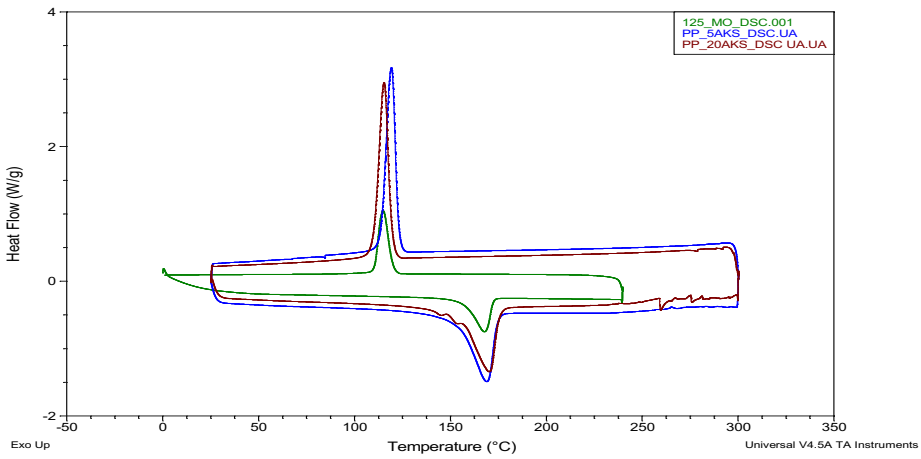

Figure 4.13 : DSC curve of Borealis PP/AKS biocomposites.

DSC curve of PP/AKS biocomposites and neat PP was shown in figure 4.13. The addition of the AKS could give a nucleating effect to the material and hence the crystallinity would increase. Due to the proper alignment of the polymer chains with the increase in crystallinity, the material also gains barrier properties through which it can protect itself from external factors such as heat, moisture, oxygen, and so on. This was crucial because biomass itself was intrinsically hydrophilic, which makes it susceptible to moisture and open air. It was expected to have the higher the biomass content, the larger the nucleating effect will be, yet after 10% filled biocomposites, the crystallization decreased which may be related to the agglomeration at higher biomass contents. Thereby, improper dispersion and poor interfacial compatibility due to the agglomeration of the biomass could influence the crystallinity degree and result in lower crystallite formation. To compare the results, $Tm_{onset,}$ Tm, ΔHm, and Xc values were determined and table 4.9 was formed according to that.

Table 4.9 : Tm_{onset}, Tm, ΔHm, and Xc values of PP and PP/AKS biocomposites.

Sample (%)	Tm_{onset} (˚C)	Tm (˚C)	ΔHm (J/g)	Xc (%)
PP	157,20	167,66	31	15
PP/5AKS	153,93	168,89	83,14	40,16
PP/10AKS	154,47	170,36	93,44	45,14
PP/15AKS	154,19	168,54	89,72	43,34
PP/20AKS	154,38	170,06	86,05	41,54

At 5% biomass content, PP/5HS had the highest thermal stability, followed by PP/5AKS, and PP/5CC had the lowest. At 10% biomass, PP/10CC had the highest thermal stability, yet the greatest mass loss also occurred in this biocomposite until 420 °C. The results were similar for 15% biomass content biocomposites, yet while

the best-performing material was PP/15HS, the worst belonged to PP/15WS. The results of 20% biomass content were similar to those of 10% content, where the best results were obtained from PP/20CC. The figure 4.14 illustrates TGA curve of the 10% biomass content biocomposites.

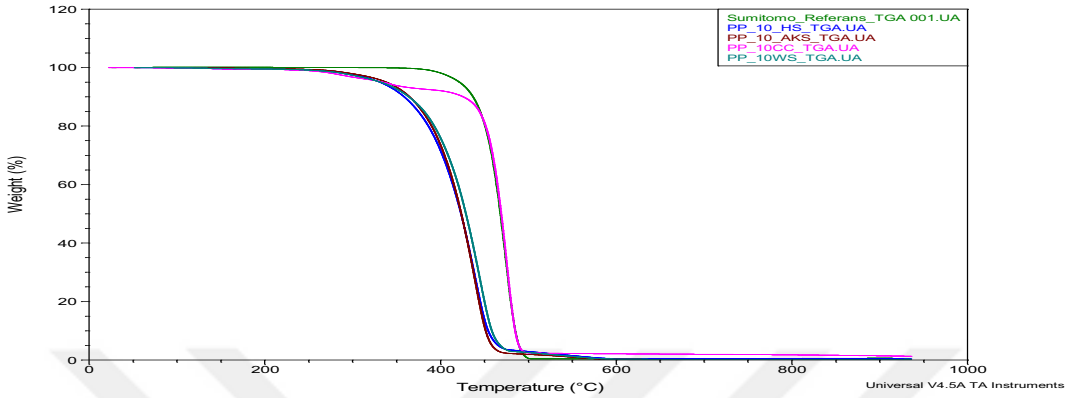

Figure 4.14 : TGA curve of Sumitomo PP biocomposites.

As expected, as the biomass content increased, the thermal decomposition of the biocomposites started earlier. The decomposition curves of PP/15AKS and PP/20AKS were almost the same, yet there was only a slightly higher thermal stability at the temperature ranges between 200°C and 400°C in PP/15AKS. There was an apparent difference between the thermal stability of PP/5AKS and the rest of the biocomposites, which was higher than others. At high temperatures after 450 °C, the thermal stability of PP/10AKS was the same as that of neat PP. However, the rest of the biocomposites had lower thermal stability, and the mass loss started earlier than in neat PP.

PP/5HS had a slightly lower Tonset than neat PP, and the curve that was closest to neat PP was also PP/5HS. The other biocomposites started to decompose earlier, and the increase in biomass content changed the decomposition curve just a little bit. So, there were no apparent changes with the increase in biomass content.

The uncompatibilized PP/HS biocomposites showed the same behavior with other biomasses, which means that as the biomass content increased, the thermal stability of those biocomposites decreased. However, the thermal stability of PP/20WS was higher than that of PP/15WS after 400 °C.

In PP/CC, there was no linear relationship between the biomass content and thermal stability. PP/10CC had the greatest thermal behavior among other PP/CC biocomposites. After Tonset, there was an apparent mass loss that came from the biomass itself, and except for that part of the curve, the thermal stability was the same after 430 °C. The impact strength of PP/10CC had the greatest value, which also confirms this result. The second-best biocomposite belonged to PP/20CC.

PP/20AKS had the lowest Hm and Xc values. This may be because the optimum amount of biomass was 20% in the case of Sumitomo PP. It may be that Sumitomo PP became more compatible with the addition of 20% biomass inside the polymer matrix, and as a result, a small amount of thermal energy would be enough to initiate crystallizing the material. The size of the crystallization peak decreased in higher biomass contents. Moreover, PP/5AKS had the sharpest peak whereas the other uncompatibilized biocomposites had broader peak with low cooling temperatureswhich shows that in higher biomass contents the crystallization becomes slower [67]. The results of PP/AKS biocomposites were shown by table 4.10.

Table 4.10 : $Tm_{onset,}$ Tm, ΔHm and Xc values of Sumitomo PP/AKS biocomposites.

Sample (%)	Tm_{onset} (˚C)	Tm (˚C)	ΔHm (J/g)	Xc (%)
PP	156,66	166,62	76,53	36,48
PP/5AKS	156,50	170,38	81,98	39,60
PP/10AKS	156,54	168,40	76,09	36,75
PP/15AKS	156,07	168,36	76,91	37,15
PP/20AKS	155,67	169,45	63,85	30,80

The Xc values of PP/HS biocomposites were much lower than PP/AKS biocomposites. However, the Xc of PP/20HS were higher than PP/20AKS biocomposite. Tm_{onset} values of PP/HS biocomposites were higher than PP/AKS biocomposites. The thermal stability was higher in PP/5HS biocomposite. Furthermore, the highest ΔHm value was also belong to PP/5HS biocomposite as depicted in 4.11.

Table 4.11 : $Tm_{onset,}$ Tm, ΔHm and Xc values of Sumitomo PP/HS biocomposites.

Sample (%)	Tm_{onset} (˚C)	Tm (˚C)	ΔHm (J/g)	Xc (%)
PP	156,66	166,62	76,53	36,48
PP/5HS	158,03	170,66	67,45	32,58
PP/10HS	155,96	169,01	74,24	35,86
PP/15HS	158,38	169,55	66,38	32,06
PP/20HS	158,12	162,38	73,45	35,48

In PP/WS biocomposites, as the biomass content increased Tm_{onset}, ΔHm and Xc values increased as depicted in the table 4.12. Yet, after 15% biomass, these values decreased. For Xc values, the alignment of biomass inside the polymer matrix may properly distributed and hence the addition of more biomass contributed to the crystallinity values and thermal stability by increasing the Tm_{onset}. Whereas at PP/20WS the biomass content, the amount of biomass may go beyond its limits and decreased those values.

Table 4.12 : $Tm_{onset,}$ Tm, ΔHm and Xc values of Sumitomo PP/WS biocomposites.

Sample (%)	Tm_{onset} (˚C)	Tm (˚C)	ΔHm (J/g)	Xc (%)
PP	156,66	166,62	76,53	36,48
PP/5WS	155,87	170,57	75,96	36,69
PP/10WS	155,94	170,07	76,22	36,82
PP/15WS	157,97	169,27	80,59	38,93
PP/20WS	156,77	168,33	67,86	32,78

Up to PP/10CC, the crystallinity values increased. The least Xc values was belong to PP/15CC. On the other hand, as the biomass content increased $Tm_{onset,}$ and Tm values increased as shown by the table 4.13.

Table 4.13 : $Tm_{onset,}$ Tm, ΔHm and Xc values of Sumitomo PP/CC biocomposites.

Sample (%)	Tm_{onset} (˚C)	Tm (˚C)	ΔHm (J/g)	Xc (%)
PP	156,66	166,62	76,53	36,48
PP/5CC	155,79	168,49	88,17	42,59
PP/10CC	155,42	169,28	84,54	40,84
PP/15CC	156,01	169,55	74,83	36,14
PP/20CC	157,00	170,01	76,94	37,16

4.3.1.3 Mechanical Analysis

In the latter, mechanical tests that had been used in this study were explained by the theory. The mechanical tests comprised of three different testing methods; (i) tensile tests which investigates tensile strength, elongation at break, yield strength, elongation at yield and elastic modulus, (ii) the other test is Izod impact test and (iii) finally, bending test which involves flexural strength and flexural modulus. The following part gives a theoretical overview about each mechanical test.

Tensile Strength is the stress that will influence the samples during the test depends on the cross-sectional area of the sample The width and thickness of the samples are

measured with a micrometer. The sample was inserted into the two grips that clamp the material to initiate the test. As the load was continuously increased, the length of the material was also measured. As a result, the engineering stress-strain profile can be formed by recording the tensile test data, as shown in Figure 4.15 The data gives the value of elastic (tensile) modulus, (ultimate) tensile strength, stress at break, and elongation (strain) at the break.

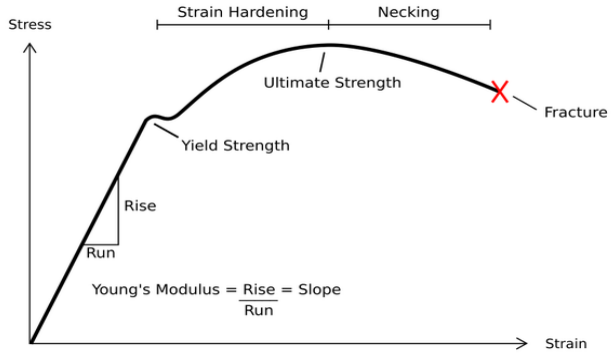

Figure 4.15 : Stress-strain diagram [68].

The stress-strain curves can define multiple characteristics of any material. The curve divides the area into two by yield strength in the first place, so-called elastic deformation, and plastic deformation. With an applied load, the material begins to deform elastically, where a sample can resume its original length after the applied force had been removed; however, with the continuum stress, the material starts to deform plastically, where a sample won't be able to turn back to its original shape henceforth. The term "ultimate tensile strength" refers to the highest point that can be attained on the stress-strain curve with a maximum elongation on the x-axis [69]. The percentage of plastic strain that was generated at the point of break was known as a material's "ductility," which measures the entire amount of permanent plastic deformation that occurs up until the fracture of the material. The elastic modulus was defined as the slope of the stress-strain curve in the elastic deformation region. The modulus of elasticity (or elastic modulus) E was the measure of tensile or compressive stiffness. Therefore, the higher the value of modulus, the stiffer the polymer will be. It determines the linear relationship between applied stress (force/unit area) and strain (change in length/original length), also called the slope of the stress-strain curve in the elastic deformation region, as depicted in the given formula; $E=\sigma/\varepsilon$. In composites, elastic modulus stands between the biomass and the matrix values.

The second factor that affects the mechanical properties of the material is flexural strength. Flexural strength also called bend strength, was said to be the stress (bend/flex) in a material immediately before a flexure test causes it to yield. Indeed, these materials frequently had subtle or significant flaws that act to concentrate localized pressures and cause localized weakening. Flexural modulus was also the same as tensile modulus (Young's modulus) for very low strains in isotropic polymers. Nevertheless, these values could not be similar in anisotropic materials, like wood. The tensile and flexural moduli of composite materials, such as fiber or particle-reinforced polymers, are frequently not equal because they are inhomogeneous mixtures of two or more materials, each with different material properties.

The final critical mechanical testing is Izod Impact Strength. The impact strength or the amount of energy absorbed by the material per unit area was then determined by dividing the energy received by the sample during fracture by the cross-sectional area. A single-point test called the Notched Izod Impact test at ISO 180 standard examines a material's ability to withstand impact by absorbing energy from a swinging pendulum. The kinetic energy required to start a fracture and keep it going until the object was fractured was known as iodized impact. It was also known as impact toughness; the area under the stress-strain curve in the tensile test had been mentioned to measure toughness, which defines the absorbed energy throughout a fracture. It can also be used to measure crack propagation. However, because of the high rate of strain exerted during the impact test compared to the low rate during the tensile test, it was different to calculate the absorbed energy. Moreover, when an extremely quick strain was applied, the material might even act brittlely. The Izod impact test involves installing the specimen vertically and impacting it with a pendulum on the same side of the notch. Figure 4.16 illustrates the pendulum impact test of polymeric materials. It calculates the energy loss of the pendulum that was coming from the energy of the material when it breaks. Simplistically, the hammer’s potential energy that was created by the impact of a material was measured before and after the test [57]. The equation (4.1) measures the E_{frac} of the material.

$$E_{frac} = m\ g\ (h_s - h_e) \tag{4.1}$$

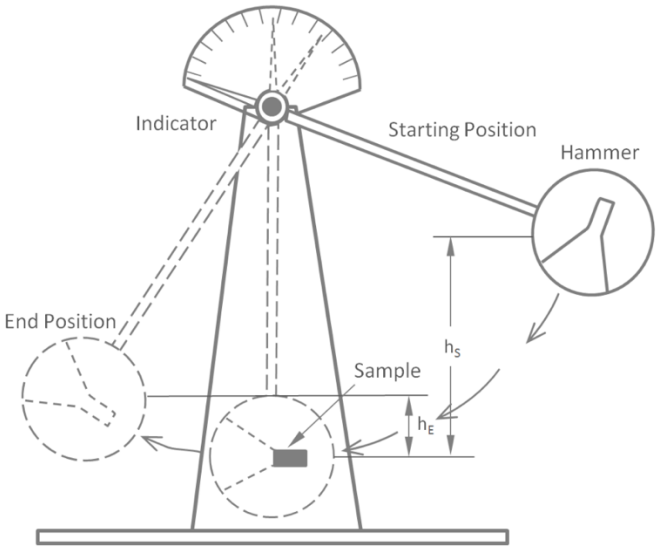

Figure 4.16 : Izod impact test [70] [57].

This part of the study investigates the effect of biomass content on biocomposites and then it compares the different types of biocomposites in terms of the kind of biomass. To confirm the effect of biomass in biocomposites, PP was compounded with AKS, HS, WS, and CC.

The tensile strength of such composites could be increased or decreased with the addition of the biomass to the matrix. Among those various shaped biomass, tensile strength is generally increased by the fiber type due to the ability to withstand transmitted stress that comes from the polymer itself. However, the biomasses with irregular shapes reduce the tensile properties since the biomass cannot withstand stresses that are imparted from the polymer matrix. Figure 4.17 demonstrates how filler loading gradually reduces the tensile strength of organic waste composites. This may be due to the particle-filled composites having no ability to transfer stress from the polymer matrix as fiber-type biomasses do. To be able to transfer stress from the biomass towards the polymer matrix, the biomass needs to had proper wetting with the matrix material. Nevertheless, the poor wetting of organic wastes caused weak interfacial adhesion between the biomasses and polypropylene matrix with increasing biomass loading [71]. The type of biomass also affected the tensile properties of the biocomposites. In lower biomass contents, the ones with PP/AKS were better. However, at 20% biomass PP/CC became higher than PP/AKS.

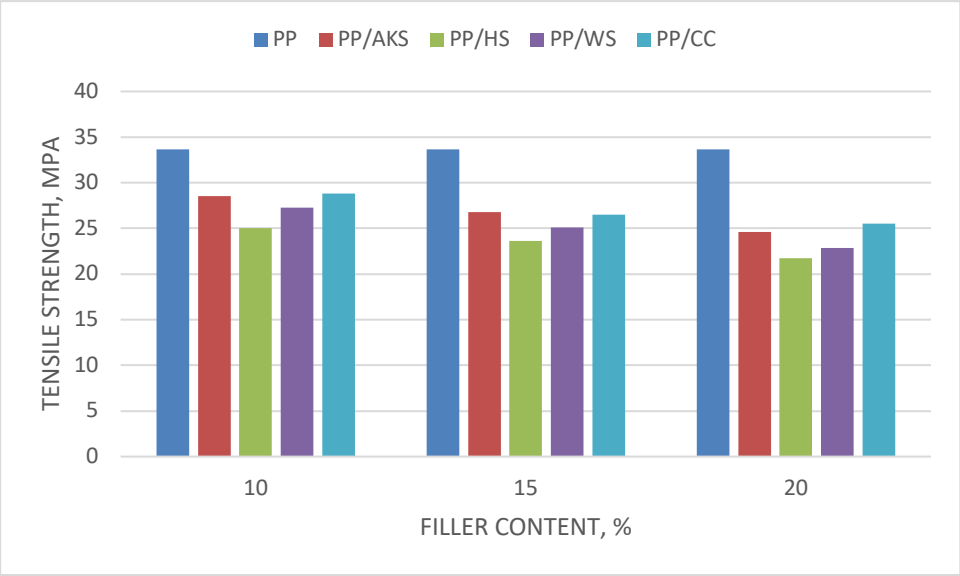

Figure 4.17 : Tensile Strength of Borealis PP biocomposites.

The addition of organic waste into the PP matrix decreased the elongation at the break and elongation at yield value. The results of elongation at break and elongation at yield were like each other. Elongation at yield values gave more accurate results than elongation at break and hence the graphical illustration was depicted in figure 4.18. Usually, elongation at yield decreases with the addition of biomass into the polymer matrix. The biomass incorporation forms a stiffer material whereby the percent elongation of reinforced composite will be lower. Contrary to tensile strength, PP/AKS had the lowest elongation at yield values amongst other biomasses. The results of PP/HS and PP/WS goes similar to one another, and they were both better at lower biomass contents. Again, at 20% biomass filled biocomposites PP/CC were superior.

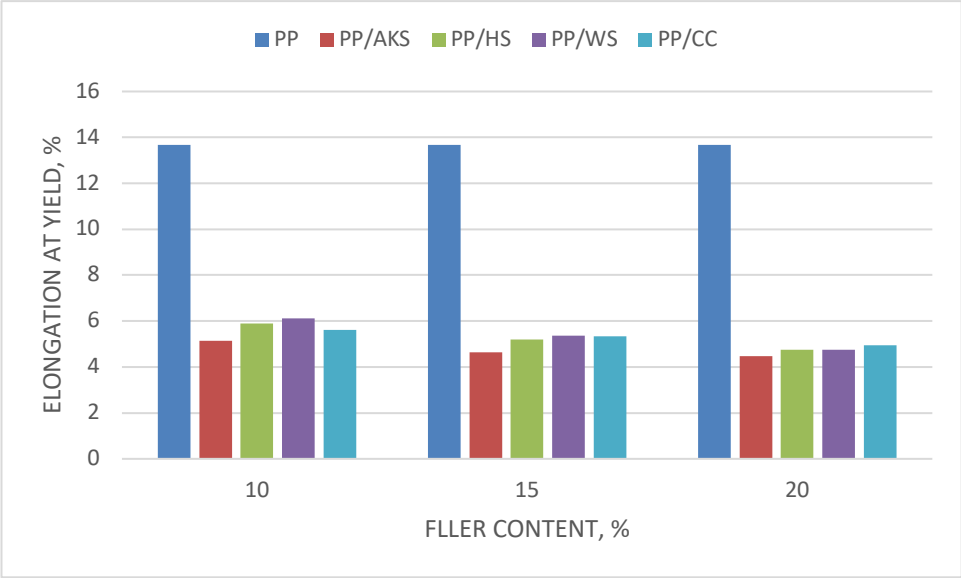

Figure 4.18 : Elongation at yield of Borealis PP biocomposites.

The elastic modulus and strength of composite materials are primarily influenced by the degree of stress transfer from the matrix to the rigid and strong biomass material as well as the reduction in mobility of the macromolecular chain structure of the polymer matrix. The stiffness of the biocomposite material was often shown by an increase in the elastic moduli [72]. As was being observed, as the organic waste loading increased, so did the elastic modulus. Figure 4.19 illustrates the elastic modulus of biocomposites. The results of PP/AKS and PP/CC were almost the same whereas the results of PP/HS and PP/WS were almost the same. The results were resembled with tensile strength of these biocomposites meaning in lower biomass contents including, 10% and 15%, PP/AKS had the highest elastic modulus whereas at 20%, PP/CC had the highest elastic modulus.

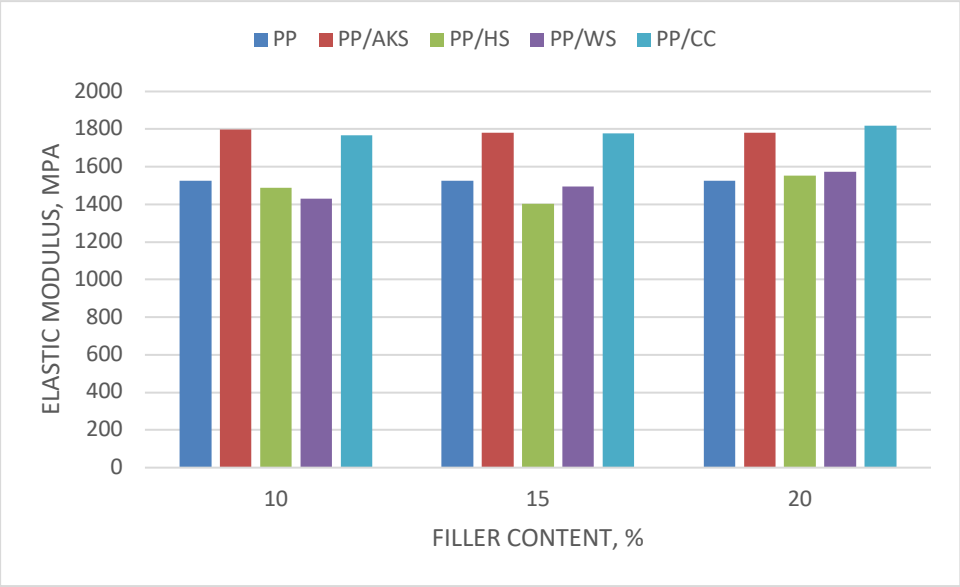

Figure 4.19 : Elastic Modulus of Borealis PP biocomposites.

Izod impact strength decreases as biomass loading rises. This finding had frequently been made and was quite expected for filled polymer systems. This issue may be brought on by inadequate polypropylene wetting of the particles, which results in weak interfacial areas and adhesion between the reinforcement and the matrix. Cracks appear along the poorer interfacial regions and travel through the polymer in the testing of impact strength. The impact strength was decreased because the following crack does not effectively prevent crack growth as the polymer region could. Adding more biomasses just expands the interfacial area, worsening the susceptibility of a material to crack propagation. Biomass inclusion was indeed considered to limit polymer mobility, reducing the system's capacity for absorbing energy throughout crack propagation. Figure 4.20 gave the results of Izod impact strength of biocomposites. PP/WS had the lowest impact value whereas PP/HS had the highest impact results in 10% and 15% filled biocomposites. At 20% filled one PP/CC turned out be highest impact strength.

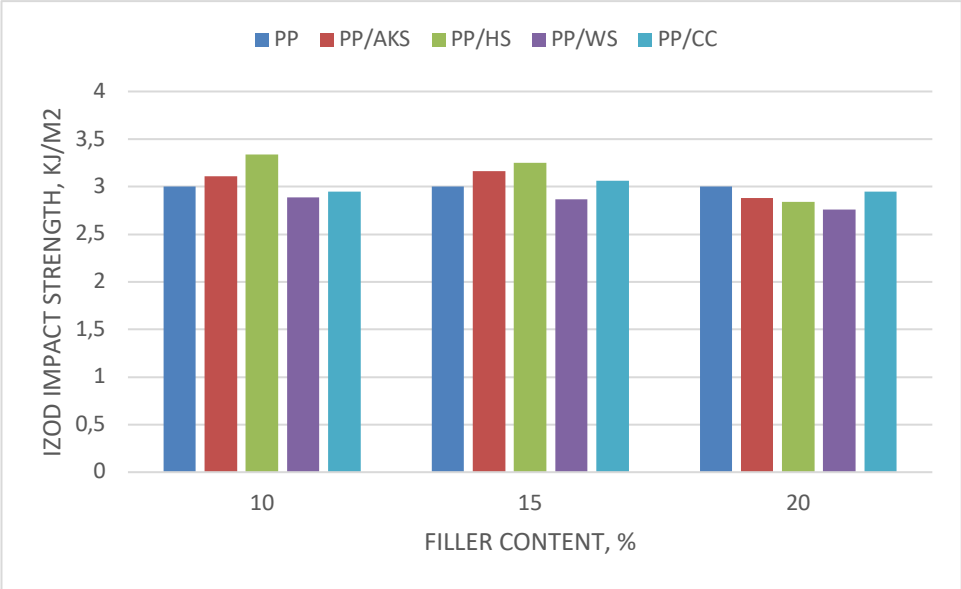

Figure 4.20 : Impact Strength of Borealis PP biocomposites.

One of the fundamental characteristics of composites was moduli (stiffness) and adding biomasses typically had as its main goal to boost the stiffness of the final product. As would be predicted, the flexural modulus continuously increases with increasing biomass content. It was a well-known fact that adding biomass causes the moduli to increase. Figure 4.21 shows the flexural modulus of biocomposites with different biomass content. The use of 10% and 15% biomass did not change the flexural modulus with the type of biomass. At 20% biomass the results were more scattered when the type of biomass changed.

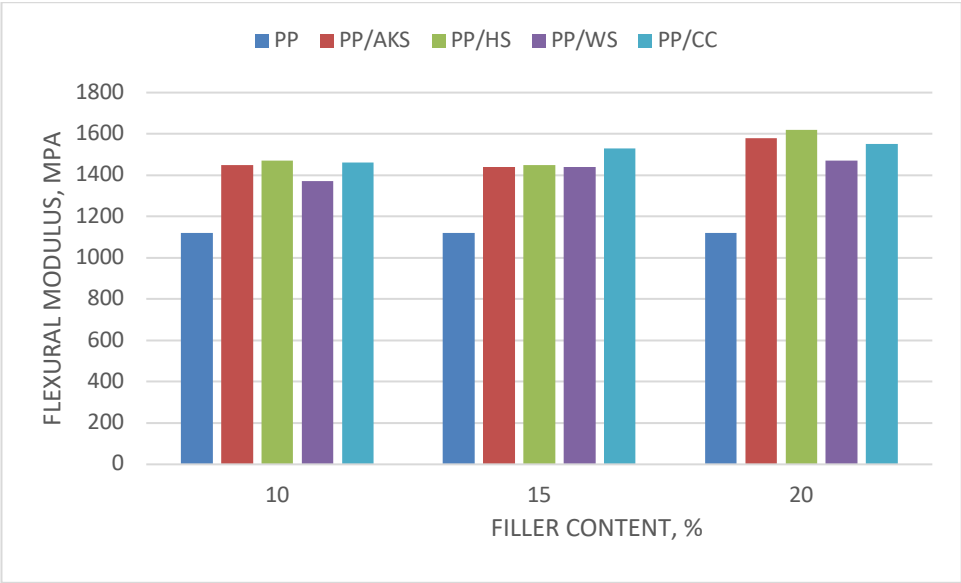

Figure 4.21 : Flexural Modulus of Borealis PP biocomposites.

Even though the results of lowest content-filled csomposite material had superior mechanical properties, we choose to proceed with the highest biomass content to reform the formulations with the additives as we were trying to use as much biomass as possible in the desired material. The best mechanical properties were obtained from PP/AKS and PP/CC.

Among all, PP/CC was superior in terms of tensile strength, yield strength, elongation at yield, impact strength and flexural strength. On the other hand, PP/AKS had the highest elastic modulus and flexural modulus values. In most cases, the mechanical results of PP/HS and PP/WS were resembling.

The tensile strength of the biocomposites decreased with increasing biomass content, as in the case of the Borealis PP matrix which is depicted in the figure 4.22.

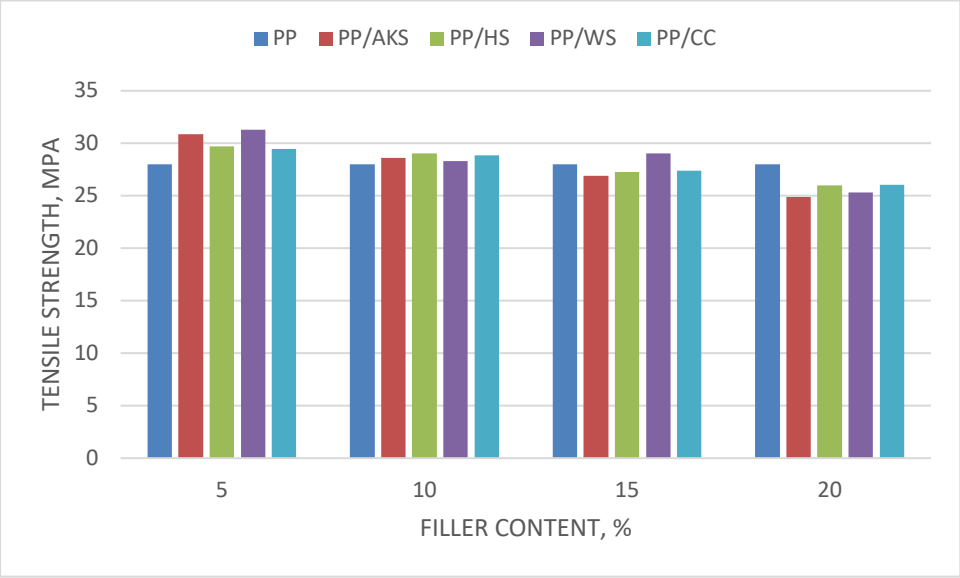

Figure 4.22 : Tensile strength of Sumitomo PP biocomposites.

The biomass inside the polymer matrix decreases the material's ability to elongate, and hence the material becomes more vulnerable to plastic deformation earlier than it should be. There was a drastic decrease when biomass was incorporated into the polymer matrix. The best results were initially obtained in the PP/5HS biocomposite; PP/10CC and PP/15CC came in the latter. Elongation at yield values was depicted in the figure 4.23 below.

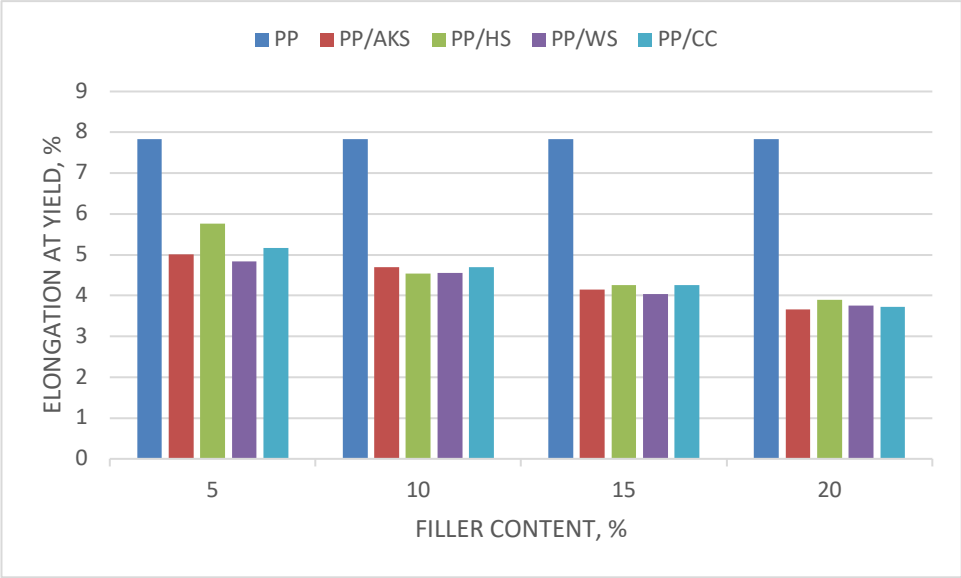

Figure 4.23 : Elongation at yield of Sumitomo PP biocomposites.

The elastic modulus of the material increased with increasing biomass content, which was also the case with the use of Borealis he125mo PP instead of Sumitomo PP. The modulus of elasticity was calculated by dividing the load by the strain. Thereby, it was known that biomass incorporation decreases the strain value, and hence the elastic modulus would increase. The higher the biomass content, the bigger the elastic modulus will be which is depicted in the figure 2.24.

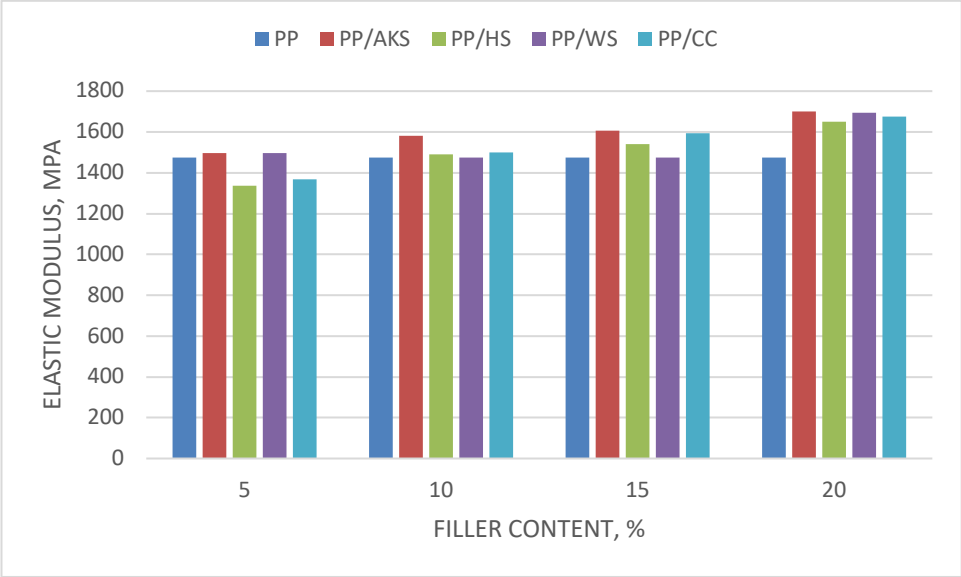

Figure 4.24 : Elastic Modulus of Sumitomo PP biocomposites.

In most cases, impact strength values increased with increasing filler content, up to 10% biomass addition. However, after 10% biomass addition, impact strength decreased as biomass content increased. Overall, the best impact strength values were

obtained from 10% biomass-filled PP biocomposites. A decrease in impact strength values after 10% filling was because the biomass particles may be accumulated on top of each other in higher amounts of biomass content. Among all, the best-performing material in terms of impact strength was PP/HS biocomposites. Both elongation at break, elongation at yield and impact strength values are expected to decrease with the addition of biomass to the polymer matrix and depicted by the figure 4.25.

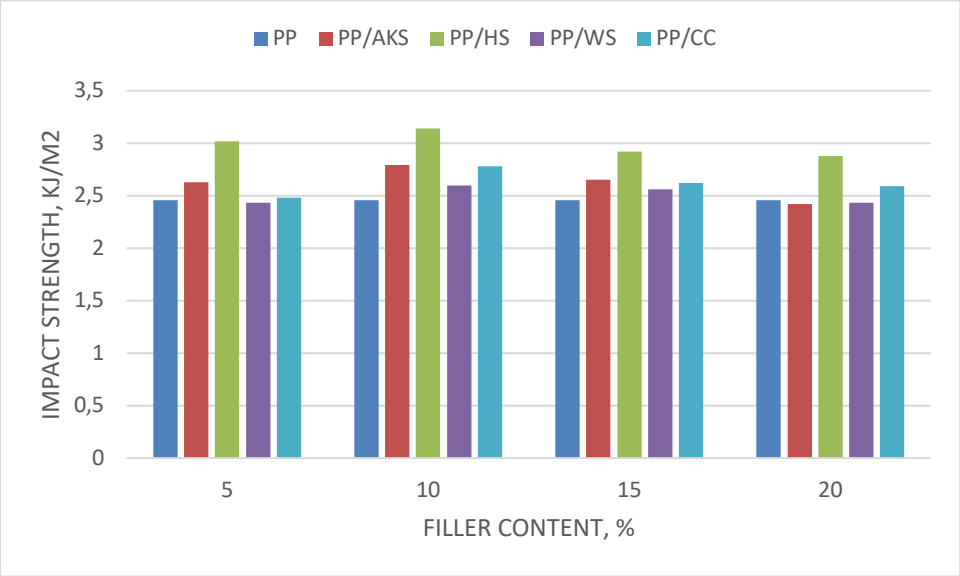

Figure 4.25 : Izod impact strength of Sumitomo PP biocomposites.

The result of flexural modulus figure 4.26 was almost the same as elastic modulus since with the incorporation of the biomass inside the polymer matrix it was expected to increase the stiffness. The more the biomass content, the higher the flexural modulus will be.

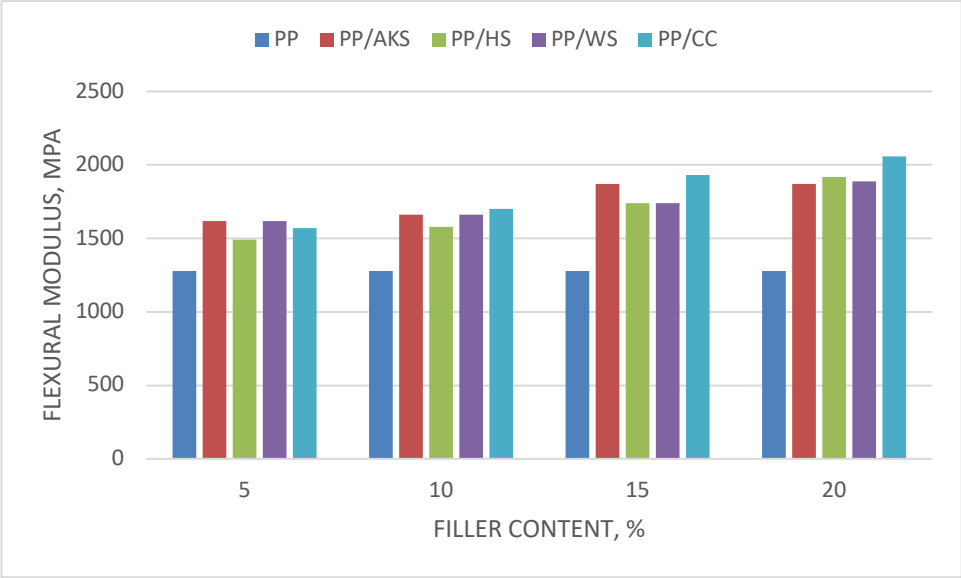

Figure 4.26 : Flexural modulus of Sumitomo PP biocomposites.

4.3.1.4 Rheological Analysis

The following part explains the rheological behavior of biocomposites. The purpose of this analysis is to investigate the behavioral change between platelets in the fluid when they are exposed to shear rate. The changing behavior is dependent on the biomass and compatibilizers inside the polymer matrix. The rheological analysis was performed with a capillary rheometer. The theories behind the capillary rheometer are as follows: A capillary rheometer was an extruder that had a die that ejected the melted polymer at high temperatures and could withstand high pressures. It had a piston that moved downward, compressed the material, and forced it through a narrow capillary die. When the piston moves downward, a shear forms between the wall and the center of the die. The flow was revealed to be laminar. The reason that we need a rheometer is that on different time scales, different effects happen that then need to be characterized by different rates of deformation. Production usually takes place in processes that contain seconds or milliseconds, such as extrusion and injection molding. The slower the process, the slower the rate of deformation will be. For instance, a rotational rheometer can only cover a certain time scale. For fast-scale profiles, a capillary rheometer would be the better option since it can also cover the time scales at milliseconds. In injection molding, the mold filling was affected by the viscosity and geometry of the runner and the cavity. These two parameters affect the shear rates, filling pressure, flow length, and clamping force. There are two kinds of

capillary rheometers for viscosity measurement: the pressure-driven type has constant shear stress, whereas the piston-driven type has constant shear rate.

A capillary rheometer was used for processing studies such as extrudate swell, degradation, and flow instabilities. Polymers are exposed to very harsh conditions throughout the melt processing, including high shear stress that causes a rate of deformation and high temperature that causes chemical conversion, which will lead to molecular degradation, along with flows with confined and complicated geometries. [1]. The melt viscosity of a material will be affected by these structural changes, and hence a change in rheological behavior will occur. The change in viscosity of a material would directly affect the processing conditions. In injection molding, if processing conditions are not arranged with a change in viscosity, short shots happen in high-viscosity cases and flash happens in low-viscosity cases. There are specific or frequently combined chemical and physical alterations that occur during conversion, which include chemical reactions, flow instabilities, and damage that will precisely alter the final polymer's qualities. It was also used to see the effects of biomass, processing aids, and product enhancers such as impact modifiers and stabilizers. In this study, the effects of biomass will be investigated.

The rheometer had a constant (controlled) piston speed, which indicates a constant shear rate, and the higher the viscosity, the higher the resistance to flow of the barrel and the higher the recorded pressure. Viscosity is a function of shear stress over shear rate, which was given in the formulation (4.1) below [1].

$$\eta = \frac{\tau}{\gamma} \tag{4.1}$$

The controlled parameters are piston speed, distance, and temperature, whereas the measured parameter is pressure. Shear stress is a load that causes a material to distort by allowing it to slide across a plane parallel to the applied force. On the other hand, the deformational change of the original length gives the shear strain value. At high shear rates, the layers of fluid glide past one another.

PP and biomass reinforced with a PP matrix act as pseudoplastic fluids that need to be processed at relatively high temperatures to reach an appropriate melt viscosity. Therefore, it necessarily involves a rheological assessment tool that can operate at such temperatures over a wide range of shear rates. As a result, the capillary rheometer was the most basic and widely used rheological device for determining the properties of

polymer rheology [3]. The capillary rheometers can simply be filled without any effort, which is essential when working with highly viscous melts at high temperatures.

Also, the shear rate as well as the geometry of the flow closely reflect the conditions that exist in procedures like extrusion and injection molding [73]. The biomasses like calcium carbonate, kaolin, and talc could create hindrances in the flow behavior and mobility of the polymer matrix chain, particularly at high biomass loadings, and result in a viscosity increase. Another consideration was the shape of the biomass particles, which could be in the form of plates, fiber, needle-like, or cubic. In this study, spherical particles were used to form a composite. These biomass particles could help the polymer flow in a well-dispersed manner, which is important for forming stress concentrators in a material [74].

The neat PP and PP/AKS biocomposites displayed non-linear pseudoplastic behavior during the flow, in which the shear stress of the material increased with increasing shear rate. This is depicted in table 4.14, where all the n values are lower than 1.

Table 4.14 : Flow index values of PP/AKS.

Samples	n (without MAPP)
PP	0.4078
PP/5AKS	0. 4022
PP/10AKS	0,3961
PP/15AKS	0,3805
PP/20AKS	0,3865

The addition of biomass to the polymer matrix increased the shear thinning behavior, and the power law index decreased accordingly. As the shear thinning behavior increases, the mobility of polymer chains increases. Normally, when biomass content increases, there is a higher chance of particles accumulating on top of each other to form agglomerates, which could hinder chain mobility and increase chain entanglement. However, in this case, the addition of biomass reduced the entanglement due to the incompatible nature of biomass and the polymer matrix. Therefore, rather than agglomerate formation, the dispersion of the biomass particles was more prominent, which facilitated the flow behavior and increased the shear thinning of the material. As a result, as the shear rate is applied, the biomass particles promote the flow of platelets without forming an interaction with the polymer matrix. Figure 4.27 depicts the shear stress versus shear rate curve of PP/AKS biocomposites.

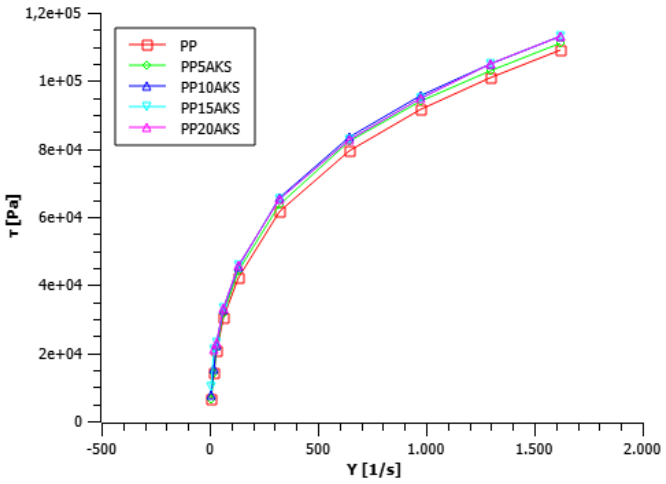

Figure 4.27 : Shear stress- shear rate curve of PP/AKS.

Apart from the investigation of shear stress with the exposure of shear rate, viscosity values were evaluated to see the effect of biomass particles inside the polymer matrix. Table 4.15 depicts the viscosity results of the PP/AKS biocomposites.

Table 4.15 : Viscosity values of PP/AKS.

PP	PP5AKS	PP10AKS	PP15AKS	PP20AKS
1030	1,03E+03	1,19E+03	1,56E+03	1,74E+04
795	7,92E+02	8,62E+02	1,17E+03	8,91E+02
6,40E+02	6,66E+02	6,87E+02	7,10E+02	7,02E+02
4,67E+02	4,85E+02	5,08E+02	5,11E+02	5,09E+02
3,26E+02	3,40E+02	3,49E+02	3,54E+02	3,44E+02
1,90E+02	1,97E+02	2,02E+02	2,01E+02	2,02E+02
1,23E+02	1,27E+02	1,29E+02	1,28E+02	1,30E+02
9 ,43E+01	9 ,66E+01	9 ,85E+01	9 ,74E+01	9 ,88E+01
7,80E+01	7,98E+01	8,13E+01	8,08E+01	8,08E+01
6,73E+01	6,82E+01	6,95E+01	6,95E+01	7,01E+01

When the shear rate was increased, the viscosity of the neat PP and biocomposites decreased progressively. This explains why pseudoplastic materials exhibit shear thinning behavior because increasing shear rate causes chain relaxation and a change in molecular orientation. The deformation caused by the shear disentangles the polymer chain, and the viscosity decreases accordingly.

The addition of biomass particles increased the viscosity of PP. This was because rigid biomass particles could impose and obstruct the flow behavior of the fluid, and hence its viscosity would increase.

The viscosity increase can be seen if there is a superior interaction between the biomass and the polymer matrix. The addition of 5% and 10% AKS biomass increased the viscosity when compared to neat PP. The better the interaction between the biomass and the matrix, the higher the tensile strength value will be. PP/5AKS and PP/10AKS had higher tensile strengths than neat PP. This was also related to the impact strength; these two biocomposites increased the impact strength value, and the better interfacial adhesion increased the viscosity of the material. Moreover, agglomeration can also increase the viscosity of the biocomposite, which was expected at higher biomass loadings. However, since the dispersion of the particles was more dominant than agglomeration, viscosity decreased as the biomass loading increased [75].

Moreover, as the shear rate increases, randomly dispersed particles align in the shear axis, which could facilitate the flow behavior of the material and reduce its viscosity. The orientation of the biomass particles is more randomly distributed at low shear rates and more aligned at high shear rates [75].

4.3.1.5 Morphological Analysis

SEM images were taken to investigate the compatibilization behavior between the AKS and PP matrices. The interaction of biomass with the matrix can be seen in figure 4.28. As the biomass content increased, the pull-out behavior and agglomeration of the biomass particles became more distinct. The intra- and intermolecular forces in the biochemical composition of biomass cause it to agglomerate at higher biomass loadings. Surface roughness was caused by improper dispersion of biomass particles, which then caused them to become more agglomerated. These results also correlated with the impact toughness of the material. While clustered biomass stiffens the material on one side, dispersed biomasses or parts that remain unfilled have higher impact strength, causing instability inside the material. These clustering particles could be seen in the PP/5AKS biocomposite. The impact strength of PP/5AKS was the lowest among other biocomposites. This is caused by improper dispersion of particles, and the small number of particles inside the polymer matrix could cause these instabilities. This could also be confirmed by the thermal values of the PP/5AKS biocomposite. Most of the time, this behavior was seen in materials with high biomass contents, which was also true for this case; PP/20AKS also formed agglomerations inside the polymer matrix.

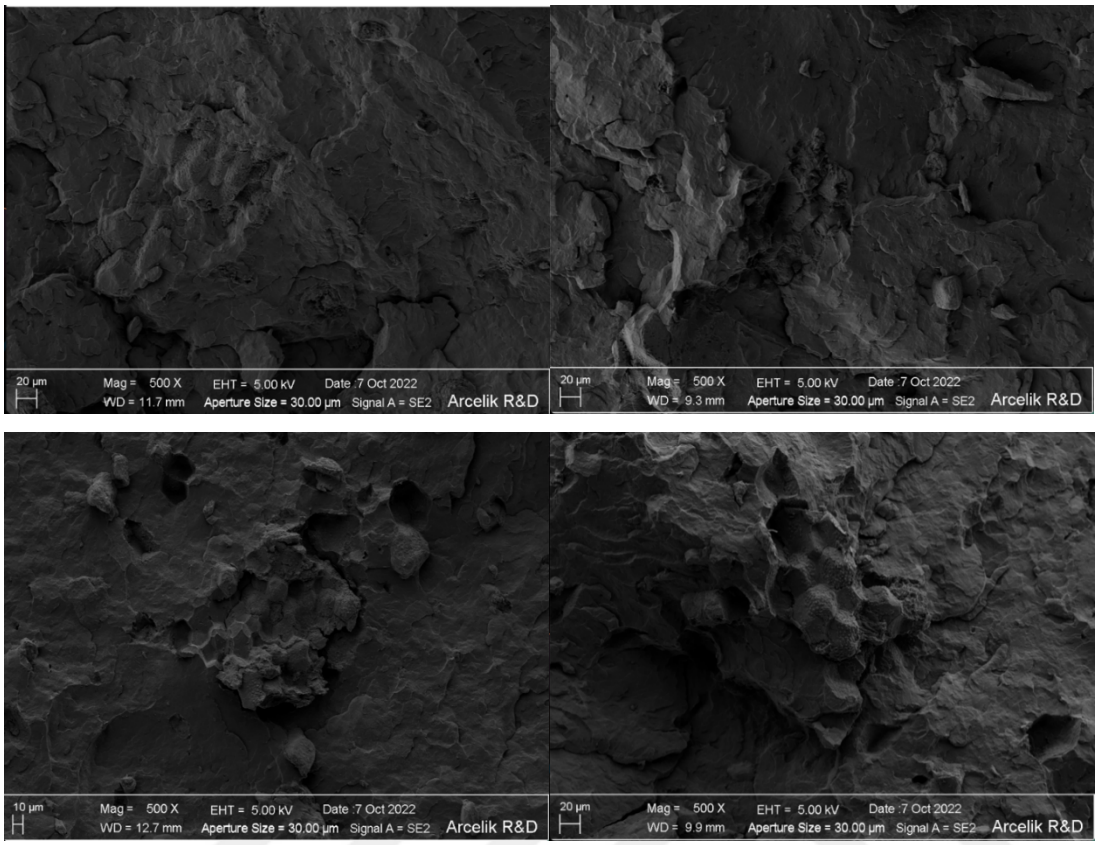

Figure 4.28 : SEM images displaying the interfacial compatibility between AKS and PP matrix.

4.3.2 The effect of compatibilizer on biocomposites

The following section describes the MAPP effect on biocomposites and how it made the biomass and matrix compatible. The root of this biomass and matrix compatibilization is esterification with the aid of anhydride. Anhydrides can be classified into two main categories: cyclic anhydrides (maleic) and non-cyclic anhydrides (such as acetic). For the scope of our project, maleic anhydride will be explained in the following. Maleic anhydride was fundamentally different from other chemical treatments in that it was utilized to improve interfacial bonding in polyolefins made from natural fibers as well as functionalize matrix polymer chains [76].

To look at the features of maleic anhydrite, a rigid, five-membered ring with a persistent dipole moment will serve as a coupling agent between the biomass and the matrix. The interconnection between the anhydrite groups of maleated coupling agents and the hydroxyl groups of those biomasses results in a bond with the polymer matrix. Mainly, through cocrystallization, the polypropylene segments of MAPP

created miscible blends with the bulk polypropylene, and the polar component of MAPP bonded chemically with a polar biomass. The maleic anhydride groups interact as nucleophiles with the biomass particles [77].

The intense interaction providing sites for mechanical anchoring would have also been aided by the surface roughness of biomasses. In addition to the previously reported mechanical anchoring, the development of a powerful link between biomass particles and PP macromolecules could be accomplished. Due to the increased rigidity of the interface, particle debonding from the matrix could be inhibited. The addition of MAPP should considerably decrease fracture toughness, particularly under impact loading conditions. Moreover, it had previously been observed that the inclusion of MAPP in composite formulations alters the crystallization behavior of PP, resulting in a reduction in crystallinity and, consequently, in matrix stiffness, yet we may not always observe a change in Tc, xc, and Tm with the addition of MAPP.

The use of the Scona modifier for MAPP compatibilization changes the mechanical and thermal behavior of the material. It was known for its ability to greatly enhance the mechanical characteristics and lower water absorption of PP natural fiber composites. E modulus values are expected to rise with increasing biomass content, but impact strength falls. The mechanical qualities of the composite material, such as bending strength and impact strength, could be dramatically enhanced using SCONA coupling agents, which significantly strengthen the bonding of biomass with the polymer matrix. Additionally, surface quality and resistance to higher temperatures are anticipated to improve. These types of modifiers are typically non-polar base polymers that undergo functionalization through grafting with various monomers. Maleic acid anhydride-modified polypropylene and polyethylene are the modifiers utilized in wood-plastic composites (WPC). The chemical structure of WPCs was like that of the natural biomasses used in this research. Therefore, the same types of modifiers are applicable for both cases. The traditional method was to graft the polymers with the monomers in the melt. However, all SCONA products are made utilizing a patented solid-phase process. A higher level of functionalization was attained via solid-phase grafting, which reduces the amount of modifier that must be present in the compound.

The amount of organic volatile organic compounds (VOC) in the products made with this process was remarkably low. Additionally, the base polymer of the modifier

experiences less damage due to the low process temperature, and the superior mechanical capabilities of the compound are reflected by the increased molecular weight that results from this. In the case of melt grafting, the degree of grafting (% w/w MAA) was in the range of 1 and 1.25 w/w%, whereas in the solid phase the degree of grafting was 1.4 w/w%. Therefore, this modifier was produced by the solid-phase process. The mechanism involves the creation of a chemically stable molecule when the maleic anhydride groups of the modifier react with the OH groups of the biomasses. The functional groups (anhydrides) that exist on the polymer backbone chemically react with OH groups to create stronger bonds. The reaction of alcohols and anhydrides forms esters as the principal product. As a result of the substitution reaction between a carboxylic acid and an alcohol, an ester molecule forms from an acid that has at least one OH group that is displaced by an OH-alkyl (alkoxy) group.

Esters had a carbonyl connecting oxygen function with two alkyl or aromatic groups. Esters can be displayed as R-COOR in text. The consequence was that the fibers were properly integrated into the matrix material, which greatly enhanced the mechanical characteristics and weather resistance of the desired product. It was critical to have the highest attainable MAH content in the coupling agent. The higher the degree of grafting, the lower the coupling agent necessary for the surface wetting of a biomass. To illustrate, wax has a greater degree of grafting, yet having a lower molecular weight than other materials cause a decrease in mechanical strength. When substituting a coupling agent with a low MAH content for a material with a greater MAH content, it was crucial to alter the amount in the present formulation. If not, the anticipated enhancement in mechanical behavior following the substitution would not happen or might even cause the values to degrade. In the study, it was proven that a coupling agent containing 0.74% MAH was used at a concentration of 3%. The bending strengths of the product are nearly equal when the same amount of a coupling agent with 1.72 MAH is employed instead. The final product had improved mechanical characteristics when the latter coupling agent was lowered to 2%.

The MAH content of the composite was always a crucial component. A far higher concentration (about 5%) was conceptually required for the modifier with reduced MAH content, but the modifier with more grafting can reach this threshold at concentrations as low as 2%. The precise values vary depending on the raw materials

utilized and each user's unique requirements. Therefore, it was usually better to examine a range of concentrations to find the ideal amount. In this research, the optimum concentration had been investigated and found to be 2%, which was the right dosage for our application.

4.3.2.1 Spectroscopic Analysis

MAPP has two distinctive peaks at 1775 cm^{-1} and around 1856 cm^{-1}. However, the addition of MAPP inside the AKS changed its distinctive peak from 1775 cm^{-1} to 1740 cm^{-1}. This is because the functional group inside the MAPP opened its ring structure to form an ester bond with the biomass. Since some of the peaks changed due to the alteration of the size and angle of the bond, we observed symmetric and asymmetric changes in the peak.

When Borealis PP is compounded with MAPP, we observe a peak at 1740 cm^{-1}. This means that MAPP reacts with AKS and forms an ester peak. This also suggests that MAPP formed cross-binding interactions with other molecules found in the OH groups of AKS. The isotacticity ratio of Borealis PP appeared to be higher. The addition of MAPP to the Borealis PP matrix increased the crystallinity values, which were analyzed by the DSC curve. Thereby, MAPP improved the properties of Borealis PP biocomposites.

The isotacticity of Sumitomo PP is lower than Borealis PP. This directly affects the crystallinity of the polymer compound. The DSC curve of Sumitomo PP biocomposites showed that, the addition of MAPP into the polymer matrix decreased the Xc values. There was only one exception, which was PP/20AKS/MAPP. Having a high content of AKS inside the polymer compound may create compulsory distribution inside the polymer matrix, and hence MAPP could not form clusters. Consequently, MAPP improved the crystallinity of the Sumitomo PP/20AKS/MAPP biocomposite.

When MAPP was added to the compound, the existence of this molecular structure was found in some of the places in the PP matrix. At those specific parts, if MAPP binds only with biomasses rather than the PP matrix, this could result in the formation of weak spots in the biocomposite because the connection between MAPP and the biomass might form clusters at those parts, and disordered particle distribution affects other properties such as impact strength. The results of Sumitomo PP biocomposites resulted in lower impact strength values with the addition of MAPP. As a result, when

biomass was added to the more isotactic PP, it contributed to the crystallinity of the biocomposite.

The addition of MAPP decreased the isotacticity of Borealis PP/AKS biocomposites. In MAPP added biocomposites with Sumitomo PP, PP/AKS/MAPP showed that the highest isotactic number belonged to PP/15AKS/MAPP. Moreover, the isotacticity increased with increasing biomass content until PP/15AKS/MAPP. In PP/5AKS and PP/20AKS biocomposites, the isotacticity decreased with the addition of MAPP, whereas in PP/10AKS and PP/15AKS biocomposites, MAPP increased the isotacticity, and the increase in PP/15AKS/MAPP was drastic. The isotactic ratios of PP/5AKS/MAPP and PP/20AKS/MAPP were almost the same. The highest isotacticity of PP/CC/MAPP biomass was PP/20CC/MAPP. The isotactic values increased in PP/5CC/MAPP and PP/20CC/MAPP. In PP/HS biocomposites, there was only an increase in isotacticity in PP/20HS/MAPP. However, the only improvement in terms of isotacticity occurred in PP/WS/MAPP biocomposites, in which all the materials showed an increase in isotacticity with the addition of MAPP. In general, those with at least 20% or low biomass content had a lower atactic rate, that is, a higher crystalline rate, than the 5–10% biomass-filled ones. Moreover, Borealis PP had a higher atactic ratio than Sumitomo PP, as illustrated by Figure 4.29.

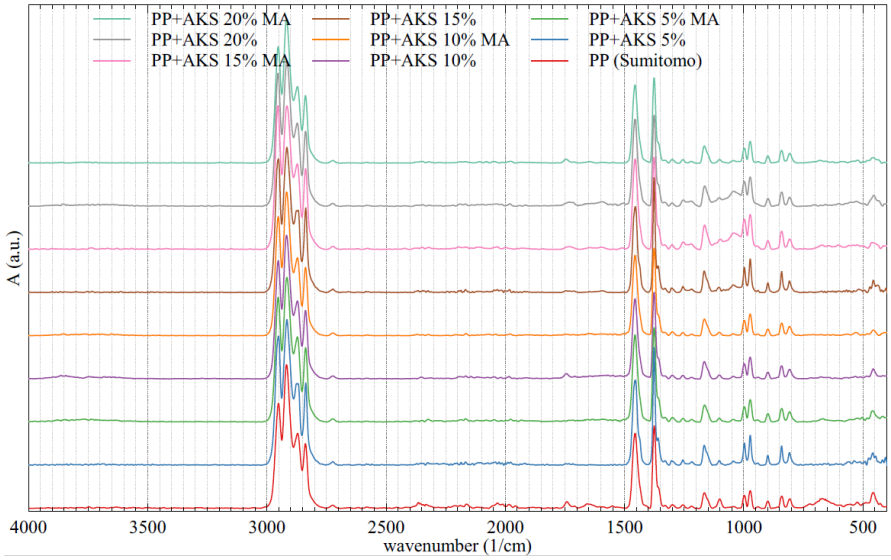

Figure 4.29 : FTIR spectra of neat PPs and their biocomposites.

4.3.2.2 Thermal Analysis

The following part continues with the thermal behavior of biocomposites. Initially, the biocomposites with Borealis PP were investigated, and then the materials with Sumitomo PP were investigated.

The compatibilized Borealis PP was investigated and compared with uncompatibilized biocomposites. In unfilled PP, there was only one decomposition step, and MAPP added compatible composite [66]. Another expectation was to lower the water content that was coming from the biomass itself, and the incorporation of compatibilizer into the polymer compound reduced the water loss, which means the amount of water content was lower in the PP/20AKS/MAPP polymer composite. In PP/20AKS/MAPP, the compatibilizer evenly distributed the biomass into the polymer matrix, and since there was no first two-step degradation in the DTG curve, it can be said that no depolymerization occurred in comparison with the uncompatibilized biocomposites. Table 4.16 depicts the mass loss steps of uncompatibilized and compatible PP/20AKS biocomposites.

Table 4.16 : Mass loss steps of PP and PP/AKS biocomposites.

Sample	T100 (˚C)	T200 (˚C)	Tmax (˚C)	(%) Residue at 600˚C	(%) Residue at 900 ˚C
PP	0,1162	0,0836	429	0,08	-
PP/20AKS	0,0856	0,6524	465	3,90	1,44
PP/20AKS/MAPP	0,1223	0,01	453	0,84	0,92

Moreover, when the material was compatibilized it was expected to have a higher Tmax value. However, while PP/20AKS had a higher Tmax value of 465°C, the compatible PP/20AKS/MAPP had a lower Tmax value (453°C). This may be due to the modified one having a reactive center (Man) and the chain can be broken more easily from there.

To investigate the melting and crystallization behavior of the biocomposites, there are different factors that affect these behaviors when MAPP is added to the compound [67]. MAPP is considered to have a low molecular weight, and when it is combined with a high molecular weight polymer, which is PP in our case, it could have a lubricant effect. The lubricant effect facilitates the flow behavior of the polymer and melting the polymer would become easier. In the case of Borealis PP biocomposites,

Tm decreased with the addition of MAPP, which indicates that MAPP could act as a lubricant. Another effect of MAPP is to bind anhydride groups to hydroxyl groups in biomasses and form covalent and acid-base interactions between them. If there is a good interaction between anhydride and hydroxyl groups, it limits the flow behavior and decreases the chain mobility. This could be the reason to obtain high Xc values in a compatible biocomposite. The third factor could be related to the interconnection of anhydride groups with each other. If MAPP molecules are not far from each other, meaning if MAPP is not distributing properly in the compound, it could result in the binding of anhydride groups within themselves. However, this fact could also improve the crystallinity of the biocomposite. Furthermore, PP has proper chain alignment without MAPP, and MAPP disembodies the chain regularity and inhibits crystallization, where it can form defects in crystallite formation. The formation of defects in the crystal structure of PP may lower the Tm values. The peak of molten PP becomes lower during cooling and has a higher peak in the case of compatibilized biocomposites. This could result in a slower crystallization degree of the biocomposite due to the incorporation of MAPP.

The DSC curve of the compatibilized Borealis PP biocomposite revealed that it had the largest crystallinity of all. As a result, due to the crystallinity effect, the material will have high molecular bonding, proper alignment, and oriented chains, and an increase in tensile strength will occur, which was also confirmed by comparing the tensile strength values of uncompatibilized versus compatibilized biocomposites. Table 4.17 illustrates the thermal transition temperatures of uncompatibilized and compatible PP/20AKS biocomposites. The increase in Tm_{onset} with the addition of MAPP showed that the compatibilizer increased the thermal stability of the biocomposite, yet neat PP had a higher Tm_{onset}. The increase in ΔHm and Xc indicated that more thermal energy was required when the material was exposed to temperature due to the high interfacial compatibility of the biomass and the polymer matrix. The high amount of Xc indicated that the increase in interfacial compatibility created hinderance between the polymer chains, and the molecular structure became more compact and aligned with the aid of the compatibilizer.

Table 4.17 : Tm_{onset}, Tm, ΔHm, and Xc values of Borealis PP and PP/AKS biocomposites.

Sample (%)	Tm_{onset} (˚C)	Tm (˚C)	ΔHm (J/g)	Xc (%)
PP	157,20	167,66	207	100
PP/20AKS	154,38	170,06	86,05	41,54
PP/20AKS/MAPP	155,15	169,29	98,16	47,42

Up to this point, the thermal behavior of Borealis PP biocomposites had been investigated. The following section explains the thermal behavior of Sumitomo PP biocomposites. Figure 4.30 depicts the TGA curve of Sumitomo PP and its biocomposites.

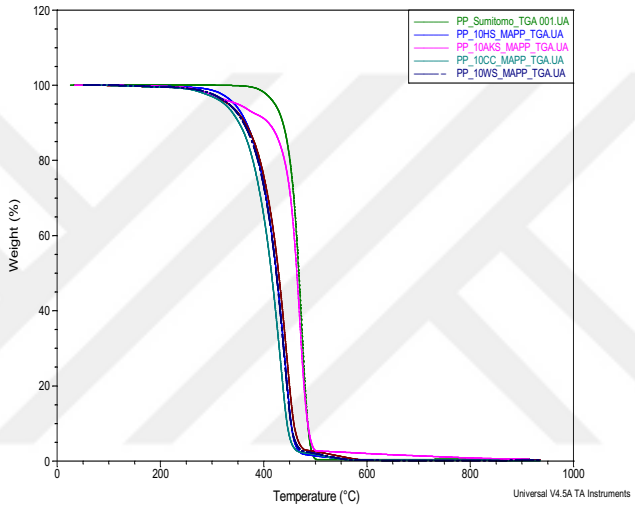

Figure 4.30 : TGA curve of Sumitomo PP compatibilized biocomposites.

The addition of MAPP increased the overall thermal stability of the biocomposites except for PP/5AKSMAPP. The thermal stability of PP/5AKS was higher than PP/5AKSMAPP. This may be because having fewer and fewer particles inside the polymer matrix did not cause any problems in uncompatibilized biocomposites because there was no binding between the biomass and the polymer matrix. This could also be seen from the differences between the impact strengths of compatibilized versus uncompatibilized PP/5AKS biocomposites. However, when MAPP was added, the bound biomass was expected to increase interfacial compatibility, but since there are fewer particles inside the polymer matrix, poor distribution may cause one side of the material to be stronger and the other side weaker, which could also affect the toughness of the biocomposites. Even though the mass loss of PP/15AKS/MAPP was

largest until 450 °C, after that temperature, its thermal stability was the same as neat PP and was higher than other biocomposites.

The same unexpected behavior occurred in PP/5HS/MAPP and PP/5AKS/MAPP, in which the addition of MAPP decreased the overall thermal properties of biocomposites, which was due to the low content of the biomass creating an instable rough surface that directly affected the impact properties of the material. The mass loss of PP, 20HS, and MAPP happened more slowly. At Tmax, PP/20HS/MAPP had a broad mass loss curve, whereas the other biocomposites and neat PP had sharp mass loss. There was no change in Tonset for PP/20HS/MAPP yet; after 400 °C, the broad mass loss change was attributed to the higher thermal stability of the biocomposite. Therefore, the addition of MAPP clearly improved the thermal stability of PP/20HS/MAPP after 400 °C. Moreover, even though the best properties were expected from PP/10HS/MAPP, PP/20HS/MAPP had a higher improvement in thermal stability at 420 °C, but still the mass loss at Tonset was larger, which was due to the high biomass content in biocomposite.

The thermal stability of PP/5WS/MAPP was higher than that of the uncompatibilized version and neat PP. This could be attributed to the proper dispersion and strong binding of biomasses, which improved the thermal properties of biocomposite materials. Because of the mechanical properties, this behavior acted in the opposite direction. PP/5HS had a higher impact strength than PP/5HS/MAPP, but the decrease in impact strength was not much in comparison with PP/5AKS and PP/5HS biocomposites. Therefore, a slight decrease in impact strength did not affect the thermal properties of PP/5HS/MAPP, yet a distinct decline also decreased the thermal behavior of PP/5AKS/MAPP and of PP/5HS/MAPP. The addition of MAPP to PP/10WS decreased the thermal properties of the biocomposite but improved PP/20WS. The mass loss after 400 °C started earlier in PP/10WS/MAPP, and hence PP/20WS/MAPP was better later at that temperature. In PP/CC, when the biomass content increased, the thermal stability decreased. The addition of MAPP lowered the thermal stability of PP/10CC and PP/20CC biocomposite. In the case of Borealis PP/AKS biocomposites, the best acting material was PP/10AKS. Therefore, the biocomposites made with Sumitomo PP were first investigated by PP/10AKS. Figure 4.31 shows the uncompatibilized and compatibilized PP/10AKS biocomposites.

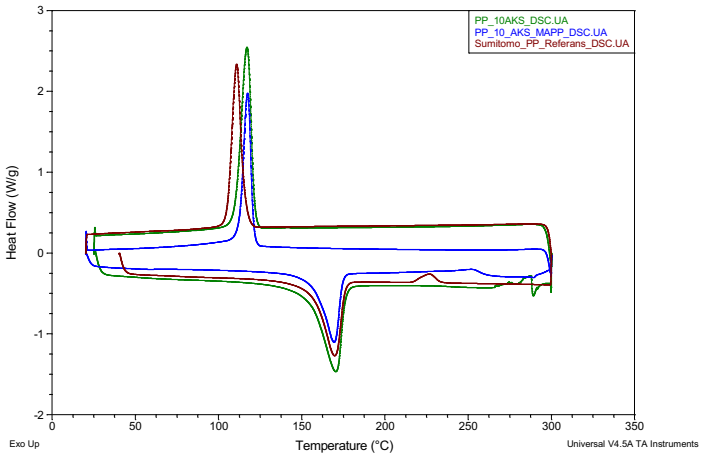

Figure 4.31 : DSC graph of lignocellulosic biomass filled Sumitomo PP biocomposites.

The Tm and Xc of Sumitomo PP were calculated as 166.62 °C and 36.48 %, respectively. There was no Tg obtained from the thermogram of PP [78]. There was no change in Tm_{onset} values with the increase in biomass content. The addition of biomass reduces chain mobility and makes the thermal decomposition of the biocomposite much more difficult, resulting in higher Tm values [79]. Because highly bonded and connected polymer chains are stronger and more difficult to melt, physical crosslinking increases Tm values. This is also true for Xc values since crystallinity increases with a decrease in polymer chain mobility. The behavior of the biomass nucleating agent caused polymer chain hinderance and increased Xc values. Lower biomass content usually results in less hinderance and lower crystallinity. However, even though the lower biomass content of the biocomposite was PP/5AKS, it had the highest Tm, Hm, and Xc values. This could be because there was no proper distribution and dispersion of particles, which resulted in more chain immobility and, hence, high thermal energy and high temperature were required to initiate crystallization [66]. The Tm of the compatibilized biocomposites decreased when compared to the uncompatibilized PP/AKS biocomposites. The only increasing value was from Tm to PP/10AKS/MAPP. This means the addition of MAPP provides more chain alignment and increases the thermal stability of the biocomposite.

The effects of compatibilization lower the Tm values by causing more defects in MAPP crystals and facilitating the melting behavior. Hm and Xc values also decreased with decreasing Tm when MAPP was added to the compound. The only differences among biocomposites belonged to PP, 20AKS, and MAPP. The only increase was

observed in the Xc and Hm values of this compatible biocomposite. This could be the reason: in environments with high biomass content, biomass tends to cluster within itself, and anhydride groups bind with each other. As a result, each particle has the same molecular structure. This may cause a hindrance due to the interconnection of the same molecules, as there is no intramolecular connection between anhydride and hydroxyl groups of biomasses. As a result, the separate and poor interconnection may result in increased interconnectivity. Table 4.18 shows the results of PP/AKS/MAPP biocomposites.

Table 4.18 : Tm_{onset}, Tm, ΔHm, and Xc values of Sumitomo PP and PP/AKS/MAPP biocomposites.

Sample (%)	Tm_{onset} (˚C)	Tm (˚C)	ΔHm (J/g)	Xc (%)
PP	156,66	166,62	76,53	36,48
PP/5AKS/MAPP	153,73	170,38	75,54	36,49
PP/10AKS/MAPP	157,73	169,41	63,03	30,44
PP/15AKS/MAPP	153,50	168,35	69,07	33,36
PP/20AKS/MAPP	154,38	168,91	69,54	33,59

The incorporation of MAPP into the PP/HS significantly reduced the overall Xc values shown in Table 4.19, indicating that cluster formation occurs within the polymer compound. Usually, it was expected that there would be an increase with the incorporation of MAPP. The cluster formation may result in lower crystallinity values. The reactive hydroxyl groups are lower in HS, in which there is a low content of cellulose and hemicellulose. The hydroxyl groups of cellulose had reactive binding sites. A low concentration of this component may reduce MAPP and HS binding. Moreover, the extractive amount of HS is highest among biomasses. The extractives may inhibit the binding of MAPP and HS by restricting the availability of binding sites for HS. As a result, MAPP may have caused hinderance within the polymer compound and decreased crystallinity values while having no effect on isotacticity.

Table 4.19 : Tm_{onset}, Tm, ΔHm, and Xc values of Sumitomo PP and PP/HS/MAPP biocomposites.

Sample (%)	Tm_{onset} (˚C)	Tm (˚C)	ΔHm (J/g)	Xc (%)
PP	156,66	166,62	76,53	36,48
PP/5HS/MAPP	161,04	168,08	34,03	16,43
PP/10HS/MAPP	156,33	169,59	68,55	33,11
PP/20HS/MAPP	156,07	168,03	37,78	18,25

The addition of MAPP to the PP/WS biocomposites increased the Xc values depicted in Table 4.20. In comparison with PP/HS biocomposites, the addition of MAPP contributed to the biocomposite in terms of crystallinity.

Table 4.20 : Tm_{onset}, Tm, ΔHm, and Xc values of Sumitomo PP and PP/WS/MAPP biocomposites.

Sample (%)	Tm_{onset} (˚C)	Tm (˚C)	ΔHm (J/g)	Xc (%)
PP	156,66	166,62	76,53	36,48
PP/5WS/MAPP	158,12	169,64	56,79	27,43
PP/10WS/MAPP	157,16	169,27	65,60	31,69
PP/20WS/MAPP	157,96	168,84	68,75	33,21

The same situation goes for this biocomposite as well; the addition of MAPP decreased the Xc, indicating less isotacticity of Sumitomo PP, which affected the alignment of the polymer chains. Table 4.21 DSC diagram showed that, in high biomass content, the size of the Tm peak was broader, and Tm was lower, meaning that in high biomass content, we observe more flaws in PP crystals.

Table 4.21 : Tm_{onset}, Tm, ΔHm, and Xc values of Sumitomo PP and PP/CC/MAPP biocomposites.

Sample (%)	Tm_{onset} (˚C)	Tm (˚C)	ΔHm (J/g)	Xc (%)
PP	156,66	166,62	76,53	36,48
PP/5CC/MAPP	156,50	171,78	64,57	31,19
PP/10CC/MAPP	156,45	164,16	78,87	38,10
PP/20CC/MAPP	156,25	169,75	72,82	35,17

4.3.2.3 Mechanical Analysis

The more organic waste we use in the compound, the more waste we convert, and the less plastic will be used. As a result, a compatibilizer was initially used in a 20% biomass biocomposite. The MAPP used in this study acts as a polymer modifier and coupling agent for cellulose-fiber-filled polypropylene, resulting in lower water uptake and higher tensile and flexural strengths [76]. Another coupling agent was also used to see the difference between two brands of the same product. Polybond 3200 and Scona 8112 TPPP were first tested in one biocomposites filled with AKS to determine the better-acting MAPP for the biocomposites. Table 4.22 illustrates the differences in mechanical strengths of Polybond 3200 and Scona TPPP 8112 MAPP.

Table 4.22 : Comparison of different grades of MAPP.

Mechanical Tests	PP (Borealis he125mo)	PP/20AKS/2mapp (Polybond 3200)	PP/20AKS/2mapp (Scona 8112 TPPP)
σ_{TS}	33,69	24,66	31,19
ε_f	7,74	3,53	9,48
σ_y	30,19	24,99	32,45
ε_y	13,68	3,24	6,07
E	1525	1586	1579
E_{frac}	3	2,31	2,91
σ_{Flex}	40	42,3	43,7
E_{flex}	1120	1370	1390

As it can be seen from the results, two different grades of MAPP resulted in different mechanical properties. Scona modifiers gain better mechanical properties for the biocomposite. This could be because of the mah content, in which Scona modifier exhibits more mah content than Polybond modifier. Moreover, the scona modifier adds one additional and important feature to the material, which is its low water absorption capability. During processing, the absence of a degassor in the extruder creates air bubbles due to the moisture inside the organic waste. Those air bubbles degrade the mechanical properties of the biocomposite. The use of the Scona modifier may have lowered this problem, and as a result, it gave better mechanical properties in comparison to Polybond 3200. The addition of a compatibilizer increased the tensile strength, elastic modulus, and impact strength. The compatibilizer also increased the elongation at break value, and hence there was a decrease in flexural strength and flexural modulus. The highest-filled compatibleized biocomposite had the worst performance. Because the Scona modifier improved the mechanical properties of PP/20AKS, the chosen MAPP was used for the other biomasses as well. Table 4.23 illustrates the mechanical test results of 20% filled, compatibilized PP biocomposites.

Table 4.23 : Mechanical test results of 20% biomass filled compatibilized PP biocomposites.

Samples	σ_{TS}	ε_f	σ_y	ε_y	E	E_{frac}	σ_{Flex}	E_{flex}
PP	33,69	7,74	30,19	13,68	1525	3	40	1120
PP/20AKS/mapp	33,23	5,19	32,54	6,22	1801	3,09	46,1	1430
PP/20HS/mapp	30,6	4,92	31,38	4,06	1878	2,81	45,2	1590
PP/20WS/mapp	31,06	4,51	31,57	3,93	1943	2,93	45,2	1540
PP/20CC/mapp	33,65	4,19	33,89	3,93	1976	3,28	50,7	1750

Tensile and impact strength had increased in all cases when the effect of the compatibilizer was examined. Elastic modulus and flexural modulus are also

increased, except for the apricot kernel shell-filled biocomposite. Elongation at break value was expected to decrease after the biomass addition, and it did so for all three cases except the apricot kernel shell-filled composite. The behavior of the apricot kernel shell composite was different from the other bio-filled composites. This was maybe due to the higher number of impurities, so those impurities like wax, oil, and pectin would inhibit the bond formation between MAPP, the apricot kernel shell, and the polymer matrix.

The compatibilized biocomposites display better tensile strength than uncompatibilized biocomposites at the same biomass content. The inclusion of MAPP, in which anhydride groups form covalent connections with the hydroxyl group of the biomass surface, gives compatibilized biocomposites their increased tensile strength. Such greater biomass-matrix contact and adhesion results in greater biomass-to-matrix stress transmission, which results in higher tensile strength.

Compatibilized organic waste-filled composites exhibit less elongation at break than uncompatibilized ones at equivalent reinforcement content. Due to better adhesion between the corn cob and the polypropylene matrix and reduced polymer mobility, the incorporation of MAPP into the composites reduced the elongation at break. It's also likely that the materials were even more brittle due to the increased stiffness of the biomaterials after the incorporation of MAPP.

At equivalent organic waste loads, the compatibilized biocomposites display greater elastic modulus than the ones that had no compatibilizer inside since MAPP provided proper biomass dispersion in the polymer matrix while also improving stress transmission at the composite interface.

Because we couldn't find the Borealis he125mo PP, we continued our search with the Sumitomo PP brand. The findings differed from those of the previous study. The mechanical test results of 5%–10%–15%–20% biomass-filled PP and compatible versions of biocomposites are depicted in figure 4.32. It was clear that the use of MAPP increased the tensile strength values of the biomass-filled PP biocomposites. The effect of MAPP was substantial in the case of PP/AKS biocomposites, in which the largest improvement occurred in their properties. Explicit improvements were also achieved in PP/CC biocomposites by the addition of MAPP, secondarily. The tensile strength

values of the biocomposites were almost the same without the use of compatibilizer. The difference between the use of compatibilizer and not using it was largest in PP/5AKS and PP/15CC biocomposites. Therefore, the highest utilization was obtained in PP/AKS and PP/CC biocomposites when MAPP was added to the compound.

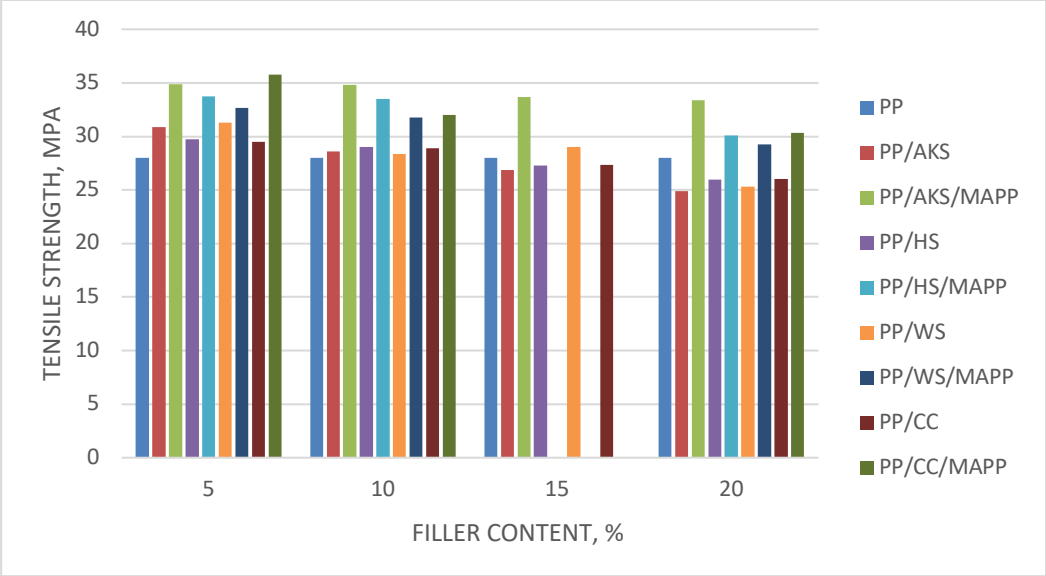

Figure 4.32 : Tensile test of Sumitomo PP biocomposites.

The compatibilized materials act differently than one another; in some cases, the compatibilizer reduced the elastic modulus, and in other cases, it was vice versa. This could be attributed to the proper mixing of MAPP with the biomass and matrix. The effect of the compatibilizer was apparent in PP/AKS and PP/CC biocomposites, meaning there was a better interaction in these polymeric materials. The best modulus of elasticity values was obtained in PP/20AKS/MAPP and PP/20CC/MAPP, respectively. Figure 4.33 shows the elastic modulus of Sumitomo PP biocomposites.

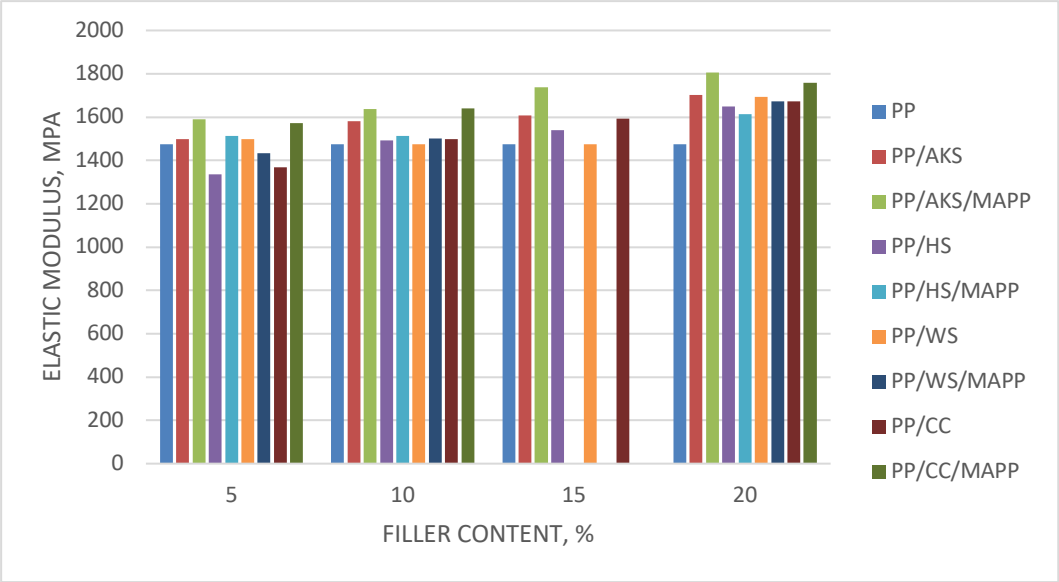

Figure 4.33 : Elastic Modulus of Sumitomo PP biocomposites.

The interesting case in figure 4.34 was that with the addition of MAPP to the compound, the impact strength values decreased when compared to those without compatibilizer, which also happened in the elongation at break and elongation at yield values.

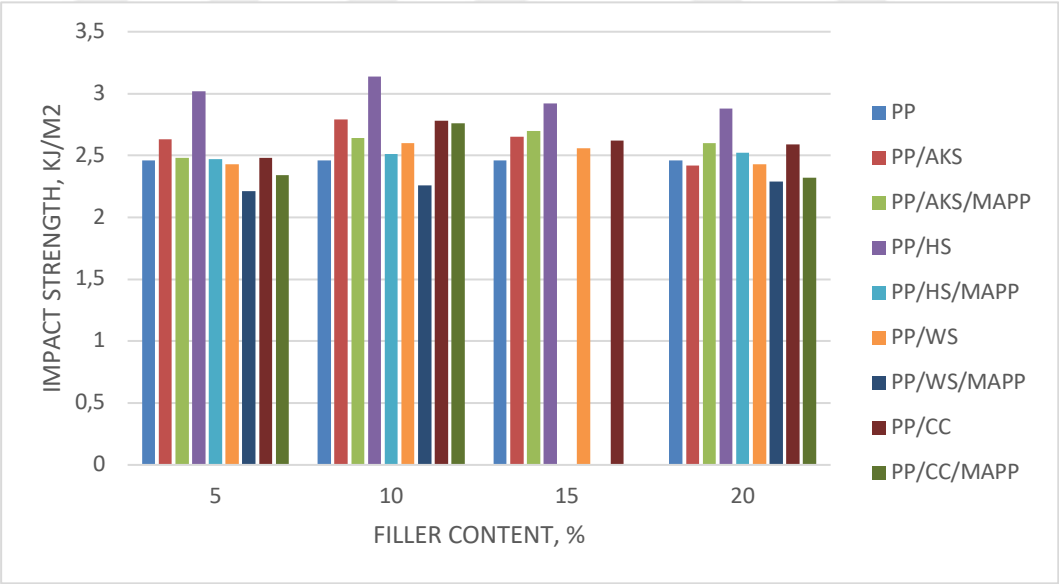

Figure 4.34 : Impact Strength of Sumitomo PP biocomposites.

Moreover, the compatibilized versions of biocomposites resulted in better flexural strength, as depicted in Figure 4.35. The highest results for incompatibilized and compatibilized biocomposite came from PP/CC and PP/CC/MAPP.

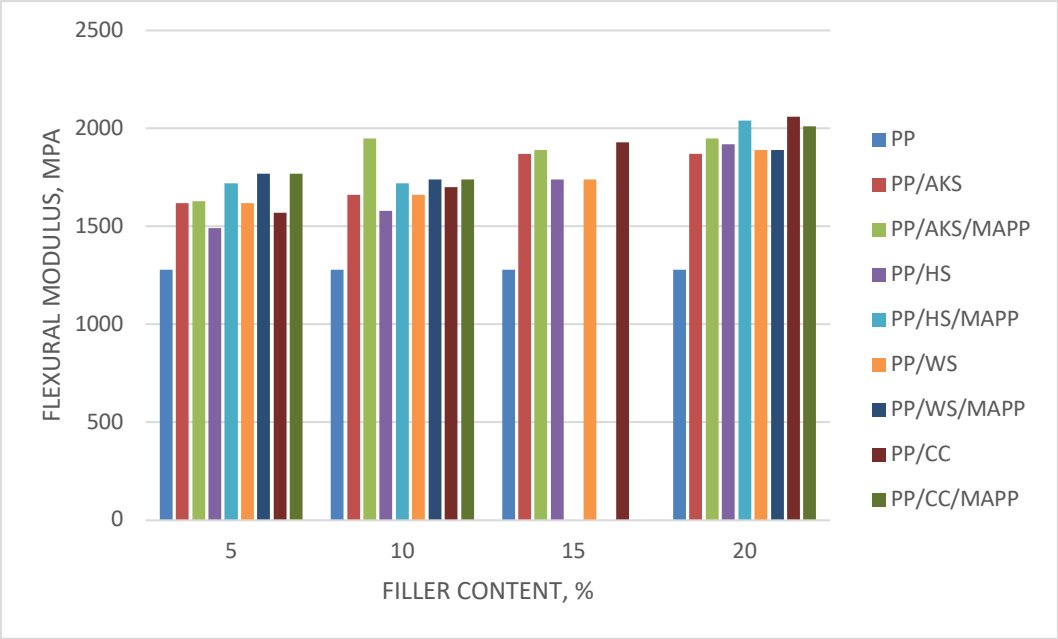

Figure 4.35 : Flexural modulus Sumitomo PP biocomposites.

4.3.2.4 Rheological Analysis

In the rheological part of the study, the compatibilized biocomposites were also investigated. The literature was reviewed to see the effect of the compatibilizer inside the polymer compound. Ariff et al. compare the flow behavior of kaolin-filled PP with and without MAPP coupling agents. The polar nature of kaolin inhibits the dispersion of the kaolin particles in the nonpolar PP matrix. When particles cannot be distributed well, it also disrupts the flow of the material and hence increases the viscosity, whereas the incorporation of MAPP facilitates the flow of the material and decreases the viscosity. Since kaolin and PP are not compatible with each other, with increasing biomass content, there will be an obstruction in the flow and the viscosity will be higher.

One study investigated the rheological behavior of treated and untreated bagasse fiber ash on polylactide matrices. The study revealed that wall shear stress decreased with increasing biomass content. The treated fibers in the composite had higher shear stress values than the untreated ones. They also found that the viscosity of the material decreased when the shear rate increased, which shows a shear thinning of the material and decreased viscosity with increasing biomass content. The treated fibers had a higher viscosity in comparison to the untreated ones in the biocomposite. When fibers were treated, the intercalation feature resulted in an increase in viscosity values [80]. Another study worked on the rheological behavior of blended short sisal fiber and glass

in low density polyethylene composites. The viscosity of the composite increased as the glass fiber content increased. The glass fiber is more compatible with the polymer matrix than short sisal fiber, and hence the compatibilized material had a higher viscosity due to the interaction between the biomass and the matrix [75]. Ogah et al. revealed that the shear rate complies with the power law equation and the agrofiber-filled high-density polyethylene shows shear thinning behavior as the biomass content increases [81]. The shear stress–shear rate curve of PP/AKS/MAPP biocomposites was drawn. Those with and without compatibilizers were compared within themselves. The evaluation of their behavior was determined by the flow index values (n) given by the equation, which are shown in table 4.24.

Table 4.24 : Flow index values of AKS filled PP biocomposites.

Samples	n (without MAPP)	n (with MAPP)
PP	0.4078	0.4078
PP/5AKS	0.4022	0,4179
PP/10AKS	0,3961	0,3839
PP/15AKS	0,3805	0,3995
PP/20AKS	0,3865	0,3882

The maximum difference occurred in the PP/20AKS, which was farther in terms of its distance from neat PP, and for compatibilized graphs, the maximum difference could be seen in the PP/10AKS/MAPP. Among all, the minimum flow index value occurred at PP/10AKS/MAPP, which was also related to the highest shear thinning behavior. The reason for the absence of shear thinning in this biocomposite was that it had the best compatibilized version among the others. In the previous cases, after 10% filling, the thermal and mechanical behavior of biocomposites decreased due to the possibility of agglomerations. Therefore, this situation could be attributed to this behavior, in which we could observe the best outcome from this biocomposite. The addition of MAPP compatibilizer inside the matrix decreased the viscosity of the polymer melt. As a result, compatibilizers reduced the accumulation of biomass particles on top of each other while limiting their hinderance and promoting the biocomposite's flow behavior. This also confirmed the tensile strength results, in which compatible biocomposites had higher tensile strength values than the ones without compatibilizer. When the biocomposites are put through the tube, they must go downward as the piston pushes toward them to compress the material. The material, however, tends to move upward and reject from the tube prior to piston compression. The material must be free

of moisture and air bubbles created by moisture must be pushed towards the capillary tube because when the high-temperature area contacts the damp material, the gas creates a vapor pressure and pushes the material out of the tube. During the processing, the air bubbles inside the granules were formed and were caused by the moisture absorptivity of the material. Without a degasser inside the extruder machine, the air bubbles are continuing to create defects, which will also impact the measurement in the capillary rheometer by ejecting the material out of the tube. The addition of a compatibilizer eased this problem, and hence it was easier to place the material into the tube with a slightly lower rejection from the plunger than without a compatibilizer.

4.3.2.5 Morphological Analysis

SEM images were taken to investigate the compatibilization behavior between the AKS and PP matrices. The interaction of biomass with the matrix can be seen in figure 4.36. The use of the Scona modifier improved the particle-matrix interaction. The biomasses inside the polymer matrix detached from the composite itself without the Scona modifier, and hence the pull-out behavior of the biomasses was observed. The compatibilization of the biomass and the polymer matrix inhibits clustering and aids in the proper dispersion of particles. As a result, the interaction between the AKS and the functional anhydride group of the maleic anhydride grafted polypropylene strengthens, resulting in a smooth surface. The increase in mechanical properties of compatible biocomposite materials also confirms this depiction.

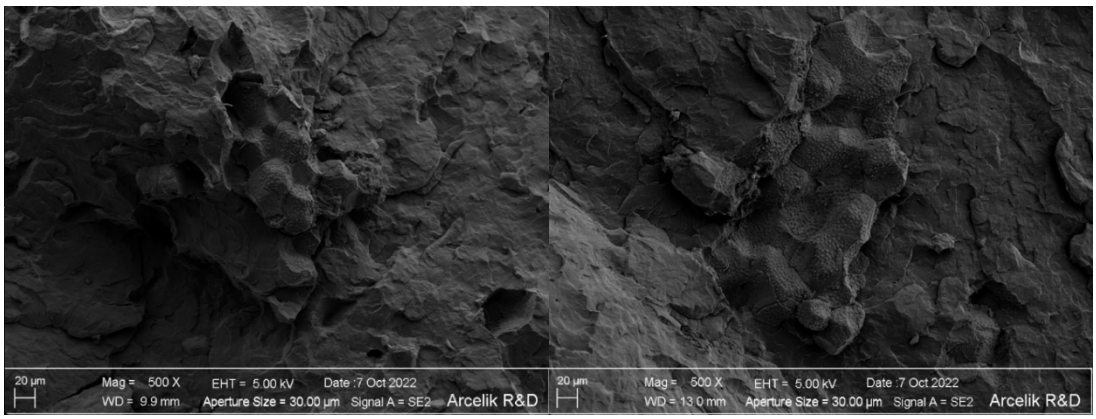

Figure 4.36 : SEM images of PP/20AKS and PP/20AKS/MAPP.

5. CONCLUSION AND RECOMMENDATIONS

The chemical composition of biomasses changes according to their type. The changing compositions include cellulose, hemicellulose, and lignin. The percent differences affect the compatibility between biomass and PP matrix due to the innate nature of biomasses, in which lignin is hydrophobic whereas cellulose is highly hydrophilic. The nonpolar structure of PP matrix makes it inherently compatible with hydrophobic biomasses rather than polar ones. The chemical composition results revealed that nutshell-type biomasses include a large portion of lignin inside their molecular structure. Among all, the highest lignin content belonged to AKS. Similar results were obtained from HS; therefore, for future work, the focus could be on this biomass to produce biocomposites. On the contrary, CC had the largest portion of cellulose. Therefore, it was expected to have poor interfacial compatibility with the polymer matrix. It was revealed that the difference between the signals of biomasses was mainly due to the ratio of lignin and cellulose.

AKS and HS started to decompose later than WS and CC. This could be due to the high lignin content of AKS and HS, whereas WS and CC have a lower hemicellulose content. The complex structure of lignin may have provided higher thermal stability than hemicellulose. The decomposition of lignin is much slower than that of hemicellulose.

The characterization of the biomasses revealed that AKS and HS had the most recent decomposition temperatures, with a larger Tonset than the other biomasses. This is due to the high lignin content of the biomass. Also, AKS had the highest total mass loss; this may be due to the large amount of non-volatile inorganic matter. Therefore, it is suggested that investigating heavy metal content by elemental analysis would be preferred.

Prior to surface modification, AKS was washed with ethanol (etOH) to remove impurities. However, when AKS is going to be esterified with SA, SA could pick up the hydroxyl groups that belong to ethanol rather than the hydroxyl groups of AKS. This may lower the yield of the surface modification. Therefore, another esterification

technique could be used for the purpose of choosing targeted hydroxyl groups that AKS owns.

Even though FTIR spectroscopy and TGA data showed that AKS was successfully modified with SA, the percent of esterified AKS could not be tested. To understand the yield of surface modification, the percentage of esterified AKS could be calculated in future work.

The biomass, matrix, and additives were previously compounded in a twin-screw extruder followed by injection molding to observe the mechanical and thermal properties of the biocomposite. The comparative effect of compatibilizers on mechanical performance was studied by tensile, flexural, and impact strengths; thermal stability was investigated by DSC and TGA analyses; and furthermore, particle distribution, particle size, and compatibility of the matrix and the biomass were characterized by SEM. As a result, the mechanical and thermal properties of biocomposites were inadequate without a compatibilizer.

The selection of biomass was critical for serial production. The biomass was chosen based on its use by secondary consumers. The nutshells and corn cobs could be collected before the second consumer. In Arçelik's previous work, spent coffee waste was collected after the second consumer. The coffee waste was not cleaned or sorted after it was collected. In some instances, unwanted substances were seen. If the unwanted external substances are not cleaned up, they could damage the mold during processing, which happened before. AKS, HS, WS, and CC wastes could be easily used in mass production.

For the polymer matrix, two different types of PP were chosen. FTIR spectra were analyzed to see the isotactic/atactic ratio. The degree of crystallization was expected to be greater if isotacticity was greater than the atactic ratio. A high degree of crystallization results in low impact toughness, high elastic modulus, and high flexural modulus. Sumitomo PP had a high isotactic ratio, and the impact toughness was lower than Borealis PP due to the crystallinity effect, whereas the elastic and flexural moduli were higher. Moreover, it was determined that the crystallinity ratio of Sumitomo PP was distinctly greater than that of Borealis PP.

The thermal analysis of Borealis PP biocomposites was different from that of Sumitomo PP biocomposites. In Borealis PP, in the first 25% portion of the TGA

graph, neat PP was more advantageous, yet in the other 75% portion of the curve, the thermal stability of neat PP was more instable than biocomposites. As a result, in high-temperature applications where biocomposites are required, they would be more advantageous than straight PP. In the TGA curve of Sumitomo PP, the thermal stability of the biocomposites decreased as the filler content increased.

So far, we have examined organic wastes such as coffee and tea, and after trying them and seeing the results, we progressed, but we made an important contribution because we were able to make an interpretation of the ratio of cellulose, hemicellulose, and lignin for the task of making a landfill decision. As a result, we have a high extractive content in HS, which leads to more impurities. WS had the least-performing material in terms of mechanical and thermal properties. CC had the highest cellulose content, which could make the biomass more hydrophilic than the other ones and affect its compatibility with the PP matrix. The best selection would be AKS. Therefore, for further studies, it would be better to proceed with AKS.

REFERENCES

[1] **Greene, J. P.** (2021). Engineering Plastics. In *Automotive Plastics and Composites* (107–125), Elsevier. https://doi.org/10.1016/B978-0-12-818008-2.00022-2

[2] **Ali, A., Bahadar, A., Khan, A., & Sanaullah, K.** (2022). Role of agricultural waste in recycled plastic biocomposites, *In Recycled Plastic Biocomposites* 165–194. Elsevier. https://doi.org/10.1016/B978-0-323-88653-6.00002-X

[3] **Batista, N. L., Olivier, P., Bernhart, G., Rezende, M. C., & Botelho, E. C.** (2016). Correlation between degree of crystallinity, morphology and mechanical properties of PPS/carbon fiber laminates, *Materials Research*, ***19***(1), 195–201. https://doi.org/10.1590/1980-5373-MR-2015-0453

[4] **Stinson, S.** (1987). Discoverers of Polypropylene Share Prize, *Chemical & Engineering News Archive*, ***65***(10), 30. https://doi.org/10.1021/cen-v065n010.p030

[5] **Park, S.-J., & Seo, M.-K.** (2011). Element and Processing, In *Interface Science and Technology* (Vol. 18, 431–499). Elsevier. https://doi.org/10.1016/B978-0-12-375049-5.00006-2

[6] **Cecchi, T.** (2021). Biocomposites from Food Waste, In *Biobased Products from Food Sector Waste* (287–310), Cham: Springer International Publishing. https://doi.org/10.1007/978-3-030-63436-0_7

[7] **Serifi, V., Tarić, M., Jevtic, D., Ristovski, A., & Šahinagić-Isović, M.** (2018). HISTORICAL DEVELOPMENT OF COMPOSITE MATERIALS, *The Annals of the University of Oradea. Economic Sciences*, *Vol. XXVII* ***(XVII)***. https://doi.org/10.15660/AUOFMTE.2018-3.3392

[8] **Liew, K. B., Goh, C. F., Asghar, S., & Syed, H. K.** (2021). Overview of Mechanical and Physicochemical Properties of Polymer Matrix Composites, In *Encyclopedia of Materials: Composites* (565–576), Elsevier. https://doi.org/10.1016/B978-0-12-819724-0.00049-5

[9] ***waste atlas the world's 50 biggest dumpsites 2014 report.*** (n.d.).

[10] **Ahmed, S., & Chaudhry, S. A. (Eds.)**. (2019). *Composites for Environmental Engineering* (1st ed.), Wiley. https://doi.org/10.1002/9781119555346

[11] **Mohanty, A. K., Misra, M., & Drzal, L. T.** (2001). Surface modifications of natural fibers and performance of the resulting biocomposites: An overview, *Composite Interfaces*, ***8***(5), 313–343. https://doi.org/10.1163/156855401753255422

[12] **Fu, S.-Y., Feng, X.-Q., Lauke, B., & Mai, Y.-W.** (2008). Effects of particle size, particle/matrix interface adhesion and particle loading on mechanical properties of particulate–polymer composites, *Composites Part B:*

Engineering, ***39***(6), 933–961. https://doi.org/10.1016/j.compositesb.2008.01.002

[13] **Zykova, A. K., Pantyukhov, P. V., Kolesnikova, N. N., Monakhova, T. V., & Popov, A. A.** (2018). Influence of Filler Particle Size on Physical Properties and Biodegradation of Biocomposites Based on Low-Density Polyethylene and Lignocellulosic Fillers, *Journal of Polymers and the Environment*, ***26***(4), 1343–1354. https://doi.org/10.1007/s10924-017-1039-9

[14] **Fuso, A., Risso, D., Rosso, G., Rosso, F., Manini, F., Manera, I., & Caligiani, A.** (2021). Potential Valorization of Hazelnut Shells through Extraction, Purification and Structural Characterization of Prebiotic Compounds, A Critical Review, *Foods*, ***10(6),*** 1197. https://doi.org/10.3390/foods10061197

[15] **AL-Oqla, F. M., Sapuan, S. M., Ishak, M. R., & Nuraini, A. A.** (2014). A Novel Evaluation Tool for Enhancing the Selection of Natural Fibers for Polymeric Composites Based on Fiber Moisture Content Criterion, *BioResources*, ***10***(1), 299–312. https://doi.org/10.15376/biores.10.1.299-312

[16] **Sohn, J., Ryu, Y., Yun, C.-S., Zhu, K., & Cha, S.** (2019). Extrusion Compounding Process for the Development of Eco-Friendly SCG/PP Composite Pellets, *Sustainability*, ***11(6),*** 1720. https://doi.org/10.3390/su11061720

[17] **Çelik, Y. H., Çelik, K. S., & Kilickap, E.** (2021). Effects of natural hard shell particles on physical, chemical, mechanical and thermal properties of composites, *Polymers and Polymer Composites*, ***29***(9_suppl), S667–S677. https://doi.org/10.1177/09673911211020717

[18] **Silva, N. G. S., Cortat, L. I. C. O., & Mulinari, D. R.** (2021). Effect of Alkaline Treatment and Coupling Agent on Thermal and Mechanical Properties of Macadamia Nutshell Residues Based PP Composites, *Journal of Polymers and the Environment*, ***29***(10), 3271–3287. https://doi.org/10.1007/s10924-021-02112-7

[19] **Barczewski, M., Andrzejewski, J., Majchrowski, R., Dobrzycki, K., & Formela, K.** (2021). Mechanical Properties, Microstructure and Surface Quality of Polypropylene Green Composites as a Function of Sunflower Husk Waste Filler Particle Size and Content, *Journal of Renewable Materials*, ***9***(5), 841–853. https://doi.org/10.32604/jrm.2021.014490

[20] **Abebayehu, S. G., & Engida, A. M.** (2021). Preparation of Biocomposite Material with Superhydrophobic Surface by Reinforcing Waste Polypropylene with Sisal (Agave sisalana) Fibers, *International Journal of Polymer Science*, ***2021***, 1–15. https://doi.org/10.1155/2021/6642112

[21] **Zia, K. M.** (2021). *Processing technology for bio-based polymers: advanced strategies and practical aspects*, Amsterdam, Netherlands ; Cambridge, MA: Elsevier.

[22] **Pilla, S.** (2011). *Handbook of bioplastics & biocomposites engineering applications*, Hoboken, NJ : Salem, Mass: Wiley ; Scrivener.

[23] Polymer processing: modeling and simulation. (2007). *Choice Reviews Online*, ***44(05)***, 44-2727-44–2727. https://doi.org/10.5860/CHOICE.44-2727

[24] **Rosato, D. V., Rosato, D. V., & Rosato, M. G. (Eds.)**. (2000). *Injection molding handbook* (Softcover reprint of the hardcover 3. ed.). New York: Springer.

[25] **Casalini, T., & Perale, G.** (2012). Processing of bioresorbable and other polymers for medical applications, In *Durability and Reliability of Medical Polymers* (49–76). Elsevier. https://doi.org/10.1533/9780857096517.1.49

[26] **Essabir, H., Nekhlaoui, S., Malha, M., Bensalah, M. O., Arrakhiz, F. Z., Qaiss, A., & Bouhfid, R.** (2013). Bio-composites based on polypropylene reinforced with Almond Shells particles: Mechanical and thermal properties, *Materials & Design*, ***51***, 225–230. https://doi.org/10.1016/j.matdes.2013.04.031

[27] **Mirón-Mérida, V. A., Barragán-Huerta, B. E., & Gutiérrez-Macías, P.** (2021). Coffee waste: a source of valuable technologies for sustainable development, In *Valorization of Agri-Food Wastes and By-Products* (173–198). Elsevier. https://doi.org/10.1016/B978-0-12-824044-1.00009-X

[28] **Cerqueira, E. F., Baptista, C. A. R. P., & Mulinari, D. R.** (2011). Mechanical behaviour of polypropylene reinforced sugarcane bagasse fibers composites, *Procedia Engineering*, ***10***, 2046–2051. https://doi.org/10.1016/j.proeng.2011.04.339

[29] **George, J., Sreekala, M. S., & Thomas, S.** (2001). A review on interface modification and characterization of natural fiber reinforced plastic composites, *Polymer Engineering & Science*, ***41***(9), 1471–1485. https://doi.org/10.1002/pen.10846

[30] **Büyükdere, B. K., Ünlü, C. H., & Atıcı, O. G.** (2022). Synthesis of surface active agents from natural waste phenolics, *Tenside Surfactants Detergents*, ***59***(2), 192–203. https://doi.org/10.1515/tsd-2021-2386

[31] **Chun, K. S., Husseinsyah, S., & Yeng, C. M.** (2016). Green composites from kapok husk and recycled polypropylene: Processing torque, tensile, thermal, and morphological properties, *Journal of Thermoplastic Composite Materials*, ***29***(11), 1517–1535. https://doi.org/10.1177/0892705715569822

[32] **Annandarajah, C., Li, P., Michel, M., Chen, Y., Jamshidi, R., Kiziltas, A., … Montazami, R.** (2018). Study of Agave Fiber-Reinforced Biocomposite Films, *Materials*, ***12***(1), 99. https://doi.org/10.3390/ma12010099

[33] **Gordelier, T. J., Thies, P. R., Turner, L., & Johanning, L.** (2019). Optimising the FDM additive manufacturing process to achieve maximum tensile strength: a state-of-the-art review, *Rapid Prototyping Journal*, ***25***(6), 953–971. https://doi.org/10.1108/RPJ-07-2018-0183

[34] **Mark, J. E. (Ed.)**. (2009). *Polymer data handbook* (2nd ed.). Oxford ; New York: Oxford University Press.

[35] **Domingos, I., Ferreira, J., Cruz-Lopes, L. P., & Esteves, B.** (2022). Liquefaction and chemical composition of walnut shells, *Open Agriculture*, *7*(1), 249–256. https://doi.org/10.1515/opag-2022-0072

[36] **Williams, C. L., Emerson, R. M., & Tumuluru, J. S.** (2017). Biomass Compositional Analysis for Conversion to Renewable Fuels and Chemicals, In J. S. Tumuluru (Ed.), *Biomass Volume Estimation and Valorization for Energy*. InTech. https://doi.org/10.5772/65777

[37] **Corbett, D., Kohan, N., Machado, G., Jing, C., Nagardeolekar, A., & Bujanovic, B.** (2015). Chemical Composition of Apricot Pit Shells and Effect of Hot-Water Extraction, *Energies*, ***8***(9), 9640–9654. https://doi.org/10.3390/en8099640

[38] **Zhao, H., Yu, Q., Li, M., & Sun, S.** (2020). Preparation and water vapor adsorption of "green" walnut-shell activated carbon by CO_2 physical activation, *Adsorption Science & Technology*, ***38***(1–2), 60–76. https://doi.org/10.1177/0263617419900849

[39] **Demirbaş, A.** (2000). Mechanisms of liquefaction and pyrolysis reactions of biomass, *Energy Conversion and Management*, ***41***(6), 633–646. https://doi.org/10.1016/S0196-8904(99)00130-2

[40] **Javier-Astete, R., Jimenez-Davalos, J., & Zolla, G.** (2021). Determination of hemicellulose, cellulose, holocellulose and lignin content using FTIR in Calycophyllum spruceanum (Benth.) K. Schum. and Guazuma crinita Lam, *PLOS ONE*, ***16***(10), e0256559. https://doi.org/10.1371/journal.pone.0256559

[41] **Ikramullah, Rizal, S., Thalib, S., & Huzni, S.** (2018). Hemicellulose and lignin removal on typha fiber by alkali treatment, *IOP Conference Series: Materials Science and Engineering*, ***352***, 012019. https://doi.org/10.1088/1757-899X/352/1/012019

[42] **Ceylan, Z., Taşar, Ş., Kaya, F., & Özer, A.** (2020). Farklı Biyokütle Atıklarının Alkali Ön İşlem Etkinliklerinin İncelenmesi, *Düzce Üniversitesi Bilim ve Teknoloji Dergisi*, 2296–2312. https://doi.org/10.29130/dubited.702096

[43] **Çelik, Y. H., Yalcin, R., Topkaya, T., Başaran, E., & Kilickap, E.** (2021). Characterization of Hazelnut, Pistachio, and Apricot Kernel Shell Particles and Analysis of Their Composite Properties, *Journal of Natural Fibers*, ***18***(7), 1054–1068. https://doi.org/10.1080/15440478.2020.1739593

[44] **Boeriu, C. G., Bravo, D., Gosselink, R. J. A., & van Dam, J. E. G.** (2004). Characterisation of structure-dependent functional properties of lignin with infrared spectroscopy, *Industrial Crops and Products*, ***20***(2), 205–218. https://doi.org/10.1016/j.indcrop.2004.04.022

[45] **Oh, S. Y., Yoo, D. I., Shin, Y., Kim, H. C., Kim, H. Y., Chung, Y. S., … Youk, J. H.** (2005). Crystalline structure analysis of cellulose treated with sodium hydroxide and carbon dioxide by means of X-ray diffraction

and FTIR spectroscopy, *Carbohydrate Research*, ***340***(15), 2376–2391. https://doi.org/10.1016/j.carres.2005.08.007

[46] **Raspolli Galletti, A. M., D'Alessio, A., Licursi, D., Antonetti, C., Valentini, G., Galia, A., & Nassi o Di Nasso, N.** (2015). Midinfrared FT-IR as a Tool for Monitoring Herbaceous Biomass Composition and Its Conversion to Furfural, *Journal of Spectroscopy*, ***2015***, 1–12. https://doi.org/10.1155/2015/719042

[47] **Aljoumaa, K., Tabeikh, H., & Abboudi, M.** (2017). Characterization of apricot kernel shells (Prunus armeniaca) by FTIR spectroscopy, DSC and TGA, *Journal of the Indian Academy of Wood Science*, ***14***(2), 127–132. https://doi.org/10.1007/s13196-017-0197-7

[48] **Gupta, G. K., Ram, M., Bala, R., Kapur, M., & Mondal, M. K.** (2018). Pyrolysis of chemically treated corncob for biochar production and its application in Cr(VI) removal, *Environmental Progress & Sustainable Energy*, ***37***(5), 1606–1617. https://doi.org/10.1002/ep.12838

[49] **Janković, B., Manić, N., Dodevski, V., Radović, I., Pijović, M., Katnić, Đ., & Tasić, G.** (2019). Physico-chemical characterization of carbonized apricot kernel shell as precursor for activated carbon preparation in clean technology utilization, *Journal of Cleaner Production*, ***236***, 117614. https://doi.org/10.1016/j.jclepro.2019.117614

[50] **Yang, H., Yan, R., Chen, H., Lee, D. H., & Zheng, C.** (2007). Characteristics of hemicellulose, cellulose and lignin pyrolysis, *Fuel*, ***86***(12–13), 1781–1788. https://doi.org/10.1016/j.fuel.2006.12.013

[51] **Purnama, P., & Kim, S. H.** (2014). Biodegradable blends of stereocomplex polylactide and lignin by supercritical carbon dioxide-solvent system, *Macromolecular Research*, ***22***(1), 74–78. https://doi.org/10.1007/s13233-014-2004-2

[52] **Ghetti, P., Ricca, L., & Angelini, L.** (1996). Thermal analysis of biomass and corresponding pyrolysis products, *Fuel*, ***75***(5), 565–573. https://doi.org/10.1016/0016-2361(95)00296-0

[53] **Guda, V. K., Steele, P. H., Penmetsa, V. K., & Li, Q.** (2015). Fast Pyrolysis of Biomass, In *Recent Advances in Thermo-Chemical Conversion of Biomass* (177–211). Elsevier. https://doi.org/10.1016/B978-0-444-63289-0.00007-7

[54] ***Recent Advances in Thermo-Chemical Conversion of Biomass.*** (2015). Elsevier. https://doi.org/10.1016/C2013-0-00403-3

[55] **Sandler, S. R.** (1998). *Polymer synthesis and characterization: a laboratory manual*. San Diego: Academic Press.

[56] **Wellen, R. M. R., Canedo, E., & Rabello, M. S.** (2011). Nonisothermal cold crystallization of poly(ethylene terephthalate), *Journal of Materials Research*, ***26***(9), 1107–1115. https://doi.org/10.1557/jmr.2011.44

[57] **Zhu, J., Liu, B., Li, L., Zeng, Z., Zhao, W., Wang, G., & Guan, X.** (2016). Simple and Green Fabrication of a Superhydrophobic Surface by One-Step Immersion for Continuous Oil/Water Separation, *The Journal of*

Physical Chemistry A, ***120***(28), 5617–5623. https://doi.org/10.1021/acs.jpca.6b06146

[58] **Andrzejewski, J., Barczewski, M., & Szostak, M.** (2019). Injection Molding of Highly Filled Polypropylene-based Biocomposites, Buckwheat Husk and Wood Flour Filler: A Comparison of Agricultural and Wood Industry Waste Utilization. *Polymers*, ***11***(11), 1881. https://doi.org/10.3390/polym11111881

[59] **Zhu, X., & Yan, D.** (2001). In situ FTIR spectroscopy study on the melting process of isotactic poly (propylene), *Macromolecular Chemistry and Physics*, ***202***(7), 1109-1113.

[60] **Lanyi, F. J., Wenzke, N., Kaschta, J., & Schubert, D. W.** (2018). A method to reveal bulk and surface crystallinity of Polypropylene by FTIR spectroscopy-Suitable for fibers and nonwovens, *Polymer Testing*, ***71***, 49-55.

[61] **Kissin, Y. V., Tsvetkova, V. I., & Chirkov, N. M.** (1972). The stereoregularity of polypropylene from IR and NMR data, *European Polymer Journal*, ***8***(4), 529-546.

[62] **İşçi, S., Ünlü, C. H., & Atıcı, O**. (2009). Polypropylene nanocomposites prepared with natural and ODTABr-modified montmorillonite, *Journal of applied polymer science*, ***113***(1), 367-374.

[63] **L. A. Hanna, P. J. Hendra*, W. Maddams, H. A. Willis and V. Zichy.** (1998). Vibrational spectroscopic study of structural changes in isotactic polypropylene below the melting point Polymer, ***29***(10), 1843-1847.

[64] **Chen, L., Wang, Y., Zhu, X., & Yan, D.** (2004). Influence of the conformational order of glassy isotactic polypropylene on its crystallization and melting behaviour. ***Polymer international*****,** *53*(2), 131-135.

[65] **Luongo, J. P.** (1960). Infrared study of polypropylene, *Journal of Applied Polymer Science*, ***3***(9), 302-309.

[66] **Mofokeng, J. P., Luyt, A. S., Tábi, T., & Kovács, J.** (2012). Comparison of injection moulded, natural fibre-reinforced composites with PP and PLA as matrices, *Journal of Thermoplastic Composite Materials*, ***25***(8), 927–948. https://doi.org/10.1177/0892705711423291

[67] **Feng, D., Caulfield, D. F., & Sanadi, A. R.** (2001). Effect of compatibilizer on the structure-property relationships of kenaf-fiber/polypropylene composites, *Polymer Composites*, ***22***(4), 506–517. https://doi.org/10.1002/pc.10555

[68] **Mansur, A.** (2011). Modeling Of Mechanical Properties of Ceramic-Metal Composites for Armor Applications, https://doi.org/10.20381/RUOR-4701

[69] **Askeland, D. R.** (1991). *The Science and Engineering of Materials*, Dordrecht: Springer Netherlands. https://doi.org/10.1007/978-94-009-1842-9

[70] **Kobayashi, T.** (2001). Impact Testing, In *Encyclopedia of Materials: Science and Technology* (4027–4031). Elsevier. https://doi.org/10.1016/B0-08-043152-6/00707-5

[71] **Zaini, M. J., Fuad, M. Y. A., Ismail, Z., Mansor, M. S., & Mustafah, J.** (1996). The Effect of Filler Content and Size on the Mechanical Properties of Polypropylene/Oil Palm Wood Flour Composites, *Polymer International*, ***40***(1), 51–55. https://doi.org/10.1002/(SICI)1097-0126(199605)40:1<51::AID-PI514>3.0.CO;2-I

[72] **Husseinsyah, S., Marliza, M. Z., & Selvi, E.** (2014). Biocomposites from polypropylene and corn cob: Effect maleic anhydride grafted polypropylene, *Advances in materials Research*, ***3***(3), 129–137. https://doi.org/10.12989/AMR.2014.3.3.129

[73] **Polychronopoulos, N. D., & Vlachopoulos, J.** (2019). Polymer Processing and Rheology. In Md. I. H. Mondal (Ed.), *Cellulose-Based Superabsorbent Hydrogels* (1–47). Cham: Springer International Publishing. https://doi.org/10.1007/978-3-319-92067-2_4-1

[74] **Ariffin, A., Ariff, Z. M., & Jikan, S. S.** (2011). Evaluation on extrudate swell and melt fracture of polypropylene/kaolin composites at high shear stress, *Journal of Reinforced Plastics and Composites*, ***30***(7), 609–619. https://doi.org/10.1177/0731684411399140

[75] **Kalaprasad, G., Mathew, G., Pavithran, C., & Thomas, S.** (2003). Melt rheological behavior of intimately mixed short sisal-glass hybrid fiber-reinforced low-density polyethylene composites, I. Untreated fibers. *Journal of Applied Polymer Science*, ***89***(2), 432–442. https://doi.org/10.1002/app.11975

[76] **Mohanty, S., Nayak, S. K., Verma, S. K., & Tripathy, S. S.** (2004). Effect of MAPP as a Coupling Agent on the Performance of Jute–PP Composites, J*ournal of Reinforced Plastics and Composites,* ***23***(6), 625–637. https://doi.org/10.1177/0731684404032868

[77] **Igarza, E., Pardo, S. G., Abad, M. J., Cano, J., Galante, M. J., Pettarin, V., & Bernal, C.** (2014). Structure–fracture properties relationship for Polypropylene reinforced with fly ash with and without maleic anhydride functionalized isotactic Polypropylene as coupling agent, *Materials & Design*, ***55***, 85–92. https://doi.org/10.1016/j.matdes.2013.09.055

[78] **Zuza, E., Lejardi, A., Ugartemendia, J. M., Monasterio, N., Meaurio, E., & Sarasua, J.-R.** (2008). Compatibilization through Specific Interactions and Dynamic Fragility in Poly(D,L-lactide)/Polystyrene Blends, *Macromolecular Chemistry and Physics*, ***209***(23), 2423–2433. https://doi.org/10.1002/macp.200800443

[79] **Mohan Bhasney, S., Kumar, A., & Katiyar, V.** (2020). Microcrystalline cellulose, polylactic acid and polypropylene biocomposites and its morphological, mechanical, thermal and rheological properties, *Composites Part B: Engineering*, ***184***, 107717. https://doi.org/10.1016/j.compositesb.2019.107717

[80] **Sitticharoen, W., Uthiyoung, C., Passadee, N., & Wongprom, C.** (2018). Surface treated bagasse fiber ash on rheological, mechanical properties

of PLA/BFA biocomposites, *Polímeros*, ***28***(3), 187–195. https://doi.org/10.1590/0104-1428.0010

[81] **Ogah, A. O., Afiukwa, J. N., & Nduji, A. A.** (2014). Characterization and Comparison of Rheological Properties of Agro Fiber Filled High-Density Polyethylene Bio-Composites, *Open Journal of Polymer Chemistry*, ***04***(01), 12–19. https://doi.org/10.4236/ojpchem.2014.41002

CURRICULUM VITAE

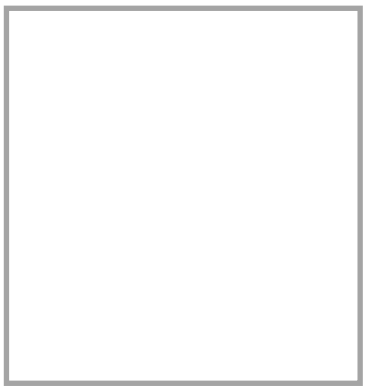

Name Surname : Eliz Gurpinar

EDUCATION :

- **B.Sc.:** 2020, Sabanci University, Faculty of Engineering and Natural Science, Material Science and Nanoengineering Department

PROFESSIONAL EXPERIENCE AND REWARDS:

- 2021-2023 Arçelik A.Ş Central R&D Advanced Materials Technologies Frontier Research Laboratory, R&D Engineer, Department of Polymer & Chemistry
- 2022 Pyramid Climbers Award Arçelik A.Ş Biocomposites Telve Duo Collaboration Developers
- 2020 October- 2021 January Imperial College London Guder Research Group Research Intern, Faculty of Engineering, Department of Bioengineering, Implantable Sensors with Bioresorbable Materials
- 2019 July-August Sika Summer Intern Quality Control and R&D Department
- 2019 June-July Henkel Summer Intern Quality Control Department

PUBLICATIONS, PRESENTATIONS AND PATENTS ON THE THESIS:

- **Gurpinar E., Unlu C., and Kovanci C.** 2022: Lignocellulosic Fillers from Organic Wastes for Polypropylene Bio-composites – ICEANS 2nd International Conference on Engineering & Applied Natural Sciences, October 15-18, 2022 Konya, Turkey.